Kobe University Repository : Kernel

PDF issue: 2024-08-26

Study of Inner Shell Excitation Effect on C-H Dissociation in Aromatic Hydrocarbon Solids

Shimoyama, Iwao

(Degree)
博士（理学）

(Date of Degree)
1999-03-31

(Date of Publication)
2014-12-10

(Resource Type)
doctoral thesis

(Report Number)
甲1914

(JaLCDOI)
https://doi.org/10.11501/3156315

(URL)
https://hdl.handle.net/20.500.14094/D1001914

※ 当コンテンツは神戸大学の学術成果です。無断複製・不正使用等を禁じます。著作権法で認められている範囲内で、適切にご利用ください。

博士論文

Study of Inner Shell Excitation Effect on C-H Dissociation in Aromatic Hydrocarbon Solids

平成11年1月

神戸大学自然科学研究科

下山 巖

DOCTORAL THESIS

Study of Inner Shell Excitation Effect on C-H Dissociation in Aromatic Hydrocarbon Solids

芳香族炭化水素固体における C-H解離に関する内殻励起効果の研究

Iwao Shimoyama

Department of Materials and Structures
Division of Industrial Science
The Graduate School of Science and Technology
Kobe University

January 1999

Acknowledgements

The author wish to express my gratitude to Professor Kazumichi Nakagawa not only for his valuable suggestions, comments, instruction and careful reading of this manuscript but also for his continuing direct guidance and encouragement.

The author is so much obliged to Dr. Kazuhiko Mase, Dr. Mitsuru Nagasono, and Dr. Shin-ichiro Tanaka at Institute of Molecular Science for their special apparatus used in this experiment, encouragement, and helpful discussion. The author is also greatly indebted to the members of EICO group for useful discussion and comment.

The author thanks to Messrs. Takeshi Mochida, Yasushi Otsuki, Hiroki Horiuchi, and Miss. Sachiko Saijo at Kobe University for their help in this experiment.

This work is supported by the Joint Studies Programs of the Institute for Molecular Science No. 7-520, No. 97-506, and the Joint Studies Program of the Photon Factory of the National Laboratory for High Energy Accelerator Organization No. 96G270. The author is obliged to the staff of the Facility for their technical help.

Contents

I . Introduction

A variety of reactions which induced by interactions between photon and matters is an important subject of photophysics and photo-process. When the photon energy is small, photon can interact with outer shell electrons to excite or ionize those. When the photon energy is large, photon can interact with inner shell electrons to excite or ionize. Such processes are called as "inner shell excitation", and the phenomena induced by inner shell excitation is called as "inner shell excitation effect" in this thesis. Inner shell excitation effect on bond breaking is essentially interesting and important because of following characteristic properties; (i) formation of multiply charged state and (ii) localization of excited state. Due to such properties, inner shell excitation are expected to cause unique reactions which are different from outer shell excitation.

Desorption induced by electron transition (DIET) is a phenomenon that neutral or ion species are emitted from a solid surface *via* electron transition induced by electron or photon irradiation. DIET proceeds through bond breaking between surface species and bulk. When photon is used to irradiate, DIET is called photon-stimulated desorption (PSD). When electron is used to irradiate, DIET is called electron stimulated desorption (ESD). Since the desorption cross sections of ESD (~ 10^{-18} cm^2) is larger than that of PSD (~ 10^{-20} cm^2), ESD is more important than PSD on the point of practical subject. However, since photon enables a selective excitation, PSD is more important than ESD on the point of study of DIET mechanism. Thus, PSD is extensively attractive to study the inner shell excitation effect on bond breaking. From previous investigations [1,2,3], PSD induced by inner shell excitation has been considered to be dominated by coulomb repulsion energy between multiple holes created by inner shell excitation in valence band. Recently, however, some researches have been reported that not only the repulsion energy but also the character of excited molecular orbital governs PSD. This means that different resonant excitations of

inner shell result in different desorption. I call this phenomenon as "inner shell resonant excitation effect" in this thesis. Ueno and Tanaka [4] reported that PSD of poly(methyl methacrylate) (PMMA) showed an obvious inner shell resonant excitation effect at O *K*-shell. In their study, desorption yield spectra of CH_3^+ and CH_2^+, showed a clear enhancement at the excitation $\sigma^*(CO\text{-}CH_3) \leftarrow 1s(O\text{-}CH_3)$, while, desorption yield spectrum of H^+ showed no enhancement at this excitation and showed a clear dip at the excitation $\pi^*(C{=}O) \leftarrow 1s(C{=}O)$. They mentioned that π^* excitation gives different decay channels from σ^* excitation. Coulman et al. [5] reported those desorption yield spectrum of total ion from condensed H_2O also showed a clear enhancement at the $4a_1 \leftarrow$ O 1s resonant excitation. Such inner shell excitation resonant effect on desorption yield has been reported for polystyrene [6] and condensed NH_3 [7].

It should be noted that inner shell resonant excitation effect arises as a consequence of fundamental interaction between photon and molecules. In most conventional PSD studies, however, excitation or ionization also contribute. I call this effect "secondary effect" in this thesis. For example, let us illustrate a schematic diagram of desorption of H^+ from benzene surface as shown in figure 1-1. In the figure, H^+ desorbed by an interaction with photon is called as "fundamental ion" and H^+ desorbed by an interaction with secondary electrons is called as "secondary ion" in this thesis. To estimate the real magnitude of inner shell resonant excitation effect, one must extract only the fundamental ions from desorbed ions.

In order to do this, I studied the inner shell excitation effect on PSD of condensed benzene and extract the fundamental effect from desorption yield using Auger electron coincidence spectroscopy. It is interesting to study the inner shell excitation effect on bond breaking of benzene because of following two reasons. (1)Benzene is a typical aromatic hydrocarbon compound which is known to have larger anti-radiation nature than another organic compounds [8, 9]. For example, as shown in table 1-1, the *G* values of H_2 and C_2H_4 products for benzene are far less than that for non-aromatic organic compounds [10, 11, 12, 13]. The reason why aromatic hydrocarbon compounds have an extended anti-

radiation nature may be attributed to the energy delocalization due to π conjugated system [14]. However, the detailed mechanism of radiation damage of aromatic hydrocarbon compounds has not been clarified. Since high energy radiation is thought to cause bond breaking induced inner shell excitation, it is important to study the elementary process of reaction following inner shell excitation. The PSD study of benzene is important because it enables us to insight the detailed mechanism of bond breaking. (2)One can compare the surface reaction and bulk reaction by using aromatic hydrocarbon compounds. When the bond breaking occurs in bulk, it must be observed as radiation damage. Assuming the elementary process of reaction in bulk following inner shell excitation is the same with that on surface, radiation damage in solid is thought to correspond to PSD on surface. Since anthracene is also typical aromatic hydrocarbon compound as well as benzene, to compare the study of radiation damage in anthracene single crystal with the study of PSD from condensed benzene is also attractive.

This thesis is organized as follows: In chapter II, basic concepts and theories of inner shell excitation effect and PSD are mentioned. In chapter III, experimental details and results for PSD of condensed benzene are shown. I also mention about the Auger electron photoion coincidence spectroscopy (AEPICO) and show the results of AEPICO spectra in this chapter. In chapter IV, physical meaning of obtained data is discussed and contributions of fundamental and secondary effect on H^+ desorption are separated. Finally, I compare the difference of C-H dissociation yield between bulk reaction and surface reaction.

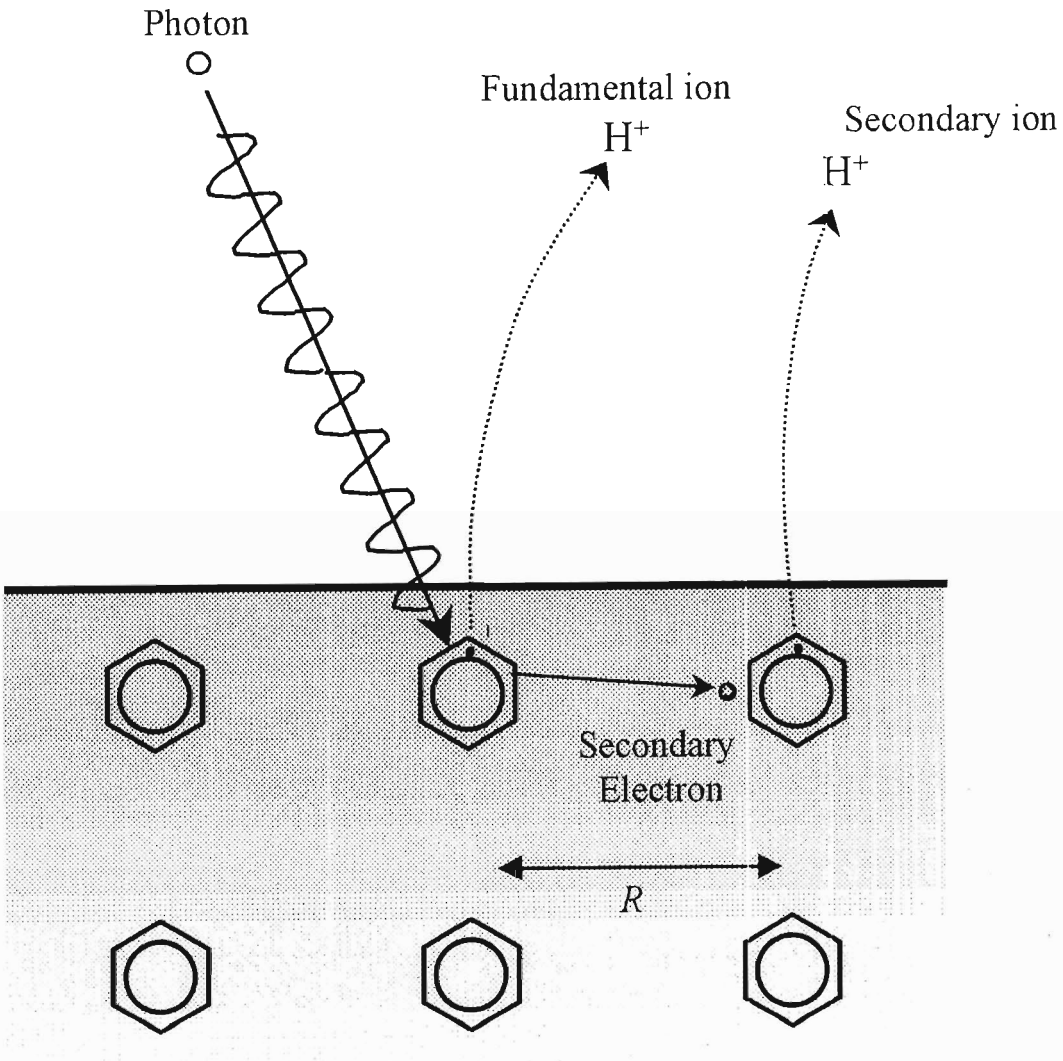

Figure 1-1.Schematic diagram of fundamental H^+ desorption and secondary H^+ desorption.
R: distance between molecules

Table 3-2: TIY/AEY intensity ratio at each inner shell excitation

$h\nu$	285eV	287eV	300eV	430eV
state	$\pi^*(e_{2u})$	X_D	ionization	ionization
TIY/AEY intensity ratio	1/4	1	1/2	1

Ⅱ. Basis of Inner Shell Excitation and Photon-stimulated Desorption

Ⅱ-1. Core decay process

At first, I describe the characteristic properties of inner shell excitation. One of the properties is formation of multiply charged state which is formed *via* a relaxation process of inner shell excitation. Figure 2-1 shows the schematic diagram of typical relaxation processes which follows inner shell excitation. In the figure, when an electron in outer shell, *e.g.*, *L*-shell, is taken out of the system, only one hole is created in the outer shell. While, when an electron in inner shell, *e.g.*, *K*-shell, is taken out of the system, a core hole is created. Since a core hole state of the system is very unstable, a core hole is filled with an electron which lies in an outer shell. The transition of electron from upper state to core hole is called as "core decay". Through the core decay, surplus energy $E_L - E_K$ is formed in the system, where E_L and E_K is energy of upper electronic state and inner shell, respectively. Principally, two competitive processes can release the surplus energy: One is non-radiative and the other is radiative process.

In the former process, the surplus energy is released by the emission of another electron. This relaxation process is called as "Auger decay process" [15]. In the final state, there are two holes in the outer shell. When the transition occurs between states which has same principal quantum number, such core decay is called as "Coster-Kronig transition". The transition probability $P_{i\to f}$ of Auger decay is described as follows [16];

$$P_{i\to f} = \frac{2\pi}{\hbar}\left|\iint \chi_f^*(\mathbf{r}_1)\psi_f^*(\mathbf{r}_2)\frac{e^2}{|\mathbf{r}_1-\mathbf{r}_2|}\chi_i(\mathbf{r}_1)\psi_i(\mathbf{r}_2)d\mathbf{r}_1 d\mathbf{r}_2\right|^2 , \quad \cdots\cdots(2-1)$$

where $\chi_i(\mathbf{r}_1)$ and $\psi_i(\mathbf{r}_2)$ are the initial wavefunctions of electron 1 and 2, $\chi_f(\mathbf{r}_1)$ and $\psi_f(\mathbf{r}_2)$ are the final wavefunctions, respectively. As described above, the operator of Auger decay is coulomb interaction. In Auger decay, the selection rules are that transitions are possible only if the initial and final states have the same

symmetries, namely, $\Delta L = \Delta S = \Delta J = 0$ [16]. Hence, optically forbidden transition can occur.

In the latter process, the surplus energy is released by emission of photon. This relaxation process is called as "characteristic X-ray fluorescence process". In this case, there is one hole in the outer shell at the final state. For a K hole, it is known that the characteristic X-ray fluorescence yield ω_X defined as following;

$$\omega_X = \frac{\text{Intensity of X-ray photon}}{\text{Intensity of X-ray photon + Auger electrons}}, \quad \cdots\cdots(2.2)$$

which has a relationship of atomic number Z as following;

$$\omega_X = \frac{Z^4}{Z^4 + a}, \quad \cdots\cdots(2.3)$$

where, for K-shell emission, a = 1.12×10^6 [17]. As shown in figure 2-2, ω_X increases as Z increases. Thus, for light element, *e.g.*, N, C, and O, the dominant core decay process is Auger decay. For example, when C K-shell electron is excited $\omega_X \approx 0.001$. And the probability of characteristic X-ray emission in the case that core hole is formed in a shallow inner shell is less than the probability in the case that core hole is formed in a deep inner shell.

Ⅱ-2. **Auger decay process**

Auger decay is the core decay process which accompanies auto-ionization and formation of multi-holes state. There are various types of Auger decay. But the processes can be divided into two main classes; one is normal Auger decay and the other is resonant Auger decay. Now, I survey these processes.

Ⅱ-2-(1). **Normal Auger decay**

Figure 2-3 illustrates a schematic diagram of simple system of a molecule which consists of K-shell (KS), valence band (VB), and an unoccupied orbital (UO). E_K, E_V, and E_{UO} are the binding energies of KS, VB, and UO, respectively. After a core electron is ionized into continuum (CO), a valence electron fills the K hole. The surplus energy $E_K - E_V$ that formed by the electron transition KS ←

VB is released of valence band by the emission of an another electron. As described above, normal Auger decay is induced by ionization of core electron. The normal Auger decay shown in Fig.2-3 is called *KVV'* Auger decay because one *K*- electron and two valence electrons take part in the Auger decay. The electron emitted from KS to CO is called as "*K*-photoelectron" and the electron emitted from VB to CO by the surplus energy is called as "Auger electron". In this case, there are two holes in valence band. I call this state as "2h state" in this thesis. Using the Koopmans' theory [18], the kinetic energy E^K_{PE} of *K*-photoelectron is expressed as follows;

$$E^K_{PE} = h\nu - E_K. \quad \cdots\cdots (2-4)$$

The kinetic energy E_{Auger} of Auger electron is described as follows [19];

$$E_{Auger} = E_K - E_{Vj} - E_{Vk} - U_{eff} + R, \quad \cdots\cdots (2-5)$$

where E_{Vj} and E_{Vk} are the binding energy of V_j orbital and V_k orbital of valence band, U_{eff} is the coulomb repulsion energy between two holes, and R is the correction term by screening of core hole. It should be noted that E_{Auger} is independent of $h\nu$ in normal Auger decay, while E^K_{PE} is dependent of $h\nu$.

Accompanying normal Auger decay, another decay processes can occur. A sudden change of effective charge induced by inner shell excitation may cause excitation or ionization of valence electron simultaneously. These phenomena are called as "shake up" and "shake off" processes. Figure 2-4 shows schematic diagrams of these processes. In the shake up process, the energy of E^K_{PE} is reduced by the energy of electron transition from outer valence to an unoccupied excited state. Since the transition energy from VB to an UO is discrete, the energy reduced *K* photoelectron shows a discrete satellite peak. There are two holes and 1 electron in the outer shell in the final state. This state is called as "2h1e state". While, in the shake off process, the energy of E^K_{PE} is reduced by the energy of electron transition from VB to CO. This continuous transition reduces the E^K_{PE} continuously. Thus, in this case, *K*-photoelectron should show a continuous structure in the low energy side of shake up satellite peak. In other words, shake off is called double Auger. There are three holes in VB at the final

state. This state is called as "3h state" in this thesis. I will show an example of these processes in chapter Ⅲ.

Ⅱ-2-(2). **Resonant Auger decay**

Consider the same picture as shown in Fig.2-3. When a core electron is not ionized but resonantly excited to an UO, the following Auger decay is called as "resonant Auger decay". Resonant Auger decay process are classified into two processes [20]; one is "spectator Auger decay" and the other is "participant Auger decay". Details description of these processes are given as following.

• **Spectator Auger decay**

Schematic diagram of spectator Auger decay process is shown in figure 2-5. In this process, the core electron is placed into an excited state as a spectator, while Auger decay proceeds by valence electrons bounded more tightly. At the final state, there are two holes and one electron in the outer shell. This state is called as "2h1e state". In this case, the kinetic energy of E_{Auger} is expressed as follows [19];

$$E_{Auger} = E_K - E_{Vj} - E_{Vk} - U_{eff} + R + E_{PCI}, \quad \cdots\cdots(2-6)$$

where E_{PCI} is the term of post collision interaction effect [21, 22]. This term is induced by the core electron excited into the UO. In the case of normal Auger decay, Auger electron feels coulomb attraction by valence two holes. On the other hands, in the case of spectator Auger decay, the coulomb attraction is weakened by the screening effect of an electron placed in UO. Consequently, E_{Auger} is shifted to higher energy than that of the 2h state. The PCI term can be negligible in the case of normal Auger decay.

• **Participant Auger decay**

Figure 2-6 shows this process. In participant Auger decay process, the excited electron is directly involved in the filling of K hole. In this case, there is only one hole in valence band. I call this state "1h state". In this case, E_{Auger} is expressed as follows [19];

$$E_{Auger} = E_K - E_{UO} - E_{Vk}. \quad \cdots\cdots(2-7)$$

Since the energy $E_K - E_{UO}$ is equal to the excitation energy $h\nu$, E_{Auger} is equal to the kinetic energy of photoelectron emitted from V_k orbital. Thus, only in this

case, the kinetic energy of Auger electron depends on *hv*.

Ⅱ–3. **Coulomb explosion**

As mentioned above, multi-hole state is created *via* Auger decay in the system. The first report of multi-hole effect to bond breaking was done by Carlson and White [23]. They irradiated X-ray of which energy was about 8 - 9 keV to CH_3I molecules. Using X-ray with this energy, they could excite *L* shell of iodine and they observed variety of multiply charged ion fractions. From this result, they proposed "Coulomb explosion" model. The initially created *L* hole of iodide produces two holes in the *M* shell *via* Auger decay. Continually, the *M* holes produces four holes in the *N* shell. Finally, eight holes are formed in the valence band of the molecule *via* "Auger cascade". This multi-hole state causes strong bond raptures due to repulsive potential between holes in the molecule. This is the coulomb explosion. In the case of molecules which consist of light elements, such Auger cascade can not occur because *L*-shell electrons constitute outer shell for light elements. But, at least, two localized holes are created in VB. By this reason, the bond ruptures are also expected for molecules which consist of light elements. Carlson and Krause [24] have reported that core ionization of small molecules which consist of C, N, and O, results in an abundance of ionic fragment. As mentioned above, unique relaxation processes and following reactions are expected for inner shell excitation.

Ⅱ–4. **Site-specific reaction**

One of the most unique reactions induced by inner shell excitation is site-specific reaction. The difference in core electron binding energies for different atoms is sufficiently large to allow selective excitation of different atoms. Thus one can create a core hole at a specific atom by tuning excitation energy at the binding energy of an atom. Since wavefunctions of inner shell are highly localized at atoms, core holes are also localized at specific site. Therefore, the following Auger decay is expected to cause different chemical reaction depending on the atomic site of the core hole and the electronic configuration of the excited state. Such reaction is called as "site-specific reaction". Moreover, even for the same element, site-specific reaction is also expected because the binding energy of inner shell for same atom is shifted by different chemical environment. Thus the site-specific bond breaking may possibly be used as a *scalpel* to selectively cut chemical bonds. First case of site-specific reaction was reported by Eberhardt *et al.* [25]. They excited C 1s of acetone (CH_3COCH_3) and measured ionic fragments of H^+, C^+, CH_3^+, O^+, CH_3CO^+, and $CH_3COCH_3^+$. Acetone has two different C: One is in the CO group and the other is in the CH_3 group. Though C^+ and O^+ yield spectra showed an apparent π^* resonance due to CO group, yield spectra of other ions didn't show π^* resonance and increased above the ionization energy of C which is belong to CH_3 group. Such site-specific reaction was observed in other molecules [26, 27]. In principle one might suppose that site-specific bond breaking can occur at the bond closest to the core excited atom. While it is reported that C^+ and CO^+ were not observed, and CH_3^+ ionic fragment yield was enhanced at the shape resonance in the case of O 1*s* excitation [28] for acetone. As shown above, in practice, bond breaking frequently occurs at bonds distant from core excited atom. It is thought that the result is due to energy transfer from core excited site to another sites through Auger decay. To control the site-specific reaction, it is necessary to study the mechanism of core decay and the complicated dissociative relaxation processes.

Ⅱ–5. **Inner shell excitation effect on bulk reaction**

As mentioned above, since inner shell excitation is also expected to cause unique reaction in bulk, several studies of inner shell excitation on radiation damage have been reported in past years. Halpern and Stöcklin [29] used monoenergetic X-rays from characteristic fluorescence of some element and studied inner shell excitation effect on Br atom of solid 5-bromodeoxyuridine (BUdR). They measured the radical concentration per unit dose by ESR and observed a resonance increase near the Br K-edge. SR is extensively useful tool to investigate such inner shell effect because it is available to use monochromatic X-rays with wide wavelength region. Using SR, Sato *et al.* [30] excited the inner shell in Ga and As of amorphous and crystalline GaAs. They measured infrared absorption spectra of defect and observed that defects were created by excitation of L shell electron, while defects were eliminated by excitation of K shell. Kondo *et al.* [31] excited Cl K shell and Br K shell of crystalline KCl and KBr at liquid nitrogen temperature. They measured absorption of *F*-center and observed no discernible increase of *F*-center formation efficiency. Kimura *et al.* [32] excited C K shell of anthracene single crystal. They measured color center formation quantum yield in the energy region $200 < h\nu < 600$ eV and observed a resonant decrease near the C K-edge. As shown above, there is variety of inner shell effects for radiation damage. The reason why there is such variety in bulk has not been clarified. Thus, it is interesting to study the difference of inner shell excitation effect between surface reaction and bulk reaction.

Ⅱ-6. Synchrotron radiation and application to processing

Synchrotron radiation (SR) is a powerful tool to study the inner shell excitation effect because of some unique properties. SR is electromagnetic wave emitted from charged particles, *e.g.*, electron or positron, moving along circular orbital (see figure 2-7). In the figure, electron circulating with radius ρ in a uniform magnetic field emits electromagnetic wave to the direction of tangent. The emission intensity distributes within a cone of which vertical angle is $1/\gamma$ from the theory of relativity, where $\gamma = E / m_0c^2$, E is electron energy, and m_0c^2 is the rest mass energy of electron. One of the most important properties of SR is that the strong light beam which energy is continuum from the infrared to the X-ray region is available. It is known that the intensity distribution of SR shows maximum at the critical wavelength λ_c as expressed as follows [33];

$$\lambda_c = \frac{4\pi\rho}{3\gamma^3}. \quad \cdots\cdots(2-8)$$

Figure 2-8 shows the intensity distribution at the SR facility, UVSOR [34]. As shown in Fig.2-8, SR is continuous light source which is also available for soft X-ray. For light element, the binding energies of inner shell lie in the soft X-ray region. Thus, using SR, the excitation energy can be tuned at a binding energy of core electron of an atom. Another properties, high brilliance, excellent directivity, well-defined polarization, and fast time structure are also very useful to study the inner shell excitation effect.

Recently, applications of inner shell excitation effect to processing have been attempted. There are many fields in the processing, *e.g.*, chemical vapor deposition (CVD), photo-etching, molecular beam epitaxi (MBE), surface modification, surface purification, and so on. Uesugi and Nishiyama [35] reported a suppression effect on the Al thermal CVD reaction on Si surface by SR irradiation. They observed that the suppression effect largely depends on the photon energy, in other words, the suppression effect is well observed by inner shell excitation, while the effect is not well observed by valence electron excitation. And Tinone *et al.* [36, 37] reported that site-specific bond scission

were observed for the PSD of PMMA tuning the excitation photon energy by SR. Since PMMA is a material which is well used photo-etching of semiconductor, this report is very interesting to develop the semiconductor processing. As shown above, inner shell excitation is expected to develop new processing method using SR.

Ⅱ-7. Inner shell excitation effect on desorption induced by electron transition (DIET)

As described in chapter Ⅰ, the study of DIET induced by inner shell excitation is extensively attractive because DIET reflects bond breaking. Moreover, since DIET is the basic process in the surface processing, the inner shell excitation effect on DIET is expected to apply the semiconductor processing and creation of new material [38]. The recent rapid progress of SR has advanced the study of inner shell excitation effect on DIET. Here, I survey three representative DIET models.

(1)Menzel-Gomer-Redhead Model

This is the first model explaining DIET phenomenon. In 1964, two theoretical models in respect of ESD were published by Menzel and Gomer [39] and independently Redhead [40]. Despite the different experimental techniques, they arrive to similar conclusions and their proposed mechanism is known as the Menzel-Gomer-Redhead (MGR) model. Figure 2-9 shows schematic diagram of this model. M and A shows a substrate and an adsorbate, respectively. In this model, desorption of A from M proceeds *via* 2 step process: (1) primary excitation and (2) escape from surface. The primary excitation is a vertical Franck-Condon excitation from the bonding ground state (M + A) to the repulsive antibonding state (M + A)* without changing the distance between M and A. Following this stage, excited electron moves along the (M + A)* potential

curve and transfers to the state (M* + A) in the excitation lifetime τ. (M* + A) is different from (M + A)* only by an excitation of the substrate. In this process, adsorbate A takes a new equilibrium distance which is located at the minimum in the (M* + A) adiabatic potential curves and receives an excess energy $E(x_0)$ - $E(x)$. As shown in Fig.2-9, there is a critical distance x_c beyond which recapture cannot occur because the excess energy $E(x_0)$ - $E(x_c)$ sufficiently large to make adsorbate escape. The MGR model is proposed in respect of desorption of neutral species with covalently bonded system. This model is supported in the case of desorption which induced by valence excitation.

(2)Knotek-Feibelman Model

For the desorption induced by inner shell excitation, Knotek-Feibelman (KF) model [41] was proposed in the case of desorbed species ionic bond system at first. Knotek and Feibelman reported that O^+ ion was desorbed from TiO_2 by Ti $3p$ shallowest core excitation. They explained this phenomenon by repulsion potential which is due to the inversion of Madelung potential induced by Auger decay. Figure 2-10 shows the schematic diagram of this model. TiO_2 is ionic compound, Ti and O are combined in the condition $Ti^{4+}O^{2-}$ at the ground state. When Ti $3p$ shallowest core electron is removed to conduction band (CB), a hole is formed in the core. TiO_2 is maximal valency compound and higher-lying electrons are lacking on the Ti atom. Thus, predominantly Auger decay is inter-atomic Auger decay. In this Auger decay process, one valence electron from the O^{2-} falls into Ti $3p$ core hole and one (or two) electron is emitted from the valence band (VB) of oxygen to release the energy of the decay. Through this decay process, O^{2-} will be changed to O^+. The charge reversal of oxygen produces the repulsive Madelung potential between Ti^{4+} and O^+ and O^+ is desorbed from the surface to relax the Madelung potential energy.

(3)Auger Stimulated Desorption Model

Auger stimulated desorption (ASD) model was proposed by Ramaker, White, and Murday *et al.* [42, 43] and is similar to the KF model. But this model

is extended to covalent, ionic, and chemisorbed system. Image a simple system illustrated in figure 2-11. In the figure, B and S shows a bulk atom and a surface atom, respectively. B and S are covalently bonded *via* bonding orbital b_0 with bond energy D in the ground state. The Auger process due to inner shell excitation creates two holes in the system and leave the system in the repulsive state b_0^{-2} with excitation energy $2E_b + U_{eff}$, where E_b is the one-electron binding energy of b_0, and U_{eff} is the effective correlation energy between two holes. Initially, S is pushed off the surface along the b_0^{-2} state. If the holes decay before critical distance R_c, S is recaptured; otherwise S gains sufficient kinetic energy to be desorbed. Beyond the R_c, S can be neutralized by electron transfer from the B and desorbed along b_n^{-2} state as a neutral species where b_n^{-2} is a bonding orbital of bulk. While, ion desorption of S^+ can proceed in the following two processes. One is a process to escape along the b_0^{-2} state. In this case, the kinetic energy of S^+ is maximum, *i.e.*, e^2 / R_0. The other is a process to escape along b_n^{-1} b_0^{-1} state. In this case, though the kinetic energy is smaller than e^2 / R_0, the ion intensity is maximum.

The most significant problem of this model lies in the time difference between holes' decay and desorption. When the multiple holes are localized in the bonding orbital b_0 for a sufficiently long time in which S exceeds the R_c, desorption can occur. While, when multiple holes decay *via* "hole hopping" before desorption, the repulsive energy is relieved and desorption can not occur. The "hole hopping" means the delocalization of holes to another atom or bond. The typical value of uncorrelated one-hole hopping times are of the order of 10^{-16} s, whereas desorption times are more of the order of 10^{-13} s. They mentioned about hole-hole correlation effect which make the one-hole hopping slow. Figure 2-12 illustrates the schematic diagram which show a hole hopping in a system with bandwidth W. When one hole resonantly hops in the valence band, the typical hopping time $\tau \approx 1/W$. When two holes are created on an atom or in a bond, the effective correlation energy between two holes is given by U_{eff}. If $U_{eff} > W$, resonant one-hole hopping is essentially blocked and $\tau \gg 1/W$ because it involves either energy transfer during the transition or a complicated multiple-

hole motion. The highly repulsive Auger final state is thus given as intrinsically long lifetime due to this correlation, possibly of the order of 10^2 times the normal one-hole lifetime. This ASD model is universally recognized as a most popular DIET model on inner shell excitation.

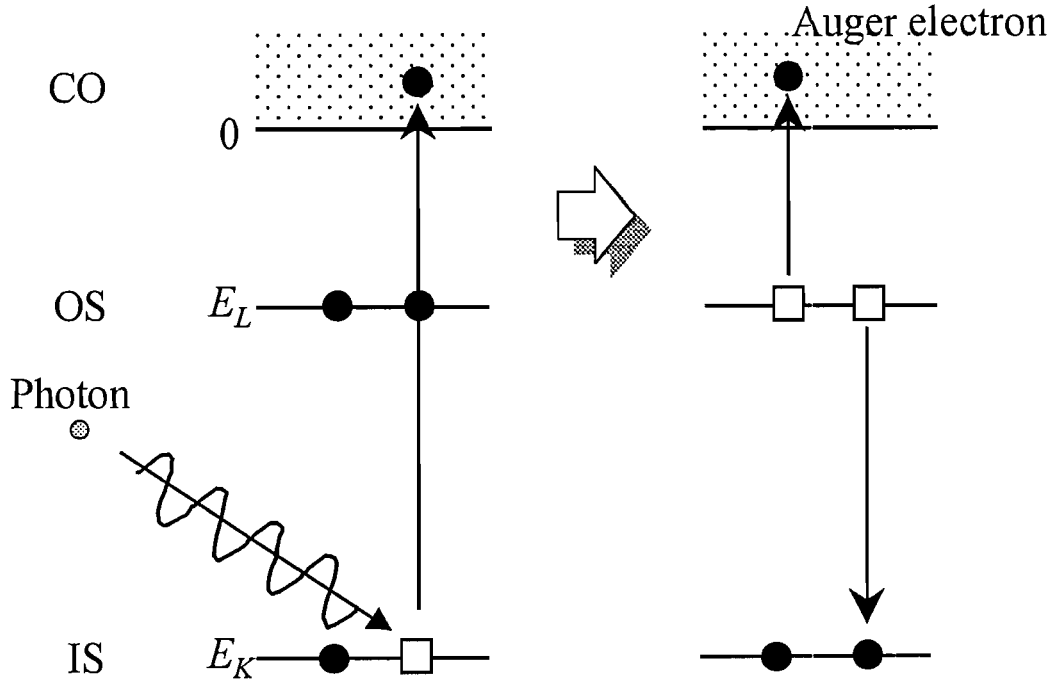

Figure 2-1-(a).

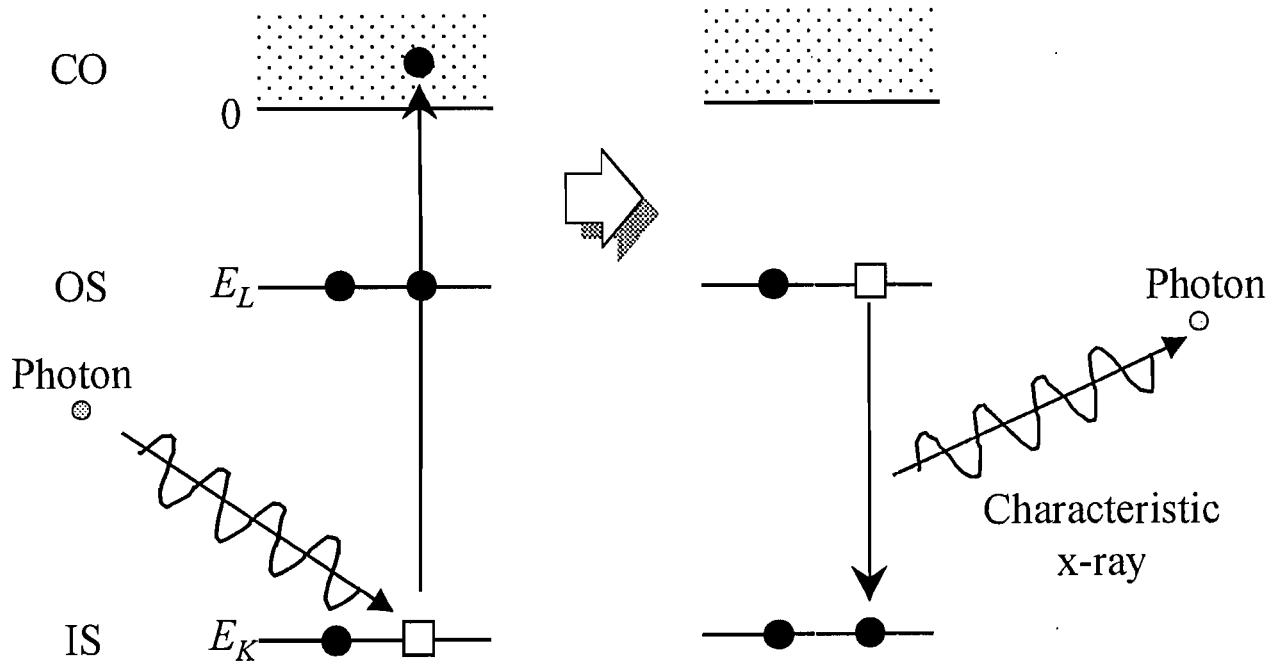

Figure 2-1-(b)

Figure 2-1. Schematic diagram of Core decay processes
(a) Auger decay process (b) Characteristic x-ray fluorescence process
C: continuum, OS: outer shell, IS: inner shell. ● : electron □ : hole
E_L: binding energies of OS, E_K :binding energies of IS.

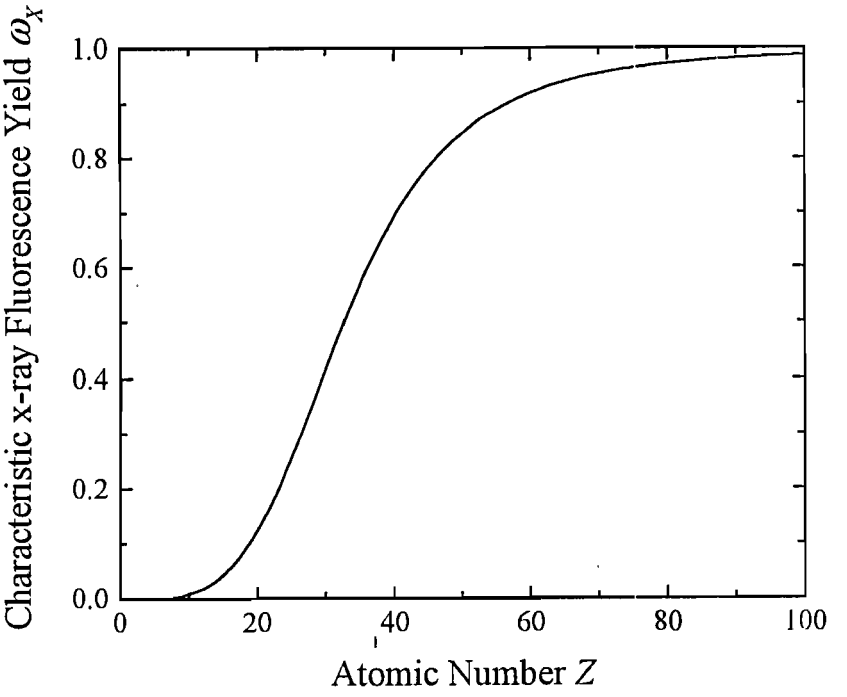

Figure 2-2. Characteristic x-ray Fluorescence Yield ω_X

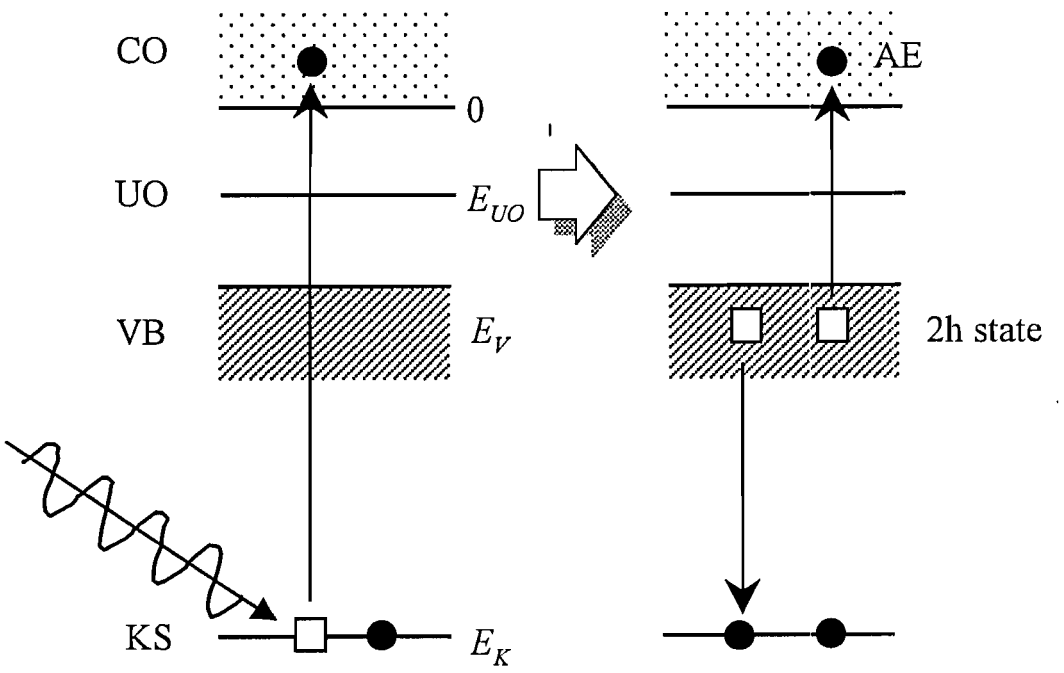

Figure 2-3. Normal Auger decay process
CO: continuum, UO: unoccupied orbital,VB: valence band, KS: *K*-shell.
E_{UO}: binding energies of UO, E_V: binding energies of VB,
E_K: binding energies of KS, AE: Auger electron.

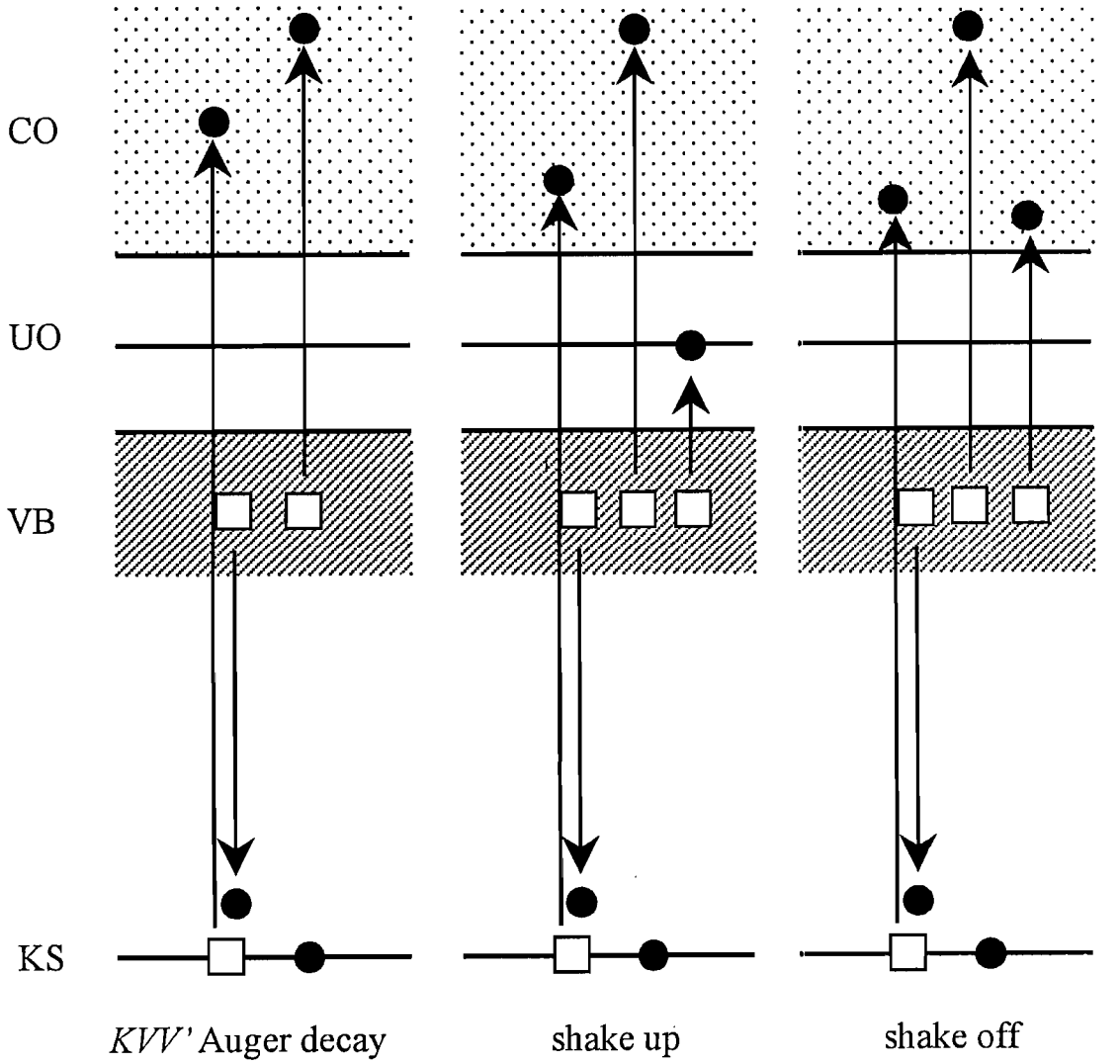

Figure 2-4. shake up and shake off processes

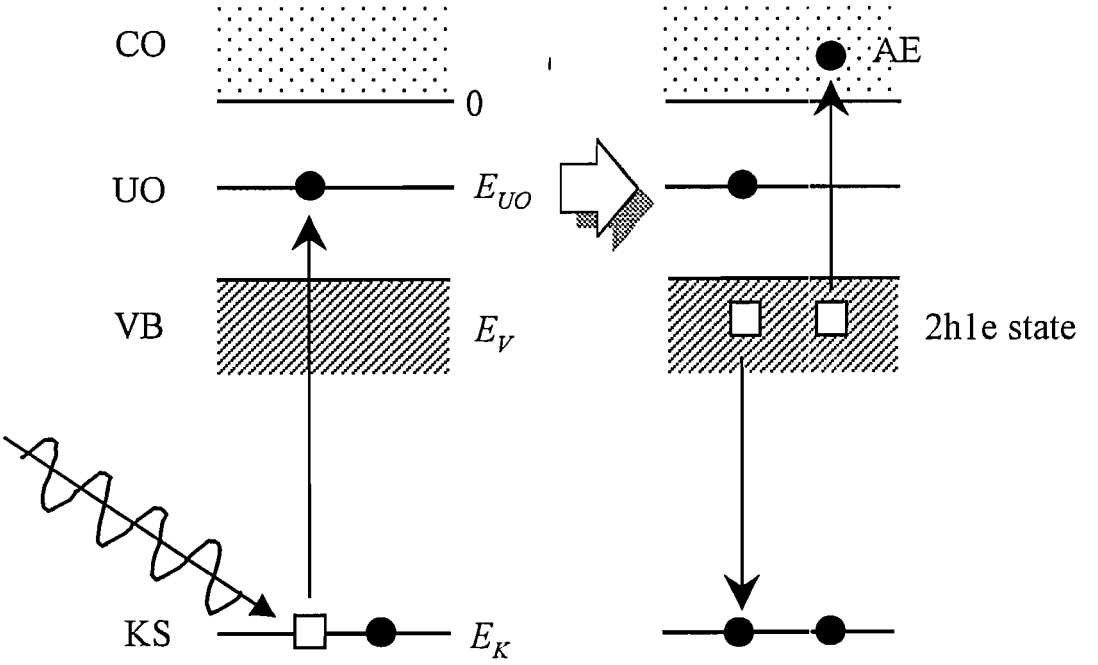

Figure 2-5. spectator Auger decay process

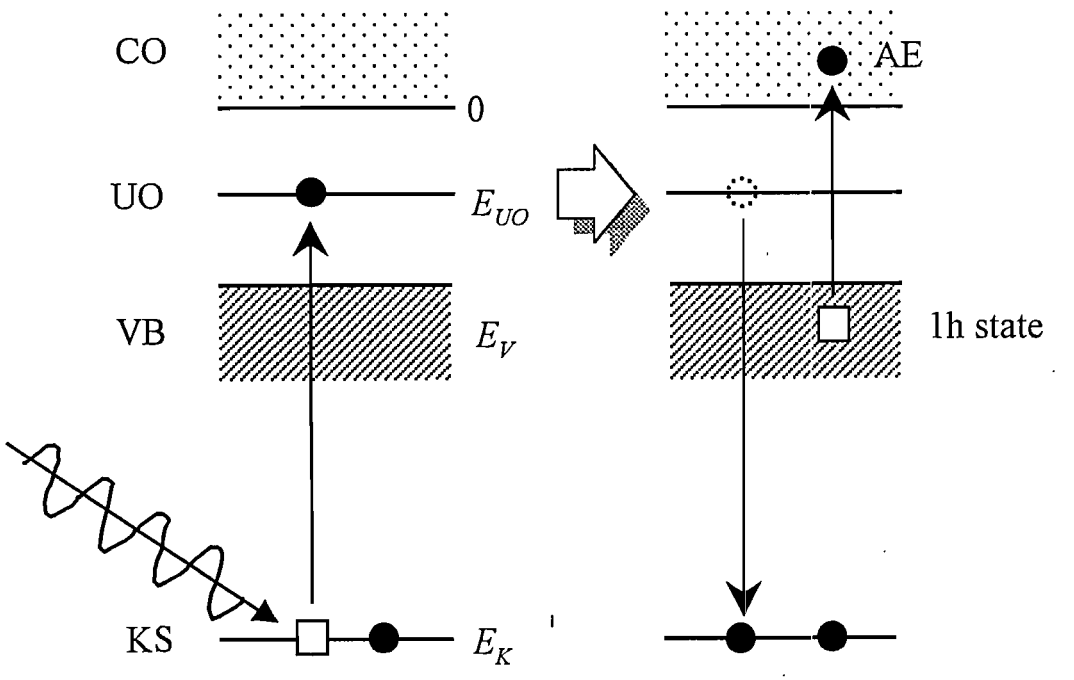

Figure 2-6. participant Auger decay process

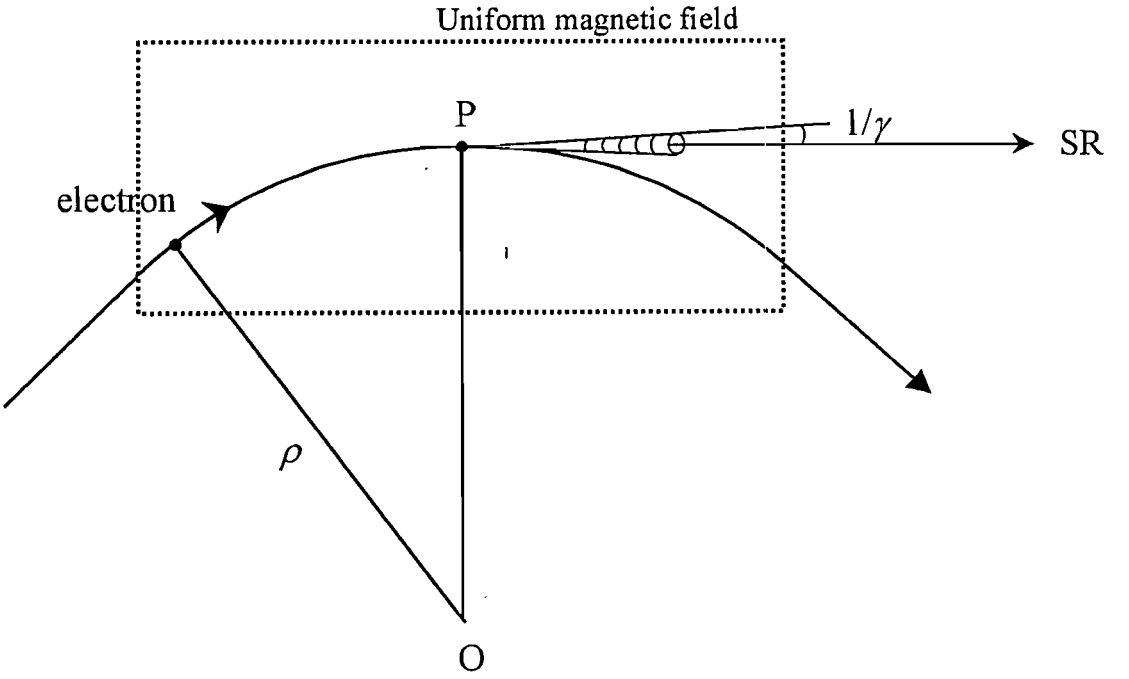

Figure 2-7. The principle diagram of Synchrotron radiation (SR).
ρ; orbital radius of electron, $\gamma = E / m_0 c^2$

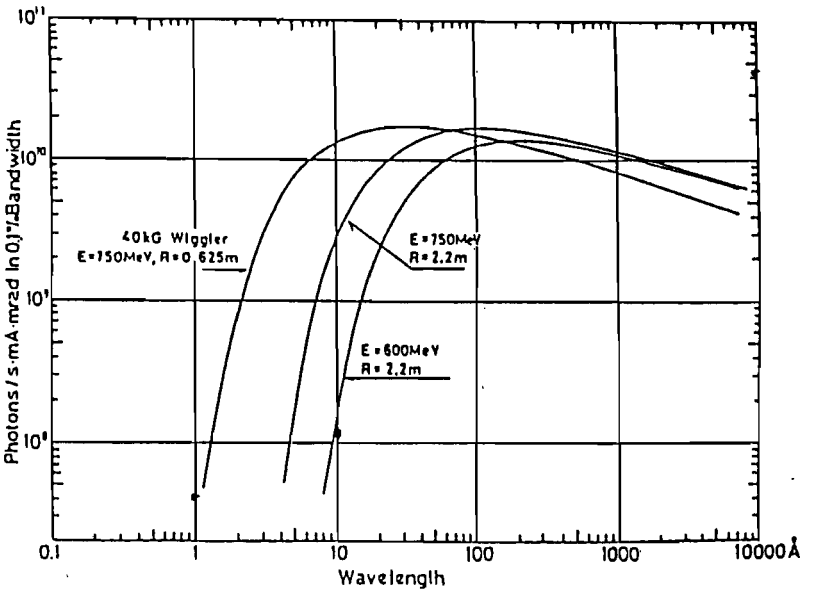

Figure 2-8. The intensity distribution of SR at UVSOR (Ref.[34])

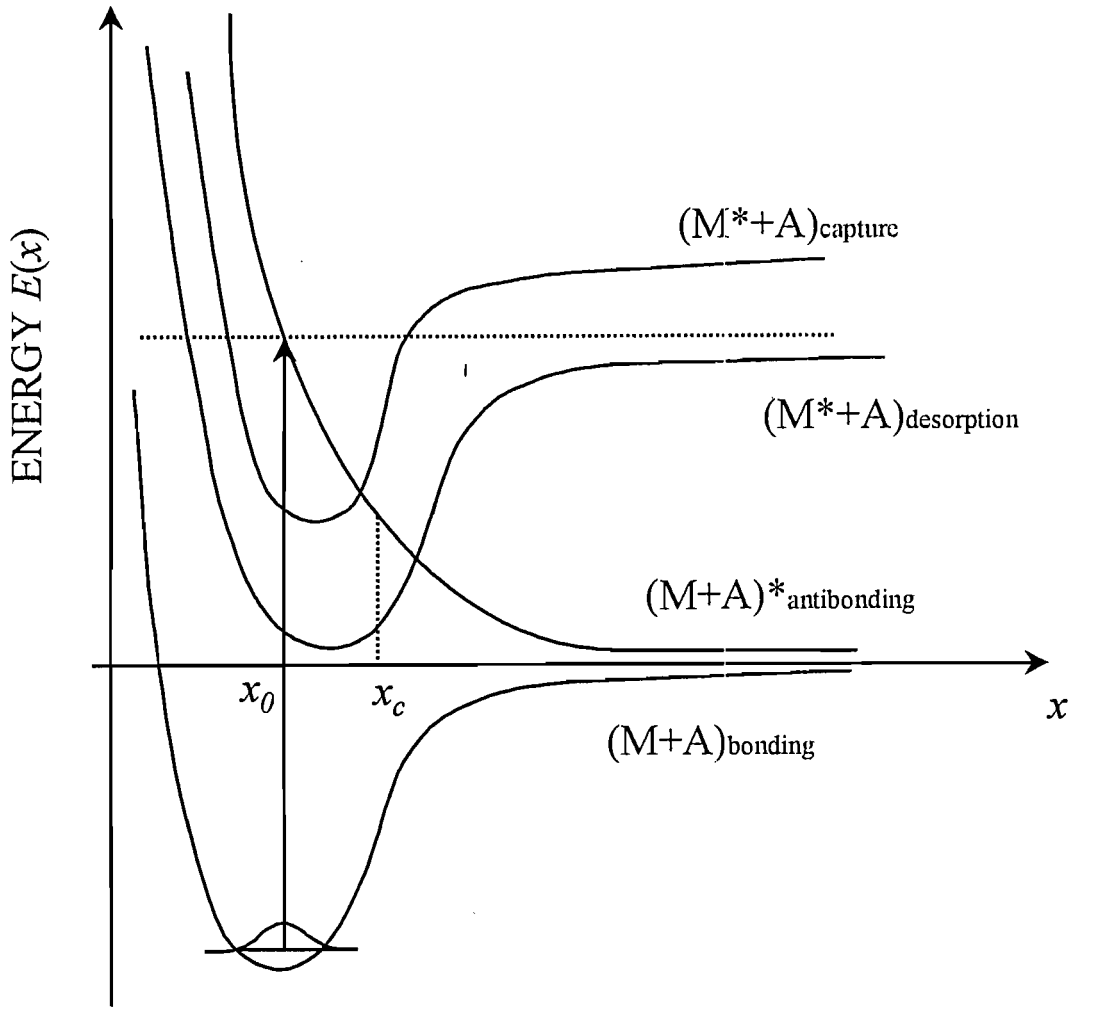

Figure 2-9. Potential energy diagram for the MGR model.
M: substrate, A: adsorbate, x_0: equilibrium distance, x_c: critical distance (Ref.[2])

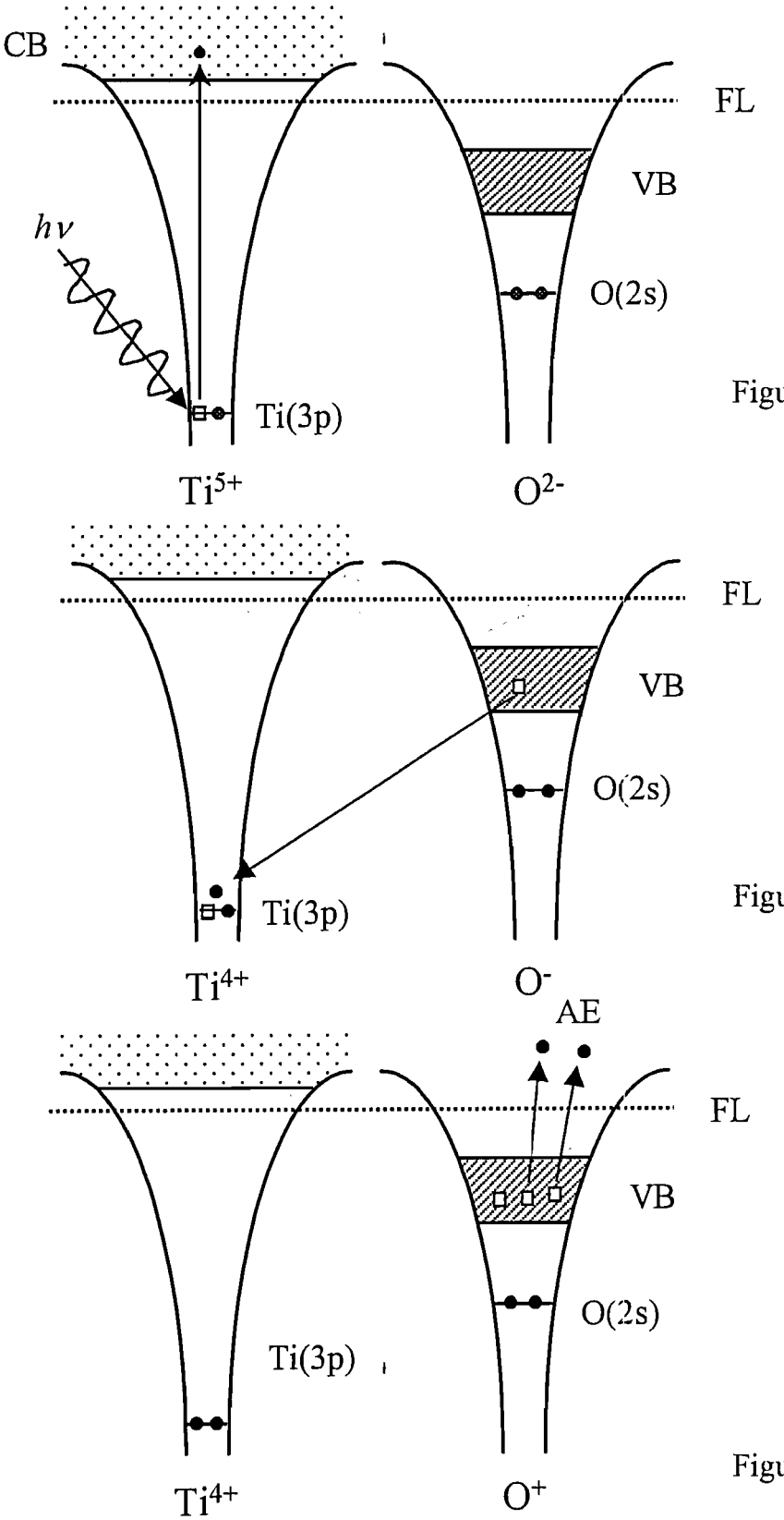

Figure 2-10. The schematic sequence for the KF model.
(a) Inner shell excitation of Ti 3p(b) Interatomic core decay
(c) Creation of multi-hole state in the O valence band
CB: conduction band, VB: valence band, FL: Felmi level,
AE: Auger electron. (Ref.[2])

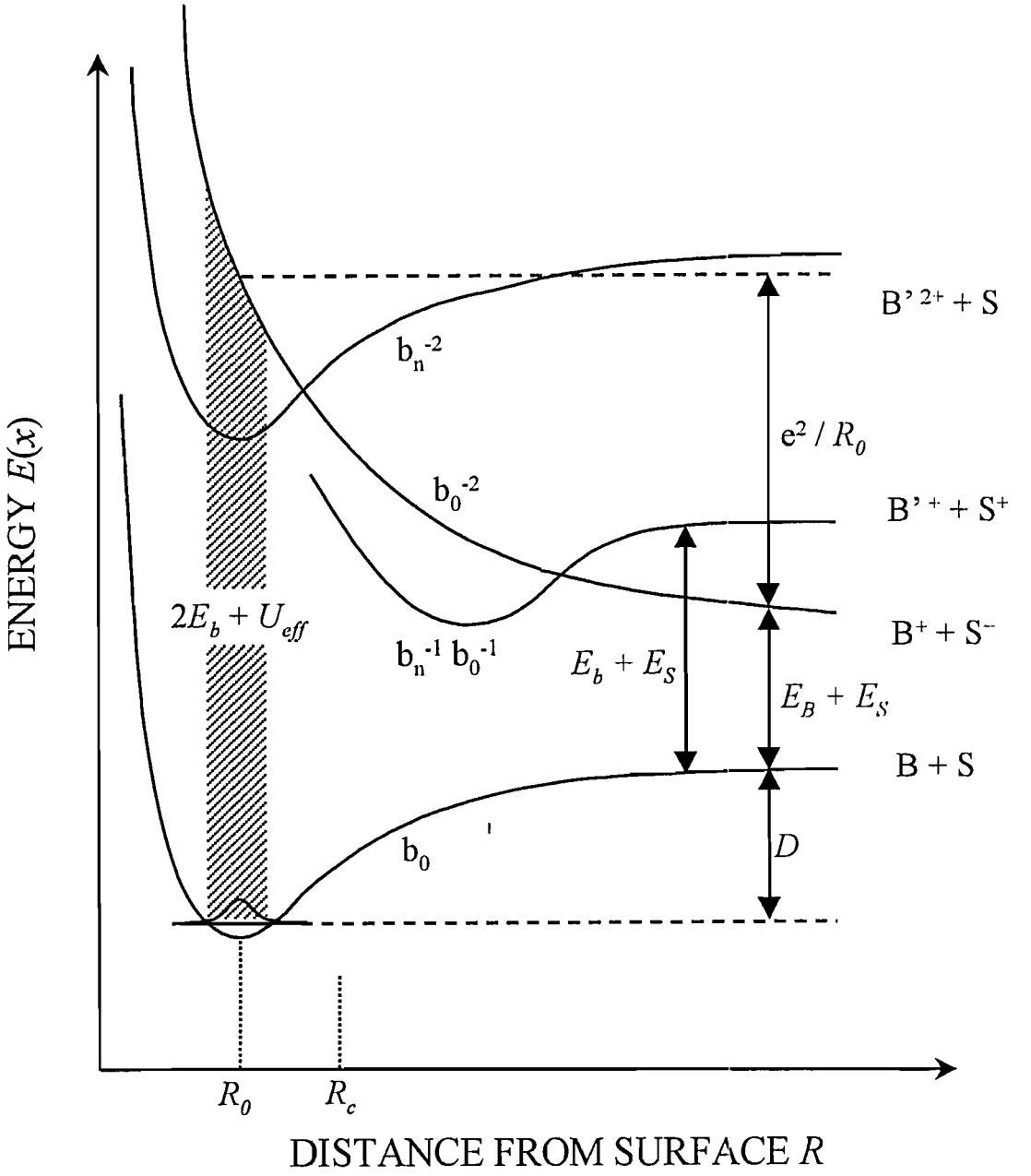

Figure 2-11. Schematic potential diagram for the ASD model.
B, B': bulk atom, S: surface atom, R_0: equilibrium distance, R_c: critical distance, b_0: ground bonding orbital, b_n, excited bonding orbital with two holes E_b: binding energy of b_0, U_{eff}: effective correlation energy, D: binding energy between B and S, E_B: energy difference between B and B^+, E_S: energy difference between S and S^+. (Ref.[42])

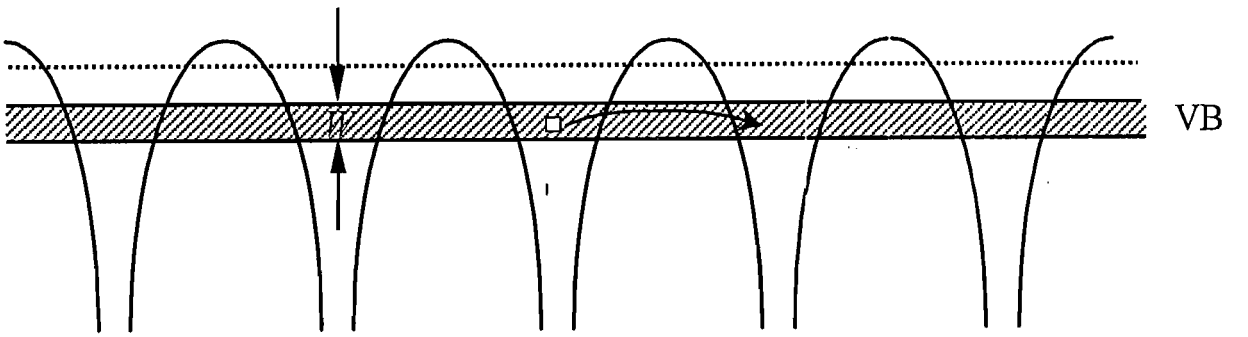

Figure 2-12-(a)

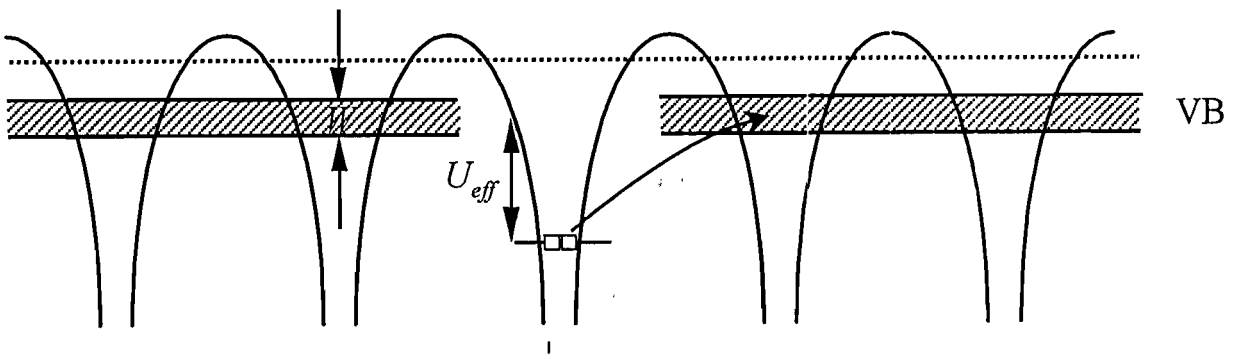

Figure 2-12-(b)

Figure 2-12. Schematic diagram of correlation between hole hopping time τ, effective correlation energy U_{eff}, and bandwidth W.
(a) Single valence hole moves with $\tau \approx 1/W$ (b) Two valence-hole state with $U_{eff} >$ W have one or two hole hopping times $\tau \gg 1/W$. (Ref.[2])

Ⅲ. Inner Shell Excitation Effect on Photon-stimulated Desorption of Condensed Benzene

In this chapter, I mention the inner shell excitation effect on photon-stimulated desorption (PSD) from benzene solid. First, experimental procedure and apparatus are discussed in section Ⅱ-1. Secondly, I show the results of near edge x-ray absorption fine structure (NEXAFS) and total ion yield spectra in section Ⅱ-2. Finally, inner shell excitation effect on desorption yield is discussed in section Ⅱ-3.

Ⅲ-1. Experimental procedure

Experiments were performed at the beamline BL-2B1 at the Ultraviolet Synchrotron Orbital Radiation Facility (UVSOR) of the Institute for Molecular Science, Okazaki, Japan. In this experiments, we measured Auger electron yield (AEY) spectra and total ion yield (TIY) spectra in an attempt to study H^+ desorption yield which reflects not only fundamental effects but also secondary effects. While, Auger electron photoion coincidence (AEPICO) spectra were measured in order to study H^+ desorption yield which reflects only fundamental effect. All apparatuses were constructed by Mase *et al.* [44]. The experiment was carried out in an ultra-high vacuum (UHV) chamber which is equipped with a coaxial cylindrical mirror analyzer (CMA), a time-of–flight mass spectrometer (TOF-MS), a sample introducing system and a cryostat. This chamber was connected to a beamline in which monochromatic soft x-ray is available. I describe details of the sample, beamline, and apparatus in following sections.

Ⅲ-1-(1) . **Sample**

Benzene (C_6H_6) sample was obtained from Aldrich Co. (HPLC grade 99.9%) and used without further purification. As a vessel for benzene, We prepared a 1/2 inch stainless tube of which one end of the tube was closed and the other end was attached with a 2/1-1/4 inch stainless union (Swagelok), a valve (NUPRO, SS-4H) and VCR connector. After evacuating air in the tube to 10^{-3} Pa with a turbo molecular pump (Varian V-60), We put liquid benzene into the tube.

Ⅲ-1-(2). **Beamline**

The most important component of this beamline is a 2-meter grasshopper monochromator (Mark X V, Baker Manufacturing Co.). Schematic diagram of this monochrometer is shown in figure 3-1. This monochrometer is based on Vodar geometry which has a constant angle α between the incidence light and normal to the grating (G) surface [45]. In the figure, a center C of Rowland circle rotates on an exit slit S_2 with an arm CS_2. The center C and an entrance slit S_1 are fixed with an arm CS_1. S_1 is codling slit which consists of a plane mirror and an one side edge mirror. G and S_1 are also fixed with the arm SG_1 with the angle α. With the horizontal motion of focusing mirror (FM), the codling slit S_1 rotates to remain the incidence angle α. In this type of monochrometer, since one can obtain a large diffraction angle β, it is applicable for an extreme grazing incidence ($\alpha \approx 90$ °). And a wide wavelength range can be covered from 600 Å (20 eV) to 15 Å (825 eV) with three gratings: 600 l/mm, 1200 l/mm, and 2400 l/mm.

We measured incident light intensity spectra I_0 with Au mesh current. Figure 3-2 shows the I_0 in the energy region from 200 eV to 500 eV. We obtained photon flux of $I_0 \approx 3 \times 10^9$ photons / sec with the resolution about 0.5 eV at $h\nu$ = 430 eV. The beam size at the sample position was about 4.5×9 mm^2.

Ⅲ-1-(3). **Apparatus**

• Coaxial Cylindrical Mirror Analyzer (CMA)

The kinetic energy of E_{Auger} has a distribution which depends on the binding energy E_B of electrons. E_{Auger} is independent of hv and analysis of the distribution of E_{Auger} gives us information of transition energy including a core orbital as described in the section Ⅱ-2-(1).

We used a coaxial cylindrical mirror analyzer (CMA) which is one of many types of electron analyzers utilizing electrostatic field in this experiment. Figure 3-3 shows the concept of such analyzer in the simplest case. An electron with the kinetic energy E_e draws a trajectory between two electrode plates which have potential difference V_D. Generally, E_0 is related to V_D by the following equation,

$$E_0 = CeV_D, \quad \cdots\cdots(3-1)$$

where C is a constant which is determined by the electrode form. When the kinetic energy of an electron is different from E_0, the electron doesn't enter at exit slit S_{ext}. Thus only the specific electron with energy E_0 can enter at exit slit by setting different voltage V_D. This is the principle of such electron analyzer. Figure 3-4 shows a schematic diagram of CMA of which the radii of inner and outer cylinder are R_1 and R_2. In this case, C is described as follows [46];

$$E_0 = \frac{eV_D}{\ln(R_2/R_1)}K, \quad \cdots\cdots(3-2)$$

where K is a constant which is determined by the incident angle α'. α' can take many different values. In the case of $\alpha' = 42°18'30''$, K becomes to be 1.31 and the trajectory of electron shows secondary convergence [46]. Since CMA has a collective solid angle (0.24 sr), it is more suitable than other electron analyzer for Auger electron spectroscopy. The construction of CMA used in this experiment is as follows. The CMA consists of a magnetic shield, semicylinders of 58-mm and 120-mm diameter, three sets of electrodes for maintaining a radial electric field, retarding grids, a cylindrical slit, and tandem micro channel plate (MCP). Most of the metallic parts of the CMA are made of SUS 316L, whose residual magnetism diminished through annealing.

Figure 3-5 shows the schematic diagram of apparatus. The voltage supplies for the CMA were controlled by a personal computer *via* a D-A converter board. Emitted electrons from sample are analyzed by CMA and detected by MCP (Hamamatsu Photonics, F4655). Electron signals were transformed to the negative NIM pulses via preamplifier (Phillips Scientific, 6954) and discriminator (Phillips Scientific, 6904, 300MHz). The NIM pules were counted by a counter (ORTEC, 996). All data was stored in personal computer (NEC, PC-9801FA). The Auger electron spectra (AES) and AEY spectra were measured by CMA.

Before measurement of Auger electrons of benzene, we measured photoelectron spectrum (PES) of Au foil with the photon energy $h\nu$ = 286.2 eV. Figure 3-6 shows the PES of Au foil. We obtained the binding energy E_B from the equation as follows;

$$E_B = h\nu - E_e - \phi, \quad \cdots\cdots (2-3)$$

where ϕ is work function; in the case of Au, ϕ = 5.1 eV [47]. As shown in Fig.3-6, Au 4*f* peak was measured near the binding energy E = 86 eV. The 4*f* peak consists of separate doublet states, *i.e.*, $4f_{5/2}$ and $4f_{7/2}$. The energy gap ΔE_B between the $4f_{5/2}$ and $4f_{7/2}$ states is about 3.7 eV. In this PES, the kinetic energy E_e of Au 4*f* peak was about 195 eV and we couldn't distinguish the two peaks. Thus we estimated the resolution $E/\Delta E$ of CMA was about 50.

• **Time-of–Flight Mass Spectrometer (TOF-MS)**

We used the time-of–flight mass spectrometer (TOF-MS) as an ion detector. TOF is an analysis technique used to identify ion of different masses and charge. Figure 3-5 shows the schematic diagram of TOF-MS. The TOF-MS consists of an electric field shield, a drift tube with an ion-extraction grid (T1), a 96-mm-drift tube (T2 and T3), a deflector, a focusing system, and MCP (Hamamatsu Photonics, F4655). The distance between a sample and T1 is 13 mm and the distance between T1 and T2 is 1 mm. A pair of conical electrodes are spot welded on both shield and T1 as a lens system. Ions desorbed from surface are collected into the drift tube by the lens system which has negative different voltage. The flight time T of an ion with mass M and charge q described as follows [48];

$$T \propto \sqrt{\frac{M}{q}}, \quad \cdots\cdots (3-4)$$

Using this relationship, the mass and charge of an ion can be identified from T. In this experiment, however, we used the TOF-MS as an only ion detector. Thus, we measured the counts of all kinds of ions desorbed from surface. Ion signals were transformed to the negative NIM pulses via preamplifier (Phillips Scientific, 6954) and discriminator (Phillips Scientific, 6908, 300MHz). The NIM pules were counted by the counter (ORTEC, 996). All data was stored in the personal computer (NEC, PC-9801FA). The ion detection efficiency was estimated to be about 0.4 [45].

• **Ultra high vacuum (UHV) chamber and sample introducing system**

Benzene sample cylinder was attached to the sample producing system equipped to the UHV chamber. The sample introducing system consists of stainless flexible tube and variable leak valve (VLV). The sample introducing system was evacuated by a turbo molecular pump and a rotary back pump. UHV chamber was evacuated by turbo molecular pumps, an ion pump, a Ti sublimation pump, and a rotary back pump. The base pressure of the UHV chamber was 3×10^{-8} Pa. Benzene thin film was formed on the Au substrate that was cooled at 80-100 K by liquid nitrogen. The temperature of the substrate was measured by W5%Re-Re26%W thermocouple. After pumping the UHV chamber and sample introducing system, we opened the valve of sample cylinder and filled stainless flexible tube with benzene gas of which vapor pressure is about 1×10^{4} Pa at room temperature. Next, opening the VLV, we introduced the benzene gas through the flexible tube to the UHV chamber. We exposed Au substrate to the benzene gas at the pressure of about 10^{-4} Pa for 100 s. On the basis of these conditions, we estimated the thickness of the benzene thin film was about 100 monolayers.

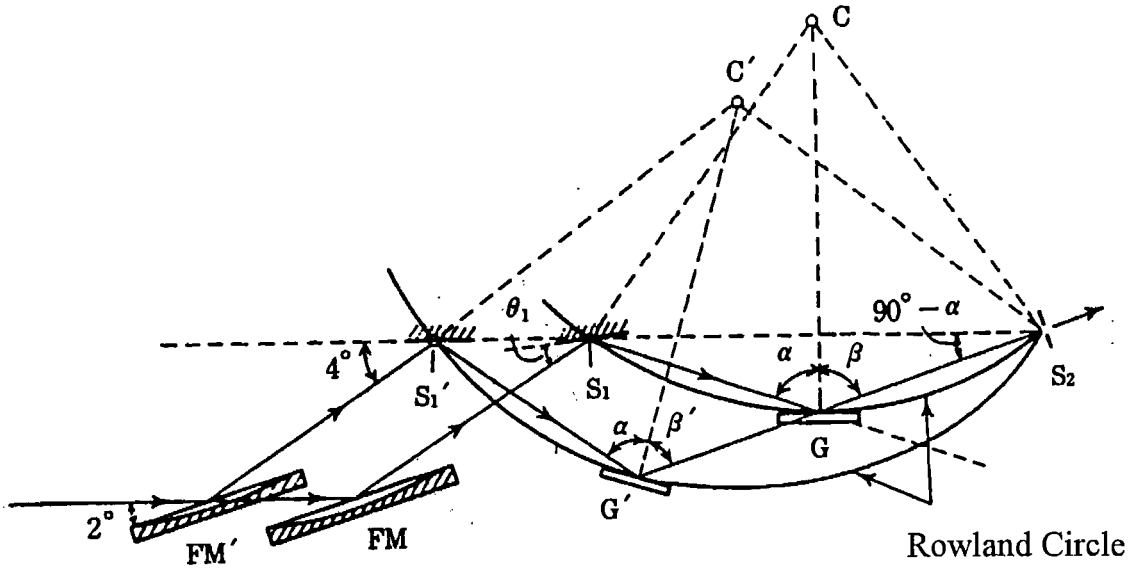

Figure 3-1. Schematic diagram of Grasshopper monochrometer
G, G': Grating, C, C': center of Rowland circle, S_1, S_1': entrance slit, S_2: exit slit, FM, FM': focusing mirror, α: incidence angle, β: diffraction angle. (Ref.[46])

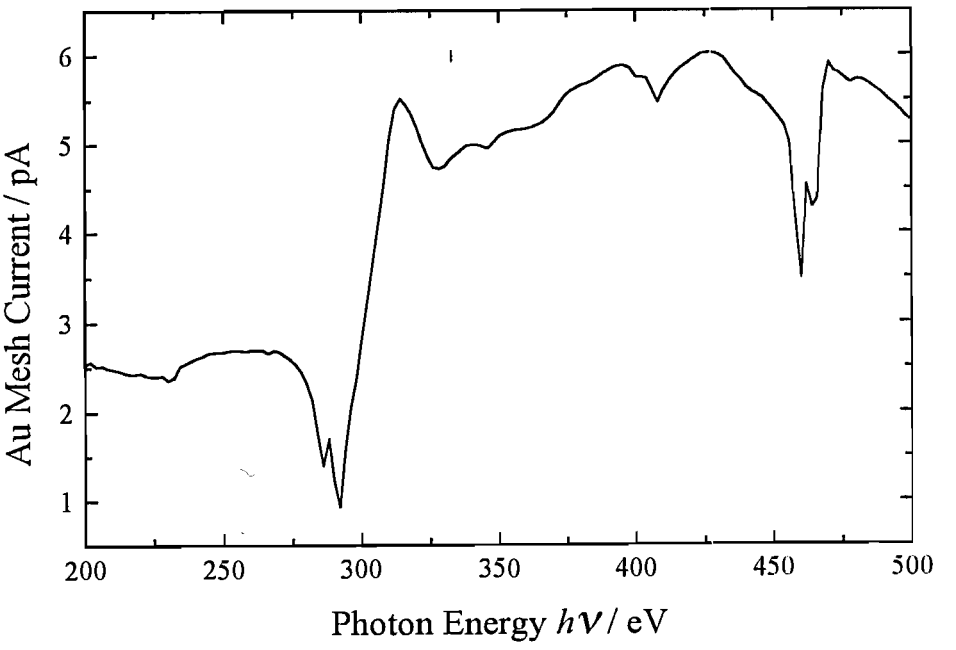

Figure 3-2. The incident light intensity spectrum of BL-2B1, UVSOR.

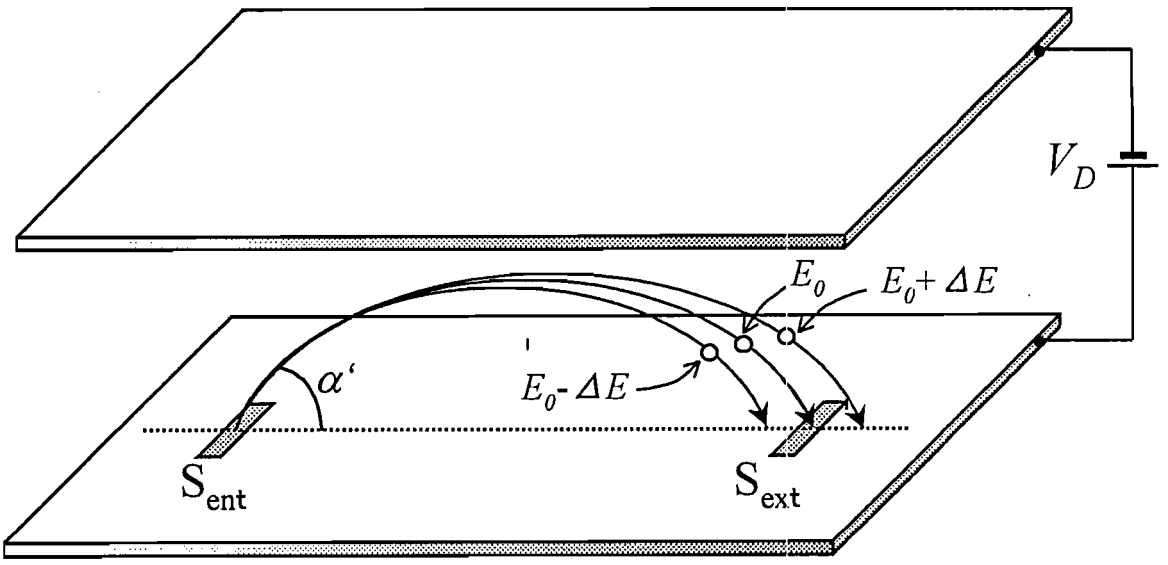

Figure 3-3. Schematic diagram of electron analyzer which uses electrostatic field. The trajectory of electrons which enter at the entrance slit S_{ent} with incident angle α' are bent by potential difference V_D between two electrode plates. Only electrons of which kinetic energy are E_0 can pass through the exit slit S_{ext}.

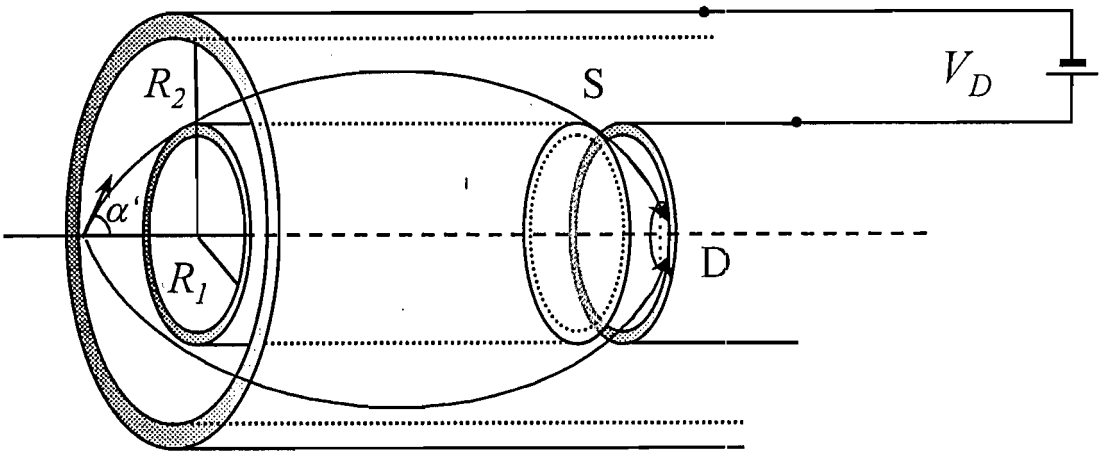

Figure 3-4. Schematic diagram of CMA

CMA has two coaxial cylinders of which radii are R_1 and R_2. In CMA, the first convergence does not depend on the incidence angle α'. Electrons are bent by potential difference between the coaxial cylinders. Only electrons which have specific kinetic energy can pass through slit S and can be detected by a detector D.

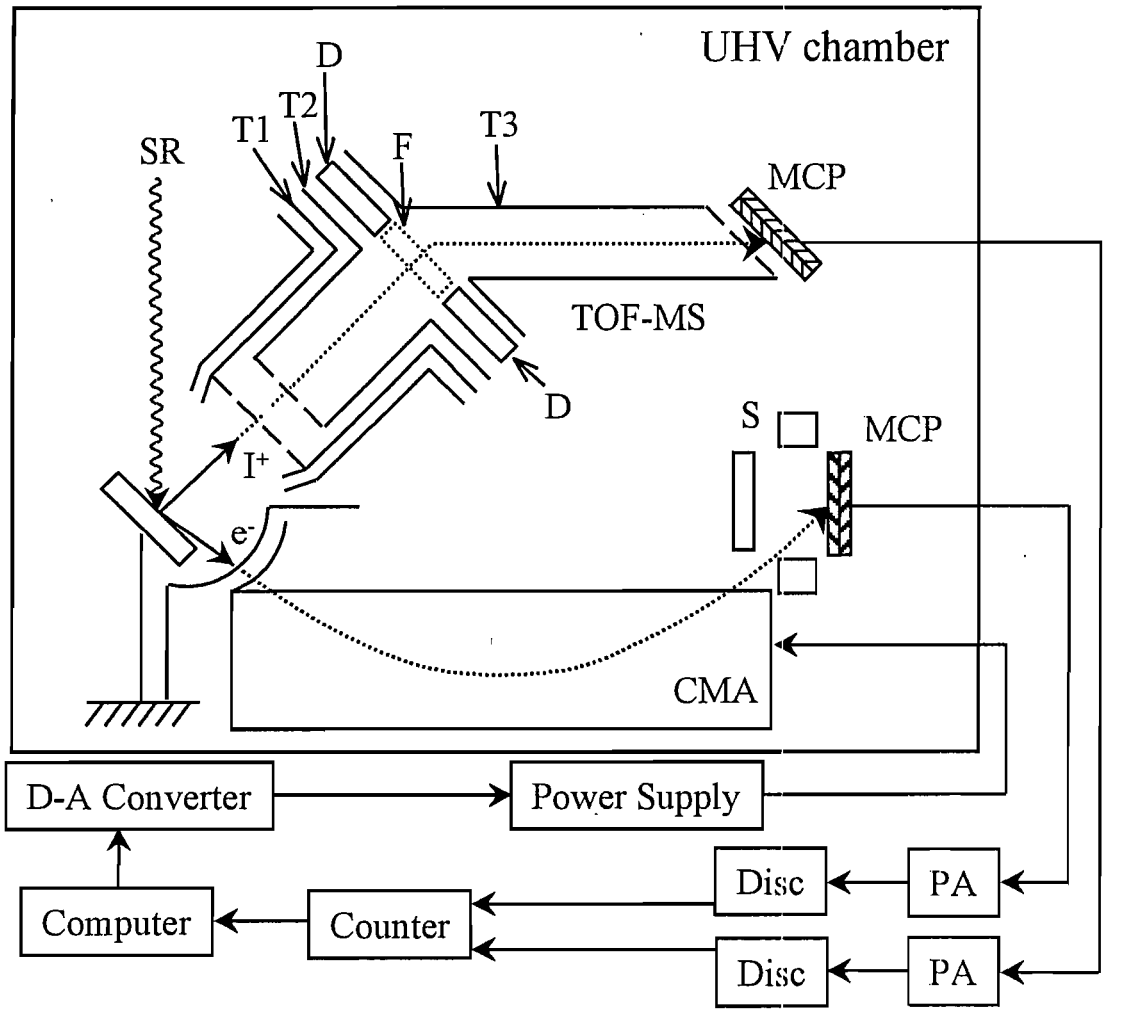

Figure 3-5. Schematic diagram of the apparatus.
PA: preamplifier, Disc: discriminator, T1: drift tube with an extraction grid T2 and T3: 95-mm-drift tube, F: focusing system, G: retarding grids, S: slit for CMA (see text for another abbreviations).
Emitted electrons (e^-) are analyzed by CMA and desorbed ions (I^+) are detected TOF-MS. (Ref.[44])

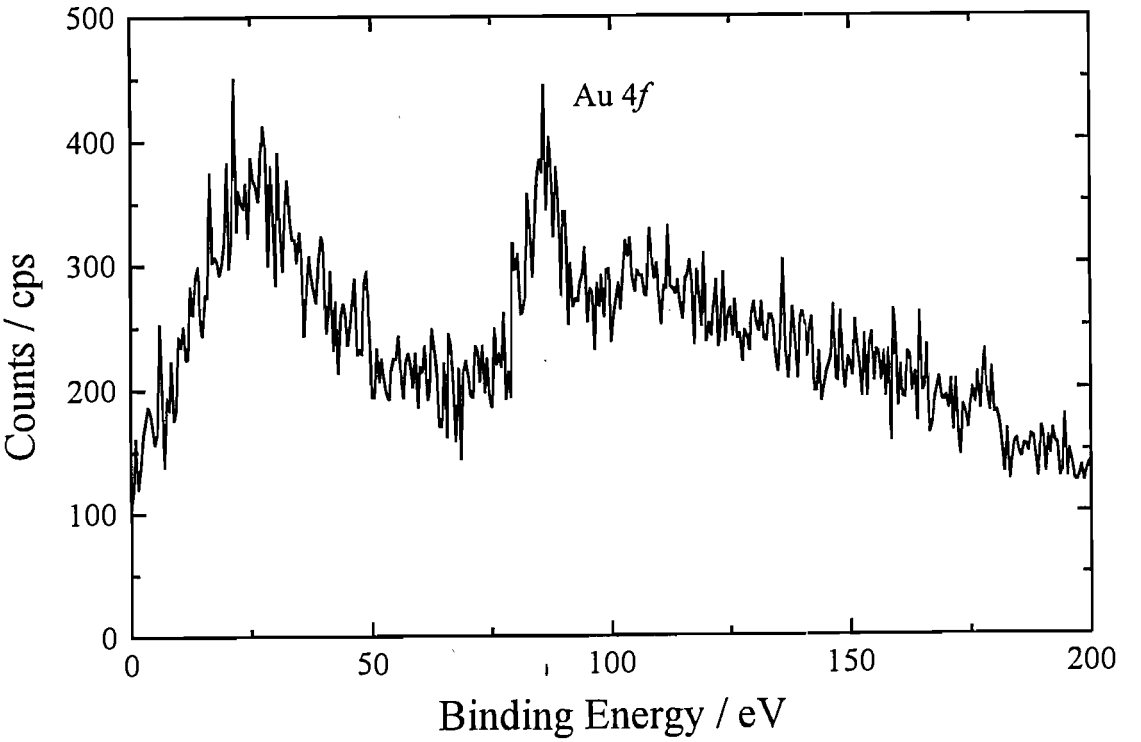

Figure 3-6. Photoelectron spectrum of Au foil.

Ⅲ-2. Auger electron yield spectra (AEY) and total ion yield spectra (TIY)

In this section, background knowledge and actual procedure for measurement of Auger electron yield (AEY) spectra and total ion yield (TIY) spectra are described. Firstly, I will mention about AEY. Secondly, I mention about TIY and show the result of calculation TIY/AEY. Comparing the previously reported calculation with our result, I discuss about the assignment of benzene NEXAFS. Finally, I show the excitation energy dependence of desorption yield and discuss about the physical meaning.

Ⅲ-2-(1). Auger electron yield (AEY) spectra

Auger electron yield (AEY) method is a technique to measure near edge X-ray absorption fine structure (NEXAFS). NEXAFS is known to reflect the transition probability from inner shell to unoccupied molecular orbital or conduction band. To measure NEXAFS, there are some technique; transmission method, electron yield method, fluorescence yield method, and reflection method. In all methods, the observed phenomena should reflect the absorption spectra. In this work, we used an electron yield method. The principle of this method is as follows. Electron yield γ is assumed to be in proportion to the absorbance of element near surface. Since the mean free path of incident photon is larger than that of electron, γ is related to absorption coefficient μ as follows;

$$\gamma \propto 1 - e^{-\mu L} \approx \mu L, \quad \cdots\cdots (3-5)$$

where L is surface depth. Thus γ is proportional to μL. As shown in figure 3-7, L depends on the kinetic energy E_e [49]. In the electron yield method, we can use three types of electrons; photoelectron, total electron, and Auger electron. When photoelectron is used for this method, one can study the difference of NEXAFS

of same atom due to chemical shift. However, there is a problem that L is not constant because the kinetic energy of photoelectron largely depends on $h\nu$. Thus, I didn't use photoelectron for this method. Next, let us consider the case that total electrons are used for this method. In total electron, the contribution of secondary electron and Auger electron are dominant. Since the secondary electron and Auger electron almost independent of $h\nu$, average value of L for total electrons are independent of $h\nu$. Consequently total electron yield (TEY) spectrum may reflect the absorption coefficient. However, there is a problem. Since benzene solid is insulator, there is a possibility that positive charge concentrates near surface. This phenomenon is called as "charge up" phenomenon. It is thought that secondary electrons having small kinetic energy largely affected by charge up. Thus we did not use total electron yield but partial electron yield method. Partial electron yield method is a technique to detect only electrons which has a kinetic energy. Since Auger electron is independent of $h\nu$ and can have high kinetic energy, we adopted Auger electron for NEXAFS in this experiment.

In this experiment, we irradiated benzene thin film with monochromatic soft X-ray at an angle of 60° to the normal benzene surface. The emitted electrons were detected and analyzed by CMA. The desorbed ions were detected by TOF-MS. At first, we measured Auger electron spectrum (AES) of benzene to determine the kinetic energy for AEY. Figure 3-8 shows AES in the case of normal Auger decay ($h\nu$ = 430 eV) in the energy region $0 \leqq E_e \leqq 400$ eV. Most intense peak at E_e = 140 eV is assigned to carbon K-photoelectron. The satellite peak beside the K-photoelectron peak is attributed to Auger shake up process because the electrons emitted *via* Auger shake up process show a discrete satellite peak as described in the section II–2-(1). While, the electrons emitted *via* Auger shake off process show a continuous structure in the low energy side of Auger shake up satellite peak. Therefore, the broad structure lying below the shake up peak is considered to attribute to Auger shake off process. The peak at $E_e \approx 340$ eV is assigned to $4f$ photoelectron of Au which is the substrate. The broad structure near 260 eV is produced *via* KVV' normal Auger decay process. Curves **A**, **B**, and **C** in the figure 3-9 show the AES for excitation energies $h\nu$ =

430 eV, 287 eV, and 285 eV, respectively. The photon energies of $h\nu$ = 287 and 285 eV correspond to the excitation energies which cause resonant Auger decay as described below. All spectra have a similar feature which has broad peak near E_e = 260 eV except the small peak near E_e = 287 eV in the curve **B**. The small peak is attributed to the carbon *K*-photoelectron which is excited by second-order light of SR. I can find that the peak energies of curve **B** and **C** are 5 ~ 8 eV higher than that of curve **A**. It is thought that this phenomenon was caused by PCI described in section Ⅱ-2-(2). Although I find a little difference in spectra **A**, **B**, and **C** each other, we measured Auger electron yield spectrum at the E_{Auger} = 260 eV because most intense peak lied near E_e = 260 eV in the all AES. I convinced that this broad structure was not affected by the extraction potential difference of TOF-MS.

Curve **A** in figure 3-10 shows the AEY spectrum in the energy region in energy region 280 < $h\nu$ < 305 eV. At this resolution, there are 6 resonances, labeled **a-f**. The obtained AEY is similar with that previously reported by Menzel *et al.* [50]. The hatched line shows the ionization potential I_P, of which value was reported to be 290.5 eV [51]. However, Menzel *et al.* [50] adopted about 1.5 eV lower energy as I_P in solid benzene, because ionization potential is shifted by polarization energy of medium around the photo absorbed molecule. Menzel *et al.* estimated the energy shift from the shift of X-ray photoelectron spectroscopy (XPS) [52]. They called this I_P as outer continuum limit. The energy I_P corresponds to the bottom energy of conduction band.

Many assignments of benzene NEXAFS have been reported, which are shown in the table 3-1. Inner shell electron energy loss spectrum (ISEELS) of gaseous benzene was measured in the energy region 280 ≦ $h\nu$ ≦ 340 eV by Hitchcock *et al.* [53]. They tentatively assigned all features as follows. A lowest intense peak was assigned to $\pi^* \leftarrow 1s$. Another features lied at 287.2, 288.0, 288.6, and 288.9 eV were assigned to Rydberg states, *e.g.*, $3s \leftarrow 1s$, $3p \leftarrow 1s$, $3d \leftarrow 1s$, and $4s$ and $4p \leftarrow 1s$, respectively. Another features lied above ionization potential (I_P = 290.3 eV) were assigned to shake up transitions. Though some differences were observed between the ISEELS and our AEY

spectrum, the outline was similar. This result indicates that the molecular nature of benzene is maintained in benzene solid. Since benzene molecules were combined by van der Waals force in solid state, benzene molecular orbital (MO) localized in the vicinity of the molecule is not largely affected by surrounding molecules. It is thought that the little differences are owing to the difference of excitation source, *i.e.*, electron and photon. In the case of photon excitation, the transition between the Rydberg states which has the same principal quantum number is forbidden. While in the case of electron excitation, however, such transition is allowed. Thus it is thought that the optically forbidden transitions were observed in ISEELS. Horsley *et al.* [51] measured ISEELS of gaseous benzene and NEXAFS of condensed (solid) benzene. Both spectra are similar to our AEY spectrum. They also measured the NEXAFS of chemisorbed monolayer benzene on Pt(111) surface with perpendicular and grazing X-ray incidence. The NEXAFS of chemisorbed benzene showed an apparently polarization dependence; the perpendicular NEXAFS showed clear two peaks that match with the positions at the photon energies 293.3 and 299.9 eV. While, grazing NEXAFS showed a clear peak at 286 eV. It is known that the NEXAFS of molecules adsorbed on surface show the polarization dependence [54, 55]. The π^* resonance dominate at grazing incidence and the σ^* resonance dominate at normal incidence, because the π^* resonance was seen when the electric field vector E of SR is perpendicular to the plane of the benzene ring and σ^* resonance was seen when the E is in the plane of the benzene ring. Thus they assigned the two peaks lied at 293.3 and 299.9 eV to σ^* resonance. Furthermore, they carried out multiple scattering (MS) $X\alpha$ calculations and assigned the features in the NEXAFS of benzene solid. They assigned first two resonances lied at 285.0, 288.9, 293.3, and 299.9 eV to the transitions $\pi^*(e_{2u}) \leftarrow 1s$ and $\pi^*(b_{2g}) \leftarrow 1s$, $\sigma^*(e_{1u}) \leftarrow 1s$, and $\sigma^*(e_{2g})$ and $\sigma^*(a_{2g}) \leftarrow 1s$, respectively. A weak feature lied at 287.2 eV in ISEELS was assigned to a $3p \leftarrow 1s$. Schwarz *et al.* [56] pointed out the contradiction of assignments by different calculations, *i.e.*, Xα [51], HAM/3 [57], and EIC [58]. Thus they calculated taking symmetry breaking into account. Benzene has D_{6h} symmetry. However, the symmetry of core excited benzene

changes from D_{6h} to C_{2v}. This is called as symmetry breaking. Moreover, several equivalent cores give a correlation effects due to several quasidegenerate canonical core orbitals. This effect, physically, emerges polarization of valence shell by an oscillating localized core hole exciton [59, 60, 61]. In addition to this effect, it is also necessary to take different relaxation of the singly occupied core shells into account. Such characteristic for core-excited states of molecules with multi equivalent cores was also taken into account to their calculation. They calculated the term value and energy of each state by *ab initio* self consistent field (SCF) equivalent ionic core virtual orbital model (EICVOM), broken symmetry individual SCF method (ΔSCF), symmetry adapted muticonfiguration SCF method (ΔMC SCF), g-Hartree method. They assigned the lowest intense peak to the transition $\pi^*(e_{2u}) \leftarrow 1s$. This MO consists of two vibrational states; $\pi^*(e_{2u}/b_1)$ and $\pi^*(e_{2u}/a_2)$. The $\pi^*(e_{2u}/b_1) \leftarrow 1s$ transition is optically allowed under C_{2v} symmetry, while, $\pi^*(e_{2u}/a_2) \leftarrow 1s$ transition is allowed only by magnetic dipole and electric quadrupole excitation. Therefore, the magnitude of $\pi^*(e_{2u}/b_1) \leftarrow 1s$ transition is much larger than that of $\pi^*(e_{2u}/a_2) \leftarrow 1s$ transition. Though the peak splitting due to this two transition was experimentally observed by Akimov [62] and Aminpirooz [63], we could not observe such splitting in our NEXAFS. This result seems to be attributed to the difference of resolution between our experiment and the other's. Peaks observed at 2 and 2.8 eV higher than $\pi^*(e_{2u})$ in ISEELS were assigned to $3s \leftarrow 1s$ and $3p \leftarrow 1s$ Rydberg transition, respectively. Schwarz *et al.* mentioned that the intensity ratio $3s/3p \leftarrow 1s$ seems unusual. They explained this phenomenon with two reasons. First, the penetrating $3s$ Rydberg orbital has significant $2p_y\sigma^*$(C-H) admixture at the $1s$-excited carbon atom. Such orbital is called as of $3s$-σ^* Rydberg valence mixed orbital. Second, strong cancellations occur in the $3p \leftarrow 1s$ transition matrix element. And they proposed the $3p$ orbital has s and d admixtures; $3d$, $4s$, and $4p$. While, the lower peak was not observed in our NEXAFS. Thus the second feature labeled **b** was thought to be assigned to $3p \leftarrow 1s$ Rydberg transition. However, Menzel *et al.* [50] concluded that this feature consists of not only $3p \leftarrow 1s$ Rydberg transition from a reason discussed below. According to their

calculation, there does not exist any state with dominant the $\pi^*(b_{2g}) \leftarrow 1s$ character. This indicates that one-electron picture is not available. Thus the peak labeled **c** was assigned to admixture $\pi^*(b_{2g}) \leftarrow 1s$ transition and shake up transition from the HOMO ($\pi^*(e_{1g})$) to give doubly occupied $\pi^*(e_{2u})$.

Ⅲ-2-(2). **Total ion yield (TIY) spectra**

Curves **B** in Fig.3-10 shows the total ion yield (TIY) spectra in the energy region $280 < h\nu < 305$ eV. Desorbed total ion species include many kinds of fragment ions. I show the TOF spectra carried out in another experiment [64] in the figure 3-11. Besides the dominant H^+ ion (peak **E**), we can also find CH_2^+ (peak **F**), $C_2H_i^+$ series (i = 1 ~ 6) (peak **C**), $C_3H_j^+$ series (j = 1 ~ 8) (peak **D**), and $C_4H_k^+$ series (k = 1 ~ 10) (peak **A**) ions. However, the intensities of desorbed ion species are quite different. I show the partial ion yield (PIY) spectra of H^+ (curve **E**), CH_2^+ (curve **C**), $C_2H_i^+$ series (curve **F**), $C_3H_j^+$ (curve **D**) series, and $C_4H_l^+$ (curve **A**) series in figure 3-12. As shown in Fig.3-12, the intensity of PIY except H^+ is 150 ~ 700 times less than the H^+ ion yield spectrum. Therefore, I regarded the TIY spectrum as a H^+ ion yield spectrum because the TOF mass spectrum of benzene thin film showed almost only H^+ ion signal. TIY spectrum shows similar tendency with AEY spectrum. This result means that TIY spectra are influenced by absorption spectra. However, there are little differences between TIY and AEY. To compare the differences, I show the result of calculation of TIY/AEY (curve **C**) in Fig.3-10. This TIY/AEY spectrum reflects the H^+ desorption yield spectrum per one photon absorbed. In the curve, one can find a clear dip at 285 eV and a peak at 287 eV, respectively. The peak at 287 eV was reported by Menzel *et al.* [50] previously to mean that the Auger initial state at this excitation energy causes strong H^+ desorption. They called this peak as X_D peak and proposed that the excitation at X_D involves a excitation to strong C-D anti-

bonding state. Moreover, the enhancement of TIY/AEY at the peak **d** also was assigned to C-D anti-bonding state. While, they didn't report the dip at 285 eV. This dip means the excitation $\pi^*(e_{2u}) \leftarrow 1s$ suppressed H^+ desorption yield. Figure 3-13 shows AEY, TIY, and TIY/AEY in the wide energy region $275 < h\nu < 460$ eV corresponding to curve **A**, **B**, and **C**, respectively. As same as Fig. 3-10, curve **A** is similar to curve **B** in this figure. However, TIY/AEY increases as $h\nu$ becomes larger. I summarize the intensity rate of TIY/AEY in table 3-2.

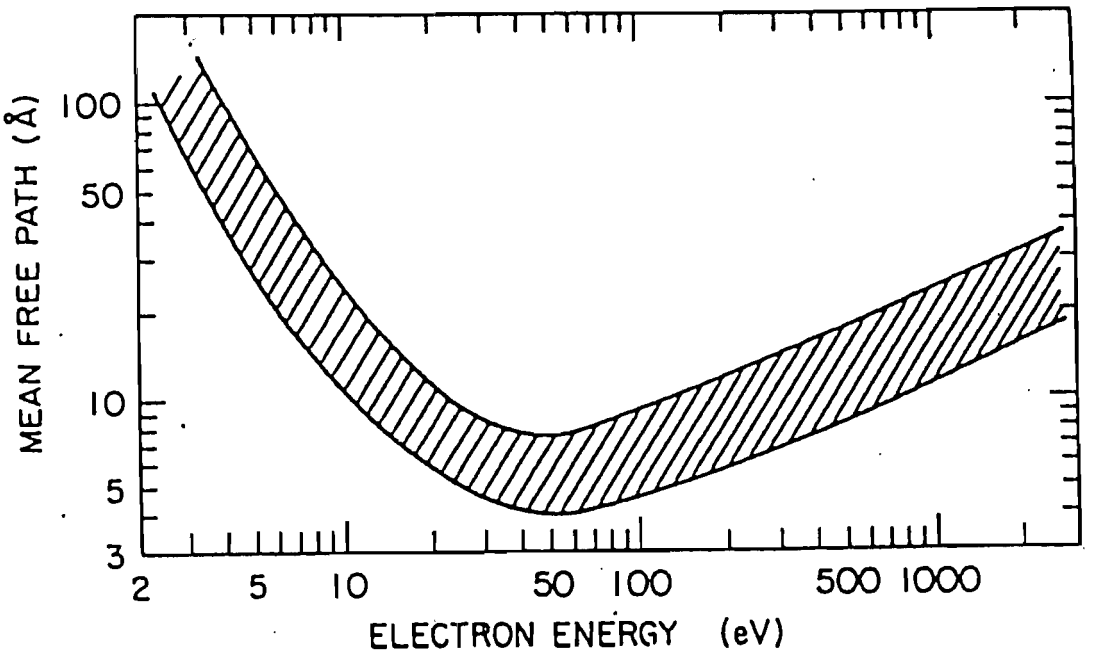

Figure 3-7. The mean free path of secondary electrons in solid [49].

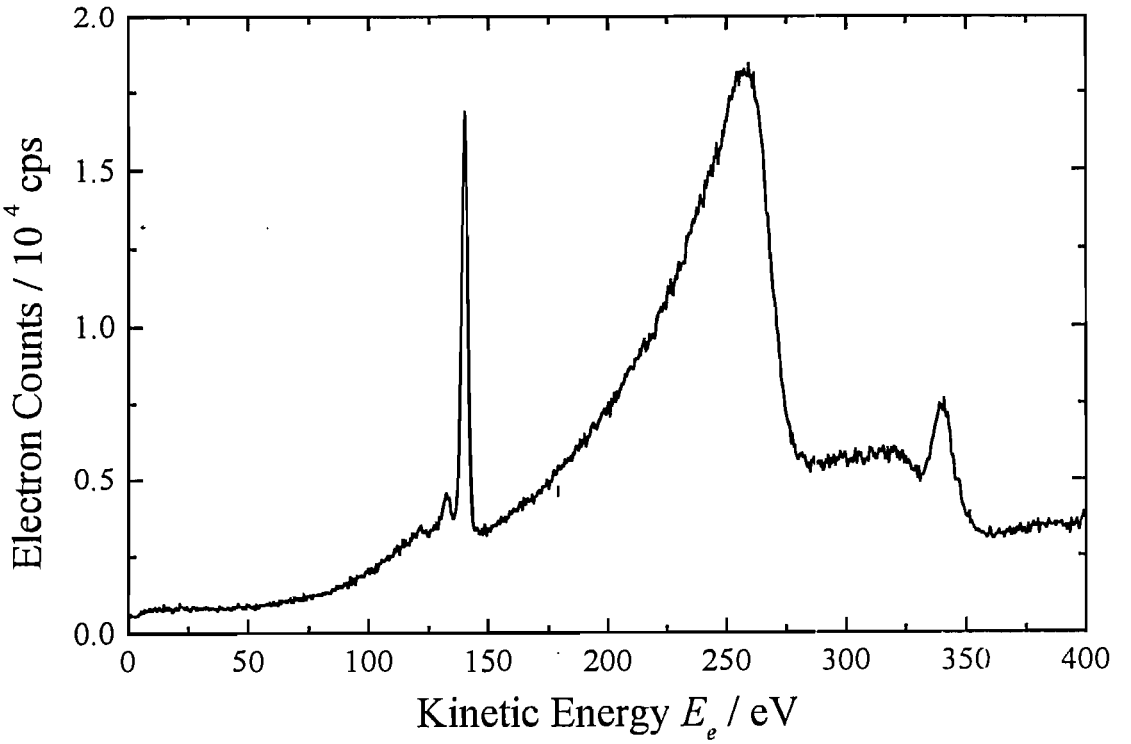

Figure 3-8. Auger electron spectrum of condensed benzene for excitation energy $h\nu = 430$ eV. See text in detail.

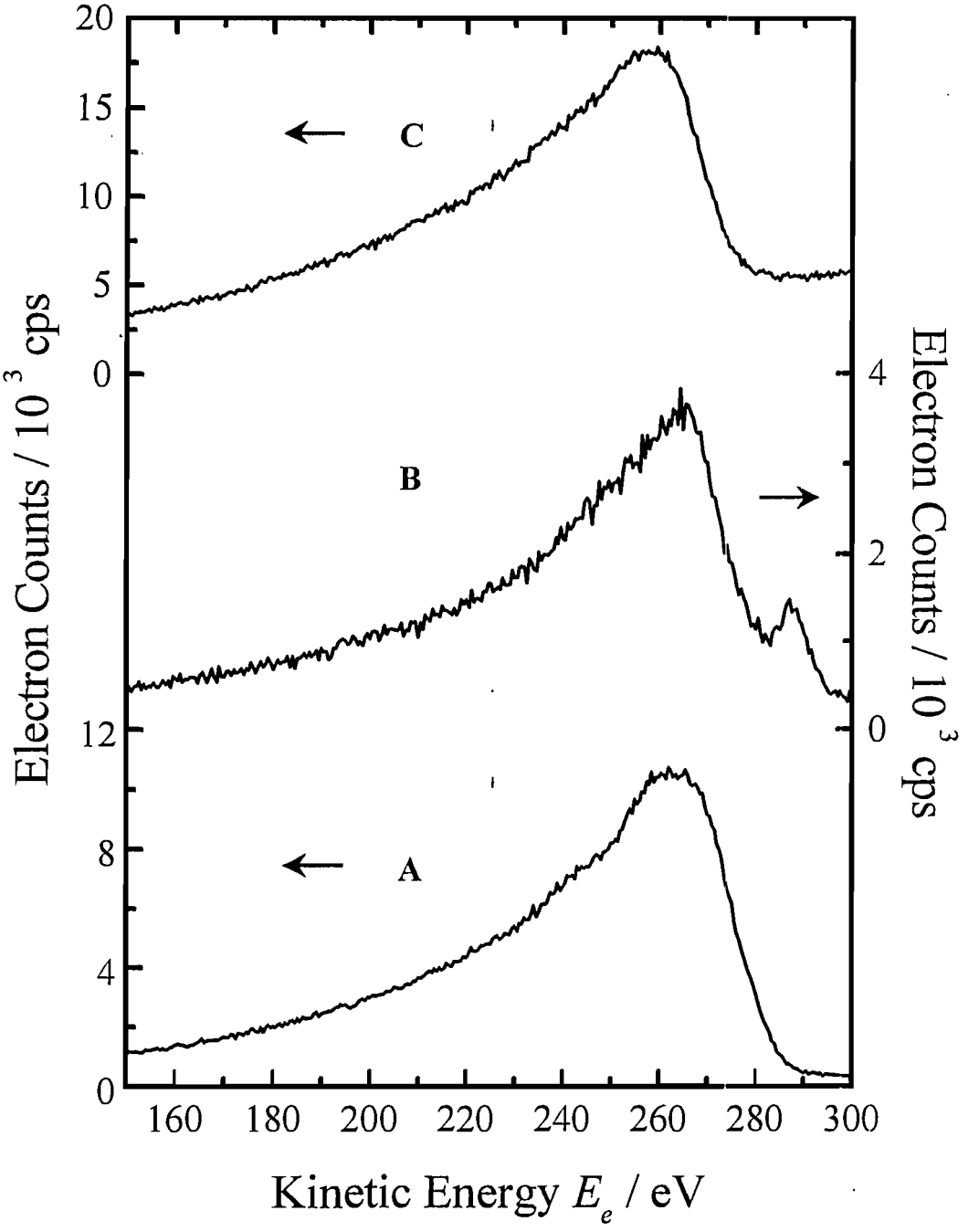

Figure 3-9. Auger electron spectrum of condensed benzene.
A: $h\nu$ = 285 eV, **B**: $h\nu$ = 287 eV, **C**: $h\nu$ = 430 eV

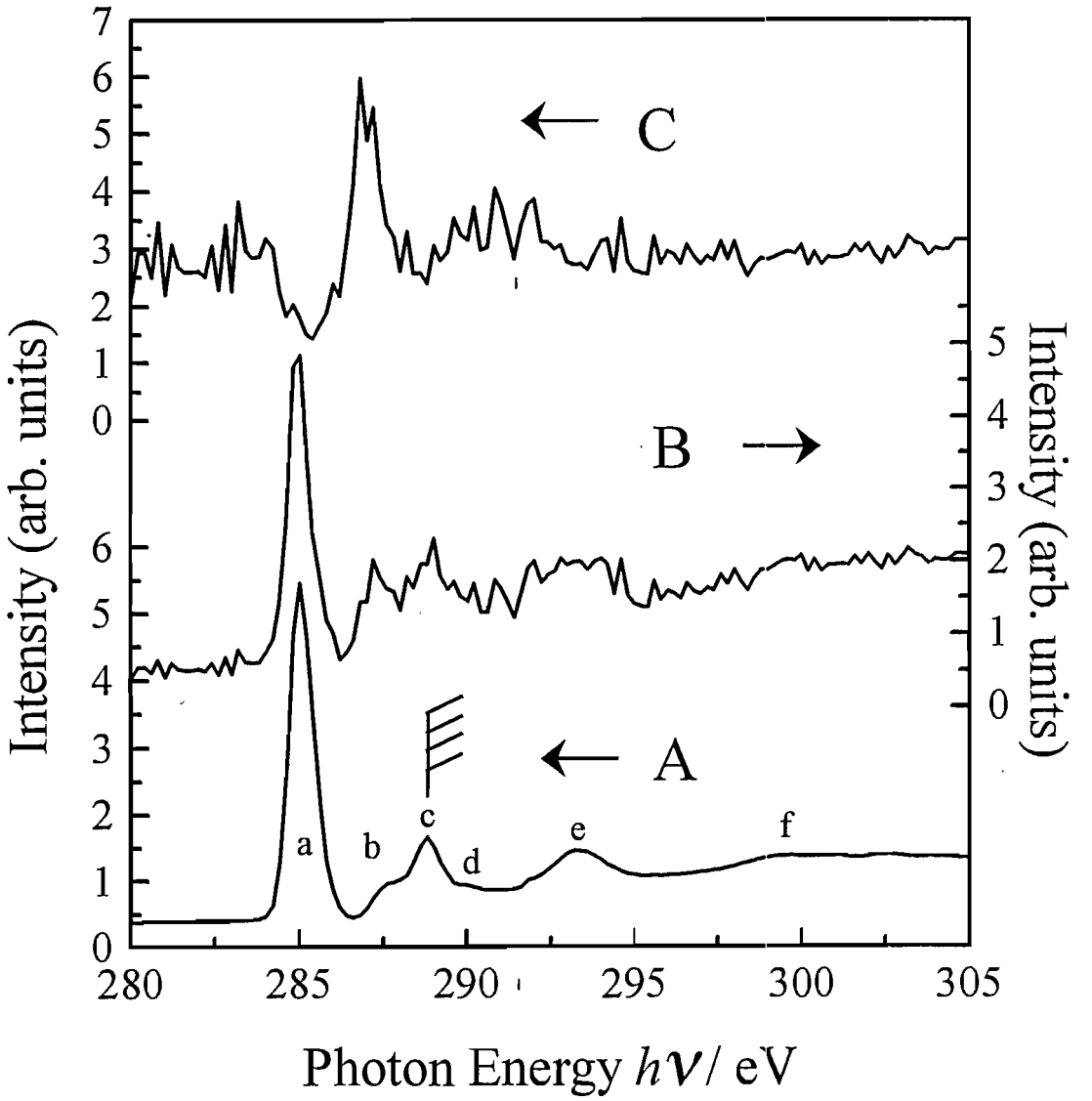

Figure 3-10. Auger electron yield (AEY) spectrum (**A**); total ion yield (TIY) spectrum (**B**); TIY/AEY spectrum (**C**). AEY spectrum was measured detecting Auger electron of which kinetic energy is 260 eV. The hatched line shows ionization potential reported in Ref.[50].

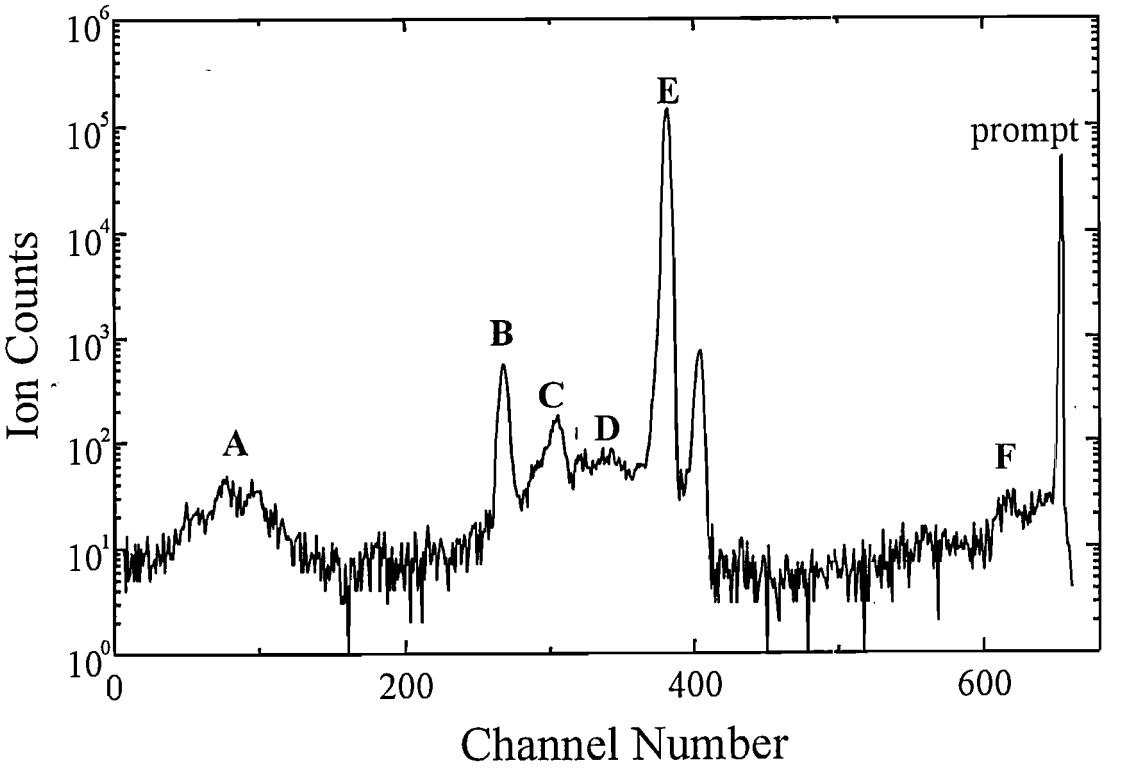

Figure 3-11. Time of Flight (TOF) spectrum of condensed benzene for excitation energy $h\nu = 380$ eV. **A**: $C_4H_k^+$, **B**: D^+, **C**: CH_2^+, **D**: $C_3H_j^+$, **E**: H^+, **F**: $C_2H_i^+$. The non-labeled peak besides peak **E** is "ghost peak" due to electron. The "prompt" peak is due to SR pulse. D^+ is contamination signal from an experiment using C_6D_6.

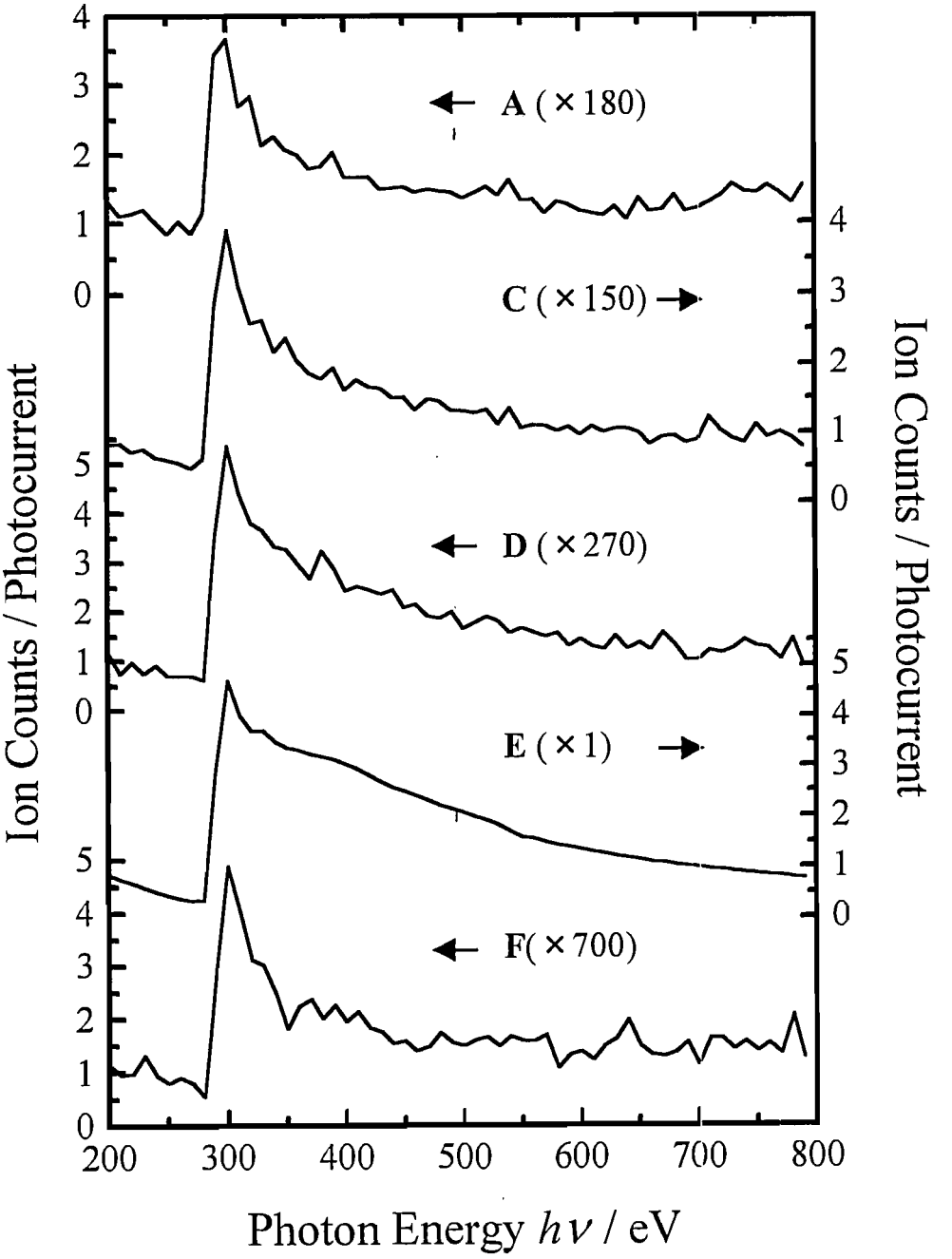

Figure 3-12. Partial ion yield (PIY) spectrum of condensed benzene.
A: $C_4H_k^+$, **C**: CH_2^+, **D**: $C_3H_j^+$, **E**: H^+, **F**: $C_2H_i^+$.

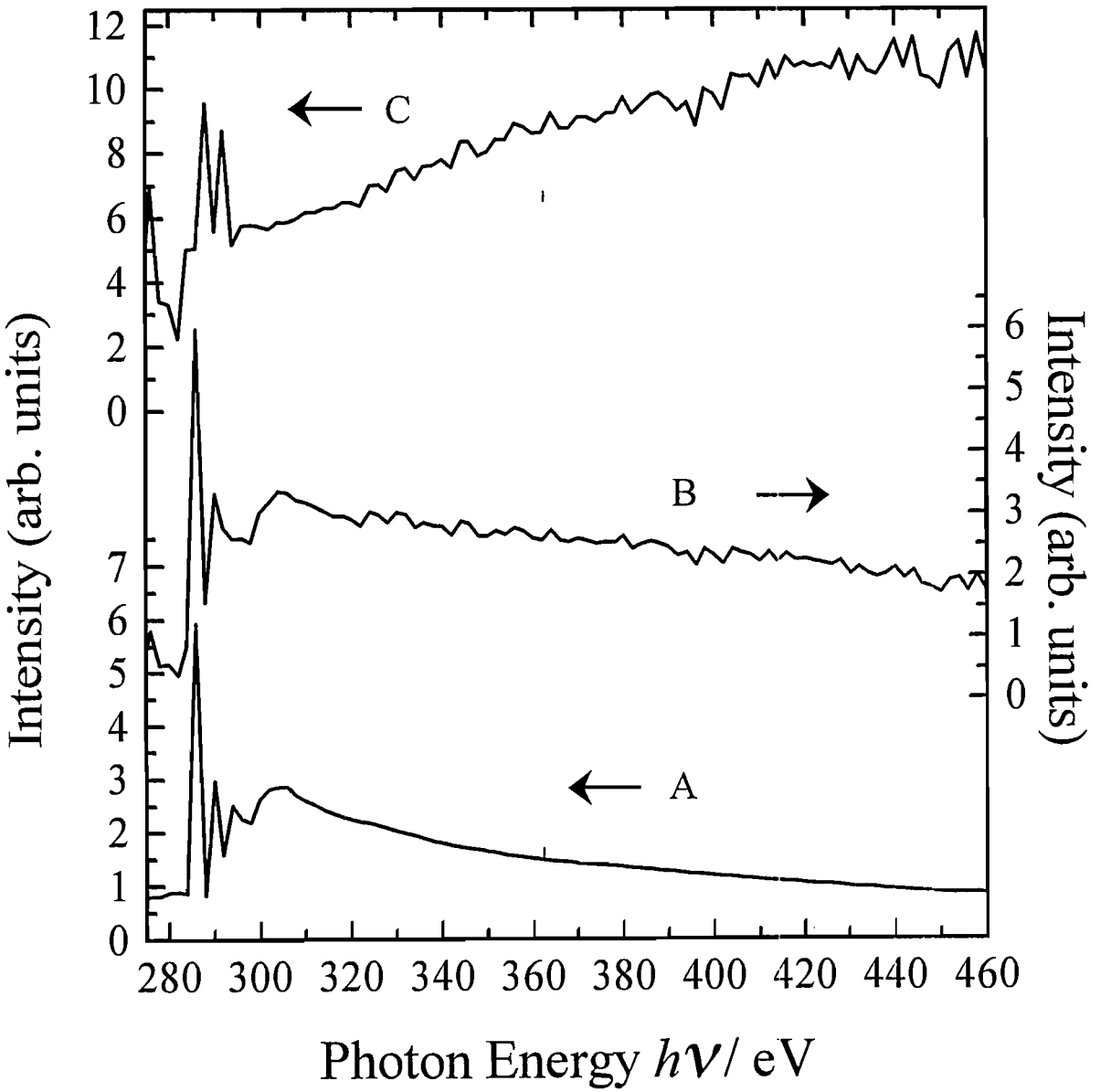

Figure 3-13. AEY spectrum (**A**); TIY spectrum (**B**); TIY/AEY spectrum (**C**) in wide energy region. The data step is about 2 eV.

Table 3-1.Assignments of benzene NEXAFS

Feature	Relative Energy (in eV)	Assignment					
		Experimental		Xα	EIC	HAM	Schwarz
		[53]	[50]	[53]	[58]	[57]	*et al.* [56]
a	0	$\pi^*(e_{2u})$	π^*	$\pi^*(e_{2u})$	$\pi^*(e_{2u}/b_1)$	$\pi^*(e_{2u})$	$\pi^*(e_{2u}/b_1)$, $\pi^*(e_{2u}/a_2)$
b	2.6	3s, 3p	C-H σ^*	—	3s, $\pi^*(e_{2u}/a_2)$, 3p	—	3s(pyσ^*CH), 3p(s, d)
c	3.8	3d, 4s, 4p	—	$\pi^*(b_{2g})$	4s	$\pi^*(b_{2g})$	3d, 4s, 4p; $\pi^*(b_{2g})$ shake
d	4.7	—	C-H σ^*	—	—	—	—
e	8.2	shake	—	$\sigma^*(e_{1u})$	$\pi^*(b_{2gs})$; $\sigma^*(e_{2g})$	—	$\pi^*(b_{2gs})$ shake; $\sigma^*(e_{2g})$
f	14.7	—	shape resonance	$\sigma^*(e_{2g})$; $\sigma^*(a_{2g})$	σ^*	—	σ^*

Table 3-2: TIY/AEY intensity ratio at each inner shell excitation

$h\nu$	285eV	287eV	300eV	430eV
state	$\pi^*(e_{2u})$	X_D	ionization	ionization
TIY/AEY intensity ratio	1/4	1	1/2	1

Ⅲ-2-(3). **Discussion**

Here, I discuss about the physical meaning of difference of the TIY/AEY intensity ratio listed on Table 3-2. First, I will deal with AES of benzene solid. Menzel *et al.* [50] measured AES at various excitation energies. I show their results in figure 3-14. Curves A, X, B, C, and D are the AES of which excitation energies correspond to features **a**, **b**, **c**, **e**, and **f** in our AEY spectrum (curve **A** in Fig.3-10), respectively. The AES which correspond to feature **a** and **b** are not apparently similar to our results (curve **B** and **C** in Fig.3-9) because of the low resolving power of the CMA used in our experiment. In spite of difference between our spectra and their spectra, both are essentially identical. Thus, I review the dependence of Auger decay process on excitation energy $h\nu$ using their AES. Curves B, C, and D were very similar. They said that this result indicates that normal Auger decay is dominant core decay process above the peak **c**. Curve A was quite different from other AES. This result implies that resonant Auger decay is dominant core decay process following the $\pi^*(e_{2u}) \leftarrow 1s$ transition. As mentioned above, there are two kinds of resonant Auger decay processes; one is spectator Auger decay and the other is participator Auger decay process. The kinetic energy E_{Auger} of Auger electron which is emitted through participant Auger decay process is the same with that of the V-photoelectron. The energy position of participant contribution is labeled by dashed lines in Fig.3-14. As shown in Fig.3-14, one can find apparent contribution of participant Auger in the curve A. However, the most part is contribution of Auger electron *via* spectator Auger decay process. Thus they showed that spectator Auger decay is predominant core decay process following the $\pi^*(e_{2u}) \leftarrow 1s$ transition. While, though the curve X mainly shows the features due to normal Auger decay, it also shows a little contribution of resonant Auger decay. In this curve, the contribution of participant Auger decay process is very small. Thus it is thought that spectator Auger decay process is important in the resonant Auger decay.

Here, I will discuss the H^+ desorption from benzene surface on the basis of ASD model. Normal Auger stimulated desorption (NASD) model can be

applicable for the desorption yields at $h\nu$ = 300 and 430 eV, while spectator Auger stimulated desorption (SASD) model can be applicable for the desorption yield at $h\nu$ = 285 eV. In regard to the desorption yield at $h\nu$ = 287 eV, there are contribution of both NASD and SASD. In the case of NASD, two holes are created in the valence band *via* normal Auger decay process (Fig.2-3). As an another possibility, there are shake up and shake off processes at $h\nu$ = 430 eV as shown in Fig.3-8. It should be noted that there are 3 holes in the valence band *via* shake up or shake off process. However, Fig.3-8 shows that the contributions of shake up and shake off process are extremely smaller than that of normal Auger decay process. Thus I regard the shake up and shake off processes as negligible.

It should be noted that the final states for excitation energies $h\nu$ = 300 and 430 eV should be the same 2h state. However, the desorption yields observed from TIY/AEY between excitation energies $h\nu$ = 300 and 430 eV are different. Why does such difference occur? To answer this problem, I propose the secondary effect on H^+ desorption. At first, I assume that secondary effect is owing to only secondary electron. There are three kinds of secondary electrons, *i.e.*, *V*-photoelectron, *K*-photoelectron, and Auger electron. Next, I assume that the magnitude of secondary effect is proportional to the kinetic energy of the electron. This assumption is confirmed from experimental results reported for various radiation scintillators, such as NaI [66] and anthracene [66], in which the pulse height is proportional to irradiation energy in the several keV energy region. On the basis of these assumptions, I illustrate secondary effect in the figure 3-15. In Fig.3-15, there are three kinds of contributions in the secondary effect; contribution of *V*-photoelectron (**V**), *K*-photoelectron (**K**), and Auger electron (**A**). In the energy region below *K*-edge, only valence shell excitation occurs. The kinetic energy E^V_{PE} of *V*-photoelectron is proportional to the excitation energy as expressed follows [18];

$$E^V_{PE} = h\nu - E_V. \quad \cdots\cdots(3-6)$$

Because E_V is much smaller than $h\nu$, the secondary effect is roughly proportional to the excitation energy. Above the *K*-edge, the greater part of excitation is inner shell excitation and valence excitation is suppressed. In the same way above the

K-edge, the contribution of *V*-photoelectron is proportional to the excitation energy in this energy region. However, since the absolute value of *V*-photoelectron decreases, the slope of contribution line for *V*-photoelectron is also suppressed. Therefore, the contribution of *V*-photoelectron is very small above *K*-edge. In the energy region in which resonant Auger decay process is dominant, Auger electron is emitted, while, *K*-photoelectron is not emitted because core electron is bounded to unoccupied molecular orbital. In this energy region, the greater part of secondary effect is due to Auger electron. In generally, the kinetic energy of Auger electron is independent of excitation energy as mentioned above part of this dissertation. In the strict sense, this description is not correct in detail. As shown in Fig.3-9, AES for spectator Auger decay is shifted to several eV higher than that for normal Auger decay. This phenomenon is caused by the screening effect of an "spectator" electron which is excited from core to unoccupied state. For this reason, the kinetic energy E_{Auger} of Auger electron depends on the excitation energy. However, the contribution of Auger electron should be considered in terms of not only the peak energy but also integrated energy because Auger electron has many kinds of kinetic energies as shown in Fig.3-9. Therefore, I regard the contribution of Auger electron as constant for excitation energy. Above the ionization potential I_P, the secondary effect includes the contribution of *K*-photoelectron. In this energy region, the contribution of *K*-photoelectron is proposal to $h\nu - E_K$. For the excitation energies $h\nu = 300$ and 430 eV, the secondary effect due to Auger contribution is same, but the secondary effect due to *K*-photoelectron contribution is quite different. I concluded that the difference of desorption yield between $h\nu = 300$ and 430 eV is attributed to the secondary effect.

Next, I consider the difference of desorption yield between the excitation energy $h\nu = 300$ and 287 eV. In this case, the secondary effect is not so difference because the excitation energy is not so different. In spite of small difference of secondary effect, the desorption yield for 285 eV was two times smaller than that for 300 eV (see Table 3-2). And the desorption yield for the excitation energy $h\nu = 287$ eV was two times larger than that for $h\nu = 300$ eV. These results can be

explained by the difference of final state. The final state of normal Auger decay is 2h state, while the final state of spectator Auger decay is 2h1e state. At the excitation energy $h\nu$ = 285 eV, an electron lies at $\pi^*(e_{2u})$. While, at the excitation energy $h\nu$ = 287 eV, an electron lies at σ^*(C-H). Therefore, it is thought that desorption yield is largely influenced by the MO character into which core electron is excited. When core electron is excited to non-bonding state, desorption is suppressed because the coulomb repulsion potential is screened by an excited core electron. On the other hands, when the core electron is excited to anti-bonding state, desorption is enhanced. This idea is firstly proposed by Mase *et al.* [67]. They proposed that the H^+ desorption probability from condensed water induced O 1*s* inner shell excitation is dominated by three factors, *i.e.*, (1)coulomb repulsion potential between two holes created by Auger transition, (2)the contributions of two holes and excited core electron to O-H bond, and (3)neutralization probability of ion on surface [68]. By the second factor, it is thought that the desorption yields for SASD are quite different from that for NASD because the ionized core electron does not give significant contribution to C-H bond. There are some studies that report such enhancement effect of desorption yield induced by inner shell excitation. Nagasono *et al.* [69] measured TIY/AEY spectra of condensed NH_3 and reported an enhancement of TIY/AEY by the excitation $4a_1 \leftarrow$ N 1*s*. Sekitani *et al.* [70] measured TIY/AEY spectra of condensed acetonitrile and reported an enhancement of TIY/AEY by the excitation C-H* $\leftarrow$ C 1*s*. These experimental results seem to support the idea. This model means that spectator Auger decay process is very important for DIET.

Keeping this in mind, let us consider an another possible explanation. When the core electron is excited to an unoccupied MO, desorption yield is usually suppressed by screening effect of the excited electron. However, if the unoccupied MO has extensively steep anti-bonding potential surface, H^+ may be desorbed before Auger decay process. This model was suggested by Menzel *et al.* [50] as "ultra fast process". In this model, PSID is dominated by not the coulomb repulsion potential but the only character of unoccupied MO. This model was proposed for H^+ desorption for the excitation $X_D \leftarrow$ 1*s* from condensed C_6D_6. It

has not been clear which model is correct, yet. To verify each model is very interesting and is subject for a future study.

As mentioned above, the difference of desorption yield between the excitations $\pi^*(e_{2u}) \leftarrow 1s$ and $X_D \leftarrow 1s$ is considered to be induced from the difference of character of MO into which core electron is excited. Hence, this inner shell resonant excitation effect is due to the interaction between photon and molecule, *i.e.*, fundamental effect. To study the true magnitude of inner shell resonant excitation effect, it should be separated from secondary effect. However, in the TIY spectrum, I detected both ions which is induced by fundamental and secondary effect. For this reason, the intensity rate of desorption yield summarized in the table 3-2 does not show the true magnitude of inner shell resonant excitation effect. Next, I examined an experiment of Auger electron photo ion coincidence (AEPICO) spectroscopy to study the magnitude of fundamental effect.

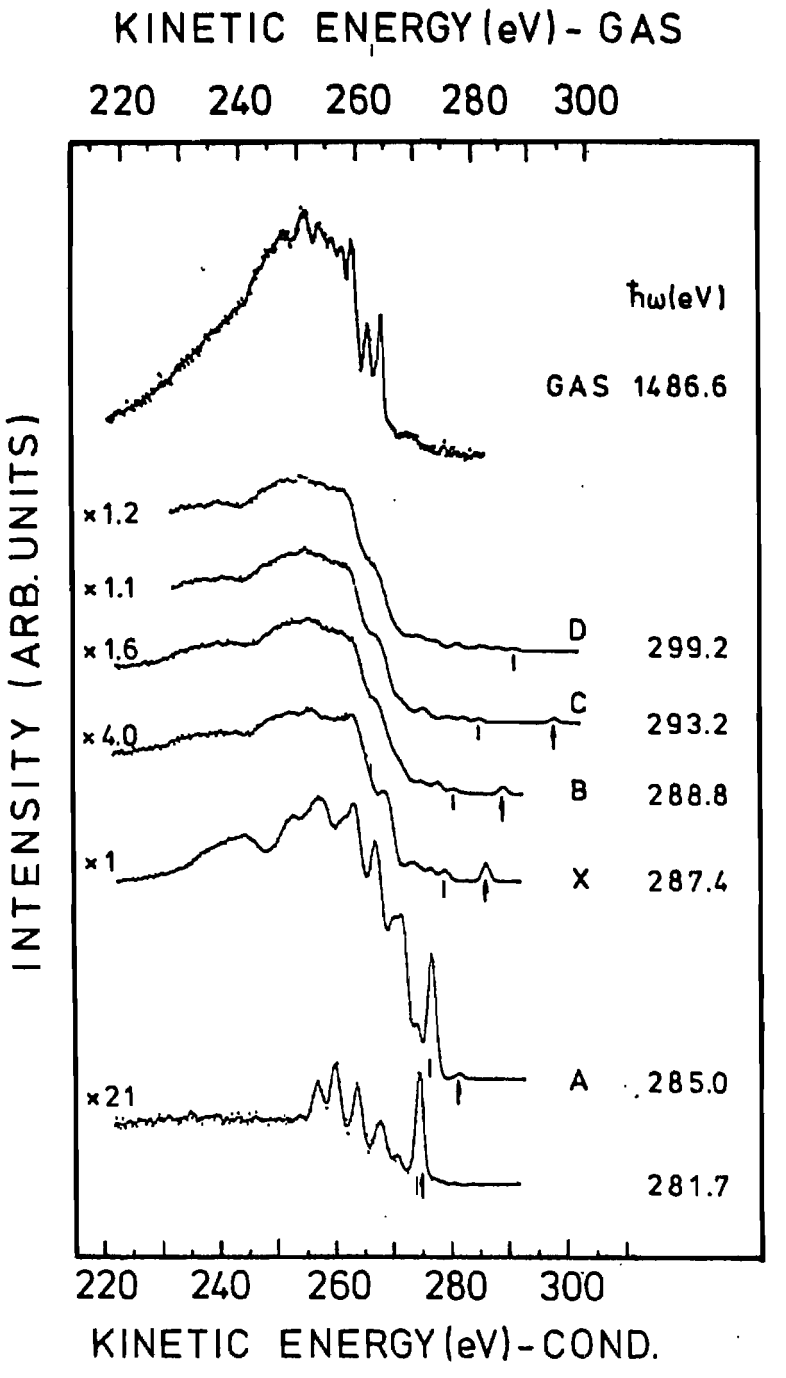

Figure 3-14. AES for condensed C_6D_6 reported Menzel *et al.* [50].
The lowest curve corresponds to prethreshold excitation. The curve on top shows the gas phase AES (Ref.[65]). The energy scale on the bottom gives the kinetic energy of the Auger electrons from solid benzene, that on top that for the gas phase molecule. The arrows indicate the C *K*-photoelectron peak excited by second order light. The dashed lines show the highest *V*-photoelectron peak.

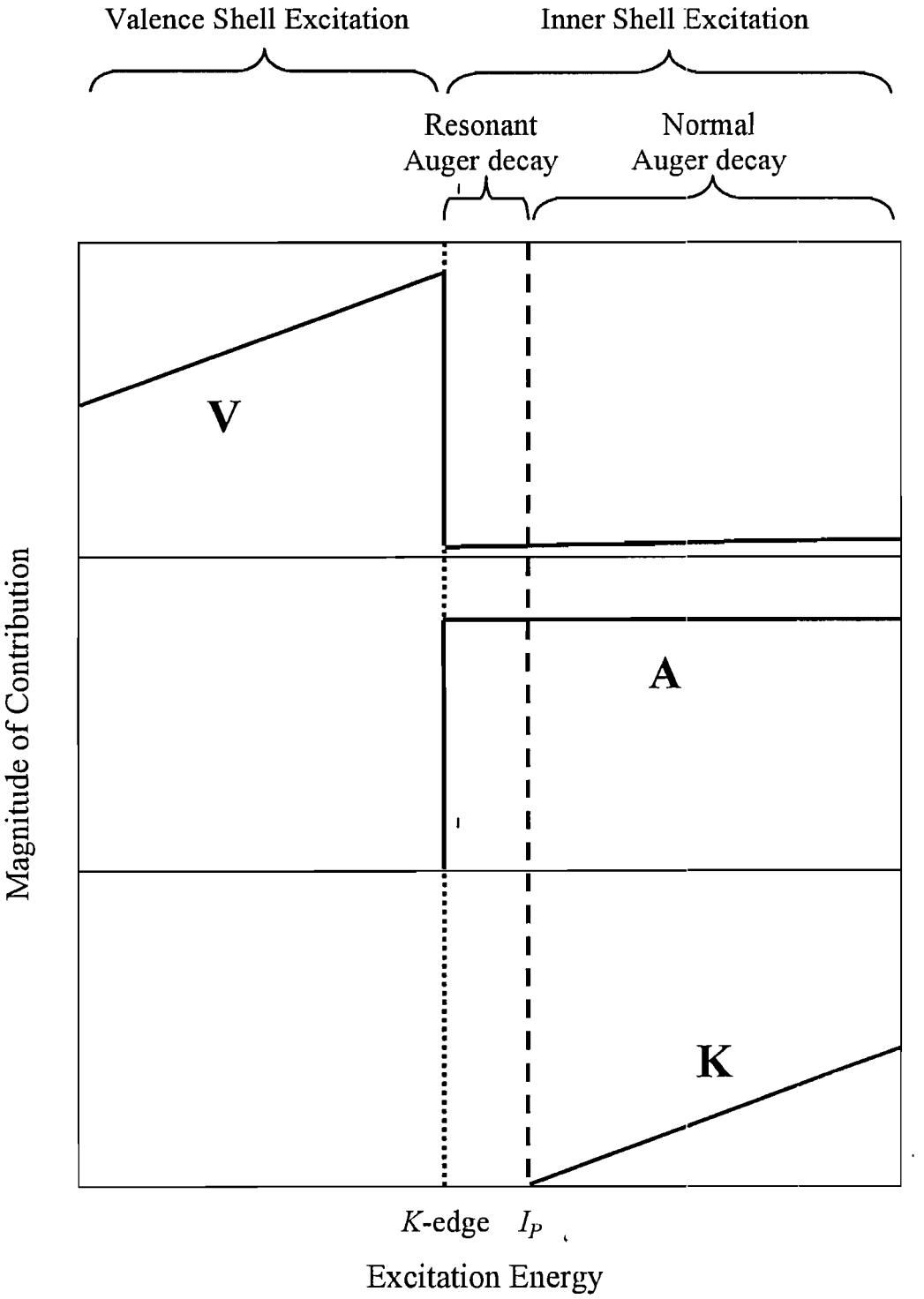

Figure 3-15. Schematic diagram of contribution of secondary effect.
V: *V*-photoelectron, **A**: Auger electron, **K**: *K*-photoelectron.

Ⅲ-3. **Measurement of Auger electron photoion coincidence (AEPICO) spectra**

Electron-ion coincidence (EICO) spectroscopy is a powerful tool to investigate the dissociation dynamics of molecules. One of the reasons is that it enables us to study the relationship between dissociation pathway and electronic transition. Especially, in the case of dissociation induced by inner shell excitation, since dissociation is closely related to Auger decay process, it is extensively important to study the relationship between dissociation pathway and Auger final states. Auger electron photoion coincidence (AEPICO) spectroscopy is a technique that is able to investigate the relationship. For many molecules, *e.g.*, N_2, [71, 72,73], CO [71, 74], N_2O [75, 76, 77], SF_6 [78], BF_3 [79], and SiF_4 [80], EICO is used and remarkable achievements for the study of dissociation have been made. Historically, the first attempt to use the EICO for the study of DIET was done by Knotek and Rabalais [81]. After this pioneering work, however, EICO spectroscopy was not applied for DIET study because of several problems due to characteristic of surface for long time. Recently, Mase *et al.* [44] developed a new EICO apparatus and succeeded to study the relationship between desorption dynamics and Auger final states.

Another reason is that EICO spectroscopy enables us to extract ions which is induced fundamental effect. Thus, I examined AEPICO experiment for condensed benzene and studied the H^+ desorption yield due to fundamental effect.

In this section, at first, the apparatus used for AEPICO and the outline of AEPICO spectroscopy are described. Secondly, I show the AEPICO spectra.

Ⅲ-3-(1) **AEPICO spectroscopy and apparatus**

I show the schematic diagrams of the apparatus and outline of AEPICO spectroscopy in figure 3-16 and 3-17. All apparatus is developed Mase *et al.* [44]. We used the same CMA and TOF-MS described in section Ⅲ-1. The experimental conditions of sample thickness, base pressure in UHV chamber, apparatus arrangement are also same with the condition for measurement of TIY and AEY. The AEPICO spectra were measured as follows. ①Monochromatic soft x-ray with energy of *hv* is irradiated on the benzene thin film. ② Following the excitation of C 1*s* electron, Auger electron is emitted and photoion is desorbed from the surface. ③Auger electron of which kinetic energy is analyzed by CMA is detected by MCP. ④The electron signal is transformed to negative NIM pulse *via* preamplifier and discriminator and triggers multichannel scaler (MCS) (Laboratory Equipment Corporation, LN-6500). This electron signal determines the starting point of TOF difference spectrum. ⑤Desorbed photoion is detected by MCP of TOF-MS. ⑥The ion signal is also transformed to negative NIM pulse *via* the preamplifier and the discriminator. The transformed ion signals is counted by MCS. The ion counts were recorded for 8 μs as a function of TOF difference between electrons and ions by the MCS. The ions desorbed from the same excited molecule which has emitted the electron give a characteristic peaks at the TOF difference spectrum (coincidence signals), while the other ions raise background counts (false coincidence signals). It should be noted that the coincidence signals are formed by ions which are desorbed by fundamental effect, while, false coincidence signals are formed by ions which are desorbed by secondary effect. Consequently, one can detect the fundamental effect by extracting the coincidence signals from the false coincidence signals. The TOF difference spectrum is called AEPICO spectrum. I measured many kinds of AEPICO spectra by scanning the kinetic energy of trigger electron.

Ⅲ-3-(2) AEPICO spectra

We measured AEPICO spectra for three kinds of excitation energies $h\nu$ = 430 eV, 285eV and 287eV. Each excitation energy corresponds specific Auger initial state as follows.The $h\nu$ = 430 eV corresponds to a excitation ionization ← 1*s*. I determined this excitation energy as a reference point because at this energy only normal Auger decay was known to occur [50]. The excitation energy of 285 eV corresponds to the excitation $\pi^*(e_{2u})$ ← 1*s*. The excitation energy of 287 eV corresponds to the X_D peak. Figure 3-18 shows a series of AEPICO spectra for excitation ionization ← 1*s* ($h\nu$ = 430eV) with a parameter of the electron kinetic energy at energy step 5 eV around the C(*KVV'*) Auger electron energy range (220 ≤ *E* ≤ 280eV). Each curve **a** ~ **l** corresponds the AEPICO spectrum for *E* = 220 to 275 eV, at energy step 5 eV respectively. Electron count rate was 4.0-7.0 × 10^3 cps and total ion count rate was 60-70 cps. Each AEPICO spectrum was accumulated for 29 min. As shown in Fig.3-18, we found clear peaks in the gate time between 420-450 ns, whereas in other TOF difference region, we found only false coincidence signals. Since we observed only almost H^+ signal in the TOF spectrum of benzene thin film, we concluded that the clear peaks in Fig.3-18 as coincidence peaks between H^+ ions and Auger electrons with each kinetic energy. Figure 3-19 shows a series of AEPICO spectra for excitation X_D ← 1*s* ($h\nu$ = 287 eV) at energy step 5 eV around the C(*KVV'*) Auger electron energy range (235 ≤ *E* ≤ 270eV). In the same manner as Fig.3-18, each curve shows AEPICO spectrum from lowest kinetic energy. Electron count rate was 1.3 - 1.9 × 10^3 cps and total ion count rate was 6 - 25 cps. The accumulation times of AEPICO spectrum was 18 min. Though the signal was small, we could also find H^+ peaks in the same gate time. Figure 3-20 shows a series of AEPICO spectra for excitation $\pi^*(e_{2u})$ ← 1*s* ($h\nu$ = 285 eV) at energy step 5 eV around the C(*KVV'*) Auger electron energy range (235 ≤ *E* ≤ 270eV). These AEPICO spectra are shown as the same manner with Fig.3-18. Electron count rate was 1.0 - 1.4 × 10^4 cps and total ion count rate was 48 - 58 cps. The accumulation times of AEPICO spectrum was 20 min. In this case, in spite of high electron and ion count rate, we couldn't find H^+ peaks in the gate time exceeding a back ground noise level.

I estimated coincidence H^+ counts to compare the intensities of coincidence H^+ signals for the AEPICO measurements of excitations; ionization , X_D and $\pi^*(e_{2u}) \leftarrow 1s$. The coincidence H^+ counts were obtained by subtracting false coincidence signal which was assumed to obey the Poisson distribution from summation of coincidence H^+ signal in the gate time. Coincidence H^+ counts for each excitation photon energy are shown in plots **a**, **b** and **c** as a function of the electron kinetic energy in figure 3-21.

On the basis of this idea, a distribution of false coincidence signals for each AEPICO spectrum essentially should not depend on the kinetic energy of triggered Auger electrons, error bars of coincidence counts were estimated as follows. I examined false coincidence signals in several TOF difference regions for each AEPICO spectrum and obtained maximum values and minimum values of false coincidence counts. Then I estimated the error at an average value of difference between the maximum value and minimum values.

The plots **a** shows the peak at 255 eV. This peak at 255 eV were confirmed by repeated measurement. These results seem to mean that H^+ is well desorbed when benzene molecules decay emitting Auger electrons which have the kinetic energy near 255eV. I can also find the peak near 255eV though the plots are somewhat scattered in plots **b**. While, plots **c** shows the peak near quite different energy, e.g., 245 and 250 eV. However, the peak in plots **c** seems incredible because I couldn't observe the coincidence H^+ signal for excitation $\pi^*(e_{2u}) \leftarrow 1s$ exceeding noise level in spite of high electron and ion count rate. I think the peak in plots **c** may appear as a consequence of some noises. Therefore, I discuss the coincidence H^+ counts for the AEPICO measurements of excitations $\pi^*(e_{2u}) \leftarrow 1s$ using an average value of the coincidence H^+ counts. In Fig.3-21, curve **A**, **B** and **C** show the C(*KVV*) Auger electron spectra for each excitation; ionization , X_D and $\pi^*(e_{2u}) \leftarrow 1s$, respectively.

In order to analyze the experiment data, I defined the experimental coincidence yield $Y(h\nu)$ for the photon energy $h\nu$;

$$Y(h\nu) \equiv [H^+ \text{ coincidence counts}] / [\text{Auger electron counts}]. \quad \cdots\cdots (3\text{-}7)$$

I obtained maximum coincidence signal at E = 255 eV for excitations ionization $\leftarrow$ 1s and $X_D \leftarrow$ 1s. I obtained that Y(430 eV) and Y(287 eV) at E_{Auger} = 255 eV were about $4.4\times10^{-6}\pm6.6\times10^{-7}$ and $4.5\times10^{-6}\pm1.7\times10^{-6}$, respectively. For the excitation $\pi^*(e_{2u}) \leftarrow$ 1s, I obtained the average value of $Y(h\nu)$ because I couldn't observe the coincidence H^+ signal enough to discuss the structure of plots c. The average value of Y(285 eV) was about $5.7\times10^{-7}\pm3.1\times10^{-7}$. I summarized the results of desorption yield obtained from TIY/AEY and $Y(h\nu)$ in the table 3-3.

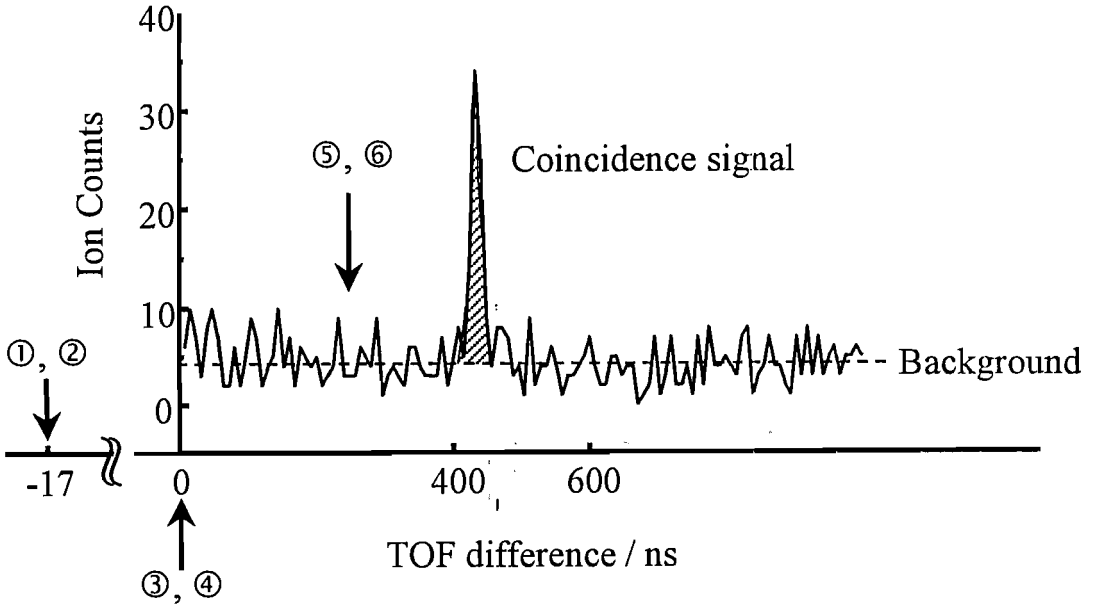

Figure 3-16. Schematic diagram of principle of Auger electron photoion coincidence (AEPICO) spectroscopy. ①Irradiation of monochromatic soft x-ray ②Excitation of inner shell ③Detection of Auger electron ④Start of multichannel scaler (MCS) ⑤Detection of photoion ⑥Count of photoion by MCS (Ref.[44])

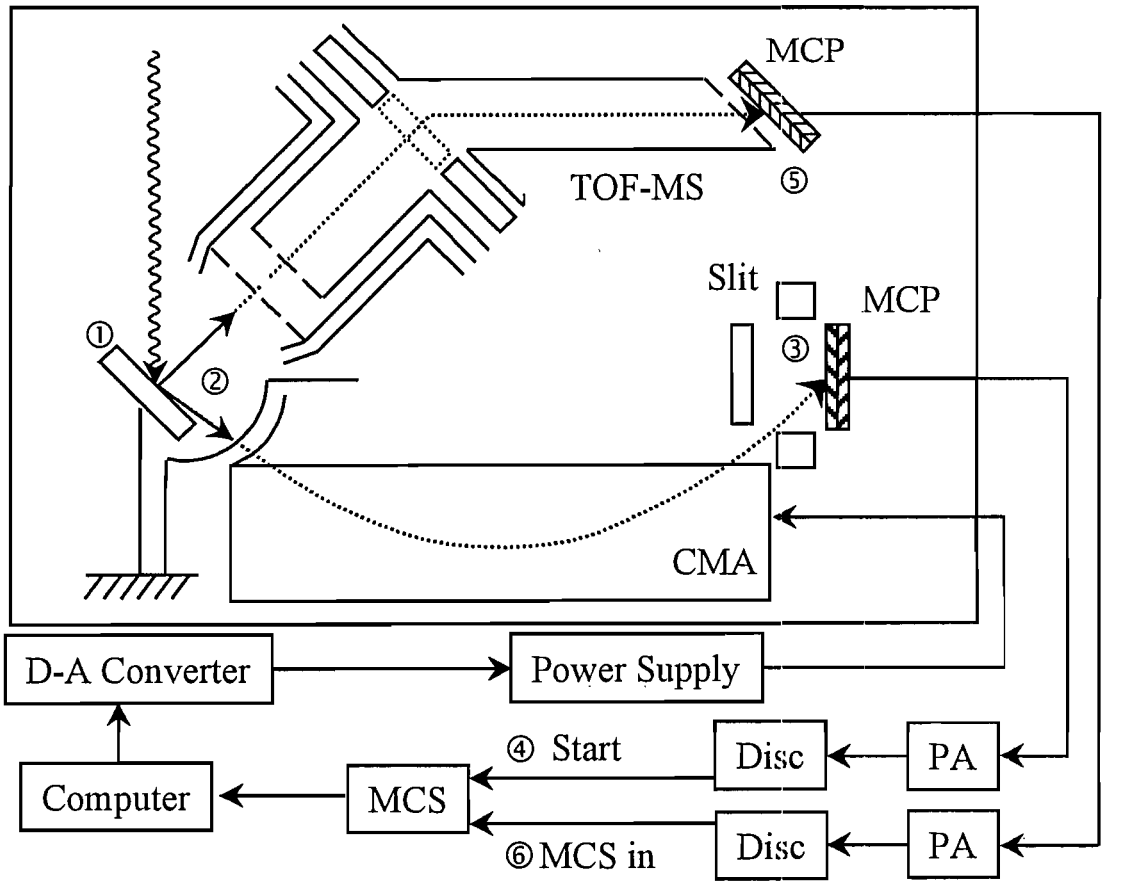

Figure 3-17. Schematic diagram of apparatus for AEPICO measurement.
①Irradiation of monochromatic soft x-ray ②Excitation of inner shell ③Detection of Auger electron by CMA ④Start of MCS triggered by electron signal ⑤Detection of photoion by TOF-MS ⑥Count of photoion by MCS. (Ref.[44])

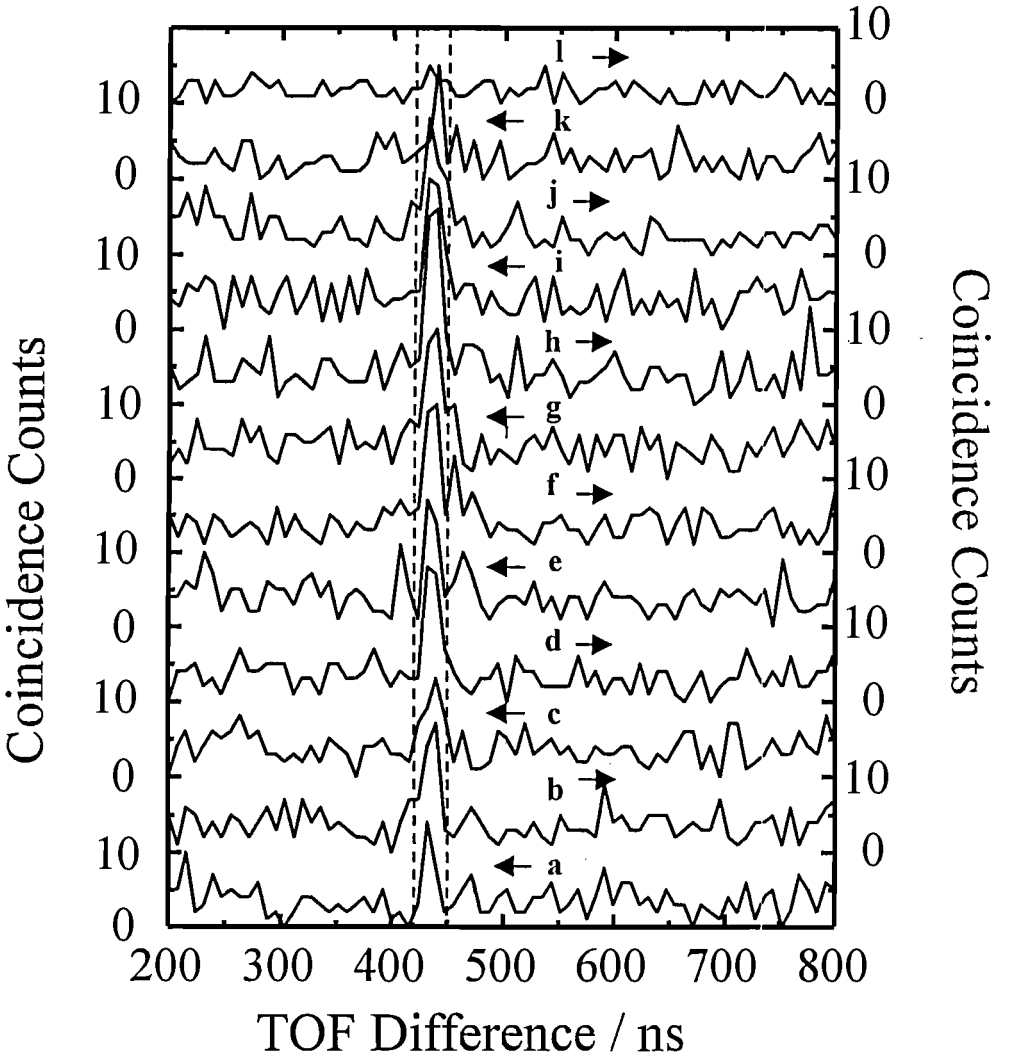

Figure 3-18. A series of AEPICO spectra for the excitation $h\nu = 430$ eV (ionization ← 1s). Curves **a**, **b**, **c**, **d**, **e**, **f**, **g**, **h**, **i**, **j**, **k**, and **l** show the AEPICO spectra at E_{Auger} = 220, 225, 230 , 235, 240, 245, 250, 255, 260, 265, 270, and 275 e, respectively. The broken lines show gate time (420 - 450 ns). Arrows indicate reference axis.

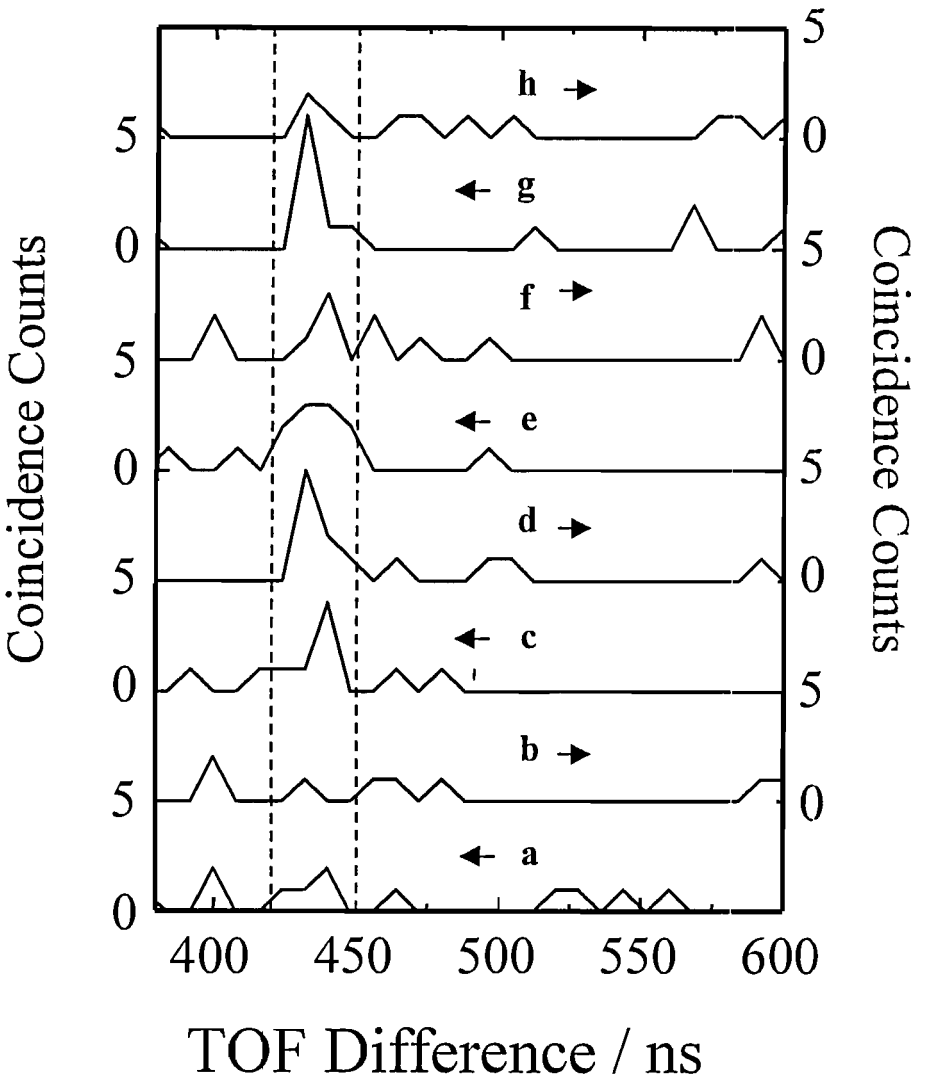

Figure 3-19. A series of AEPICO spectra for the excitation $h\nu = 287$ eV ($X_D \leftarrow 1s$). Curves **a**, **b**, **c**, **d**, **e**, **f**, **g**, and **h** show the AEPICO spectra at $E_{Auger} =$ 235, 240, 245, 250, 255, 260, 265, and 270 eV, respectively. Arrows indicate reference axis.

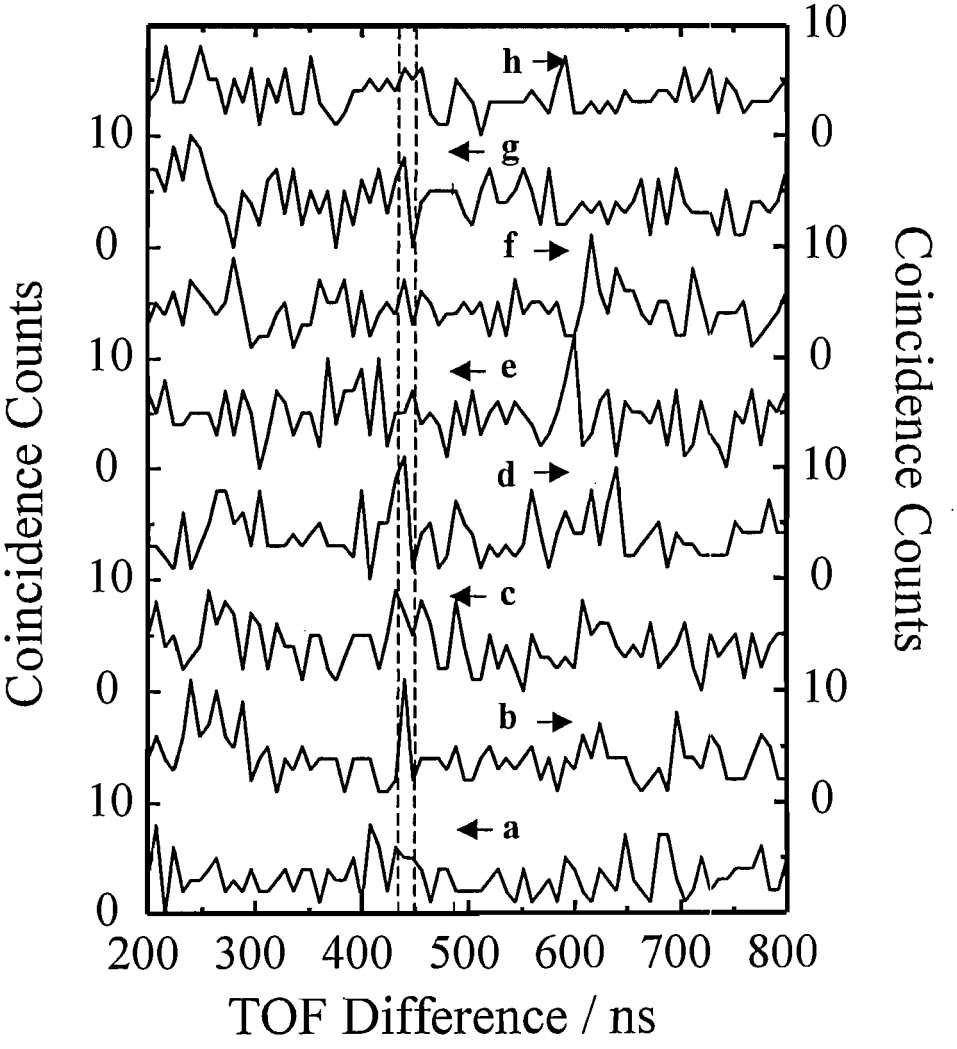

Figure 3-20. A series of AEPICO spectra for the excitation $h\nu = 285$ eV ($\pi^*(e_{2u}) \leftarrow 1s$). Curves **a**, **b**, **c**, **d**, **e**, **f**, **g**, and **h** show the AEPICO spectra at E_{Auger} = 235, 240, 245, 250, 255, 260, 265, and 270 eV, respectively. Arrows indicate reference axis.

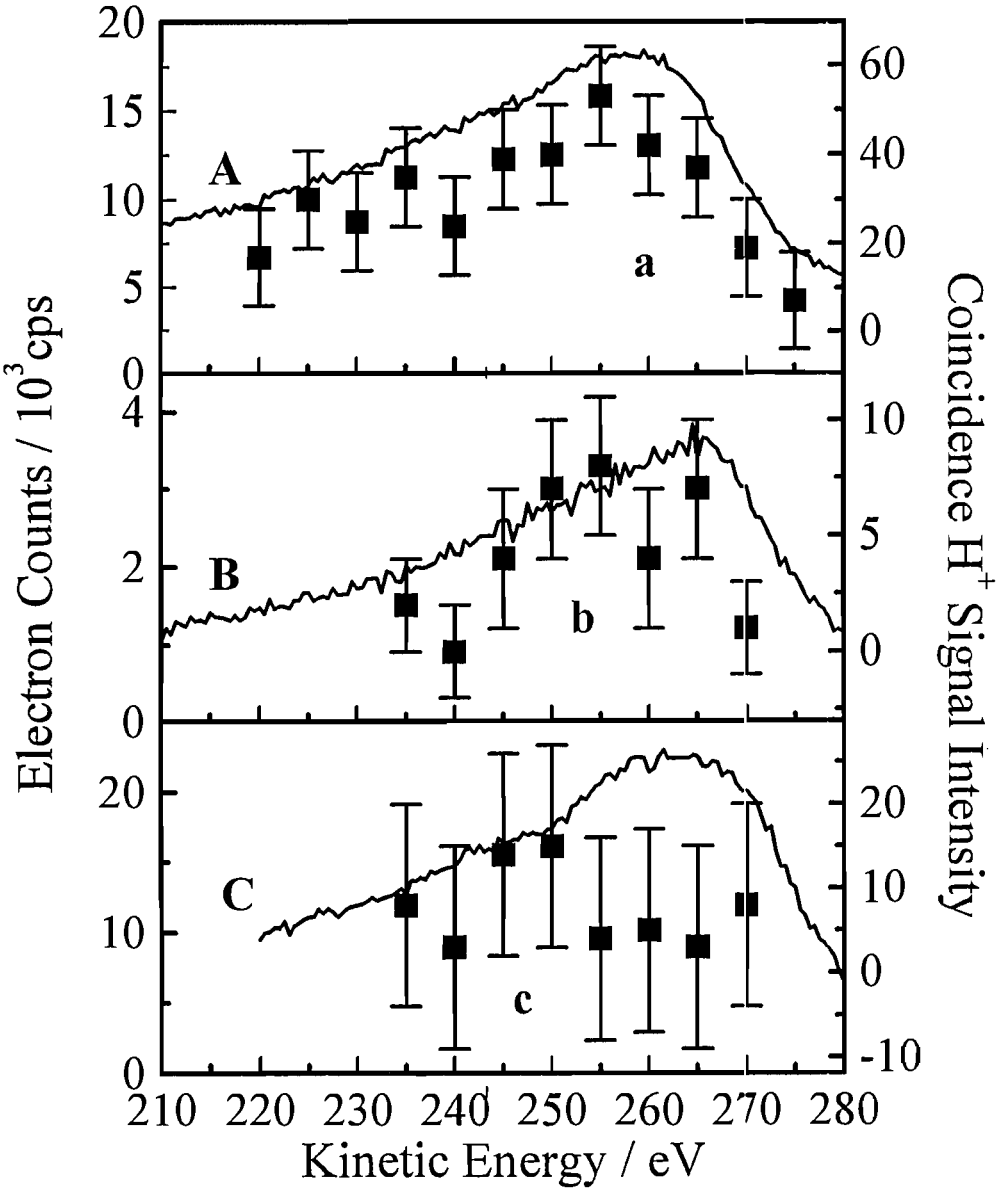

Figure 3-21.Curves **A**, **B** and **C** show AES for excitations ionization ← 1s, X_D ← 1s and $\pi^*(e_{2u})$ ← 1s, respectively. Plots **a**, **b** and **c** show the coincidence H+ counts for excitations ionization ← 1s, X_D ← 1s and $\pi^*(e_{2u})$ ← 1s, respectively. See the detail in text.

Table 3-3: TIY/AEY intensity ratio and coincidence yield $Y(h\nu)$ at each inner shell excitation

$h\nu$	285eV	287eV	300eV	430eV
state	$\pi^*(e_{2u})$	X_D	ionization	ionization
TIY/AEY intensity ratio	1/4	1	1/2	1
Y($h\nu$)	5.7×10^{-7} $\pm3.1\times10^{-7}$	4.5×10^{-6} $\pm1.7\times10^{-6}$	—	4.4×10^{-6} $\pm6.6\times10^{-7}$

Ⅳ. C-H dissociation yield and 3 step model

In this chapter, I discuss about the physical meanings of TIY/AEY and $Y(h\nu)$. TIY/AEY and $Y(h\nu)$ were dealt as the desorption yield per photon absorption in above discussion. However, I will derive that TIY/AEY reflects the C-H dissociation yield due to fundamental and secondary effects, while $Y(h\nu)$ reflect the C-H dissociation yield due to only fundamental effect by an assumption, *i.e.*, "3 step model". I discuss about a relationship between fundamental and secondary C-H dissociation yields. I mention the real magnitude of inner shell resonant excitation effect by comparing the contribution of fundamental and secondary for C-H dissociation. Next, I refer to color center formation (CCF) yield in anthracene single crystals and CCF reflects the C-H dissociation yield in bulk. Finally, I discuss the relationship between the C-H dissociation observed in surface and bulk.

IV-1. **3 step model**

At first, I start to discuss about the physical meaning of TIY/AEY. Now I assume that Auger electron emission and H^+ desorption can be described by "three step model" [82]. The schematic diagrams of this model are shown in figure 4-1 and 4-2. In this model, the process of Auger electron emission consists of three steps; (Ⅰ) photoabsorption and Auger decay, (Ⅱ) arrival of Auger electron to the surface and (Ⅲ) escape from the benzene surface. On the step (Ⅰ), benzene molecules are excited by soft x-ray to emit Auger electrons. Number $n(h\nu, E_A)$ of Auger electron emitted in a depth x~$x+dx$ from the surface is;

$$n(h\nu,E_A)=I_0\mu(h\nu)\exp\{-\mu(h\nu)x\}P(h\nu,E_A)dxdE_A, \quad \cdots\cdots\cdots\cdots(4-1)$$

where I_0 is irradiation photon number, $\mu(h\nu)$ is absorption coefficient at the photon energy $h\nu$, and $P(h\nu, E_A)$ is Auger decay probability of a molecule excited by photon with energy $h\nu$. Due to this Auger decay, a molecule emits Auger electrons which have kinetic energy of $E_A \sim E_A + dE_A$ (in this chapter, I describe the kinetic energy of Auger electron as E_A). On step (Ⅱ), emitted Auger electrons are scattered by benzene molecules before the arrival to the solid surface. The probability $S(E_A, x)$ with which Auger electron emitted at depth x arrives to the surface without scattering are;

$$S(E_A,x) = B(E_A)\exp\left(-x/L(E_A)\right), \quad \cdots\cdots\cdots\cdots(4-2)$$

where $B(E_A)$ is a parameter to designate how much fraction of emitted Auger electrons have momentum to the surface, $L(E_A)$ is the escape depth for Auger electrons having kinetic energy E_A. The maximum value of $B(E_A)$ may be 1/2 in the isotropic crystals. On the step (Ⅲ), Auger electrons arriving to the surface are partly scattered by surface potentials. I express the penetration probability $T(E_A)$ of Auger electrons having kinetic energy E_A through the surface potential. I also express the detection efficiency of CMA to be $D(E_A)$. Consequently, total Auger electron number N_{Auger} detected by a detector from solid benzene surface

which is excited by photon energy $h\nu$ and has kinetic energy $E_A \sim E_A + dE_A$ can be expressed follows;

$$N_{Auger}(h\nu, E_A) = \int_x I_0 \mu(h\nu) \exp\{-\mu(h\nu)x\} P(h\nu, E_A) B(E_A) \exp\left(-\frac{x}{L(E_A)}\right) T(E_A) D(E_A) dx dE_A. \quad \cdots\cdots (4-3)$$

In Eq. (4-3), integration is performed with respect to x but not to E_A. Because E_A is fixed at E_A = 260 eV for AEY measurement for carbon K-shell excitation. Consequently, using Eq. (3-3), AEY is expressed as follows;

$$\text{AEY} = \frac{N_{Auger}}{I_0} = \int_x \mu(h\nu) \exp\{-\mu(h\nu)x\} P(h\nu, E) B(E) \exp\left(-\frac{x}{L(E)}\right) T(E) D(E) dx dE. \quad \cdots\cdots (4-4)$$

Next, I discuss about TIY. In the same manner as AEY, if I assume 3 step model for H^+ desorption, desorbed H^+ counts can be expressed follows;

$$N_{H^+}(h\nu, E_H) = \iint_{E_H, x} I_0 \mu(h\nu) \exp\{-\mu(h\nu)x\} \eta_d^t(h\nu) B^{H^+}(E_H) \exp\left(-\frac{x}{L^{H^+}(E_H)}\right) T^{H^+}(E_H) D^{H^+} dx dE_H \quad , \quad \cdots\cdots (4-5)$$

where $\eta_d^t(h\nu)$ is the total C-H dissociation yield which includes the contributions of fundamental and secondary effect. $B(E_H)^{H+}$, $L(E_H)^{H+}$ and $T(E_H)^{H+}$ are parameters for H^+ and they are similar with the case of Auger electrons. D^{H+} is a detection efficiency of TOF-MS. It should be noted that $\exp\{-x / L(E_H)^{H+}\}$ are thought to be negligible because it is known that escape depth of H^+ ion is so small. Thus I put this factor to be the unity. And it should be noted that $\eta_d(h\nu)$ includes the neutralization probability of dissociated H^+. In Eq. (4-5), integration is performed with respect to x and E_H because in our experiment all hydrogen ions with various kinetic energies are detected. Using Eq. (4-5), TIY is expressed as follows;

$$\mathrm{TIY} \approx \frac{N_{H^+}(h\nu, E_H)}{I_0}$$

$$= \iint_{E_H, x} \mu(h\nu)\exp\{-\mu(h\nu)x\}\eta_d^t(h\nu)B^{H^+}(E_H)\exp\left(-\frac{x}{L^{H^+}(E_H)}\right)T^{H^+}(E_H)D^{H^+}dxdE_H \quad , \qquad \cdots\cdots(4-6)$$

As shown in Fig. 3-10, TIY shows a similar tendency with AEY, because TIY reflects the $\mu(h\nu)$ as expressed in Eq. (4-6). This means that the larger $\mu(h\nu)$ is, the larger the intensity of TIY is. Physically, when $\mu(h\nu)$ is large, photons are absorbed at deep from surface. This decreases the escape probability on step Ⅱ. Using the Eq. (4-4) and (4-6), TIY /AEY are expressed as follows;

$$\frac{\mathrm{TIY}}{\mathrm{AEY}} = \frac{\iint_{E_H, x} \mu(h\nu)\exp\{-\mu(h\nu)x\}\eta_d^t(h\nu)B^{H^+}(E_H)T^{H^+}(E_H)D^{H^+}dxdE_H}{\int_x \mu(h\nu)\exp\{-\mu(h\nu)x\}P(h\nu, E_A)B(E_A^t)\exp\left(-\frac{x}{L(E_A)}\right)T(E_A)D(E_A)dxdE_A.} \qquad \cdots\cdots(4-7)$$

As shown in Eq. (4-7), TIY/AEY consists of many parameters. I examined Eq. (4-7) carefully and as a first approximation I transformed it into more simple equation as following. Firstly, since $\mu(h\nu)$ is not a function of x and E_A, thus $\mu(h\nu)$ is cancelled out. Secondly, since the Auger electron energy E_A was fixed at E_A = 260 eV, I assumed that $B(E_A)$, $L(E_A)$, $T(E_A)$ and $D(E_A)$ are independent from $h\nu$. Thirdly, since I collected all hydrogen ions with various kinetic energies, I regarded $B(E_H)^{H+}$, $T(E_H)^{H+}$ and D^{H+} are also independent from $h\nu$. Fourthly, since it is clear that Auger decay is caused upon excitation at $h\nu$ = 285 eV, 287 eV and 430 eV, I regarded $P(h\nu)$ in the Eq. (4-7) as P(285 eV) ≈ 1, P(287 eV)≈ 1 and P(430 eV)≈ 1. Consequently, as a first approximation Eq. (4-7) can be simplified to be;

$$\frac{\mathrm{TIY}}{\mathrm{AEY}} \approx \mathrm{C}\cdot\eta_d^t(h\nu) \quad , \qquad \cdots\cdots(4-8)$$

where C is a constant. Hence, it is driven that TIY/AEY reflects the total C-H dissociation yield $\eta^t_d(h\nu)$.

Nextly, I discuss about the physical meaning of coincidence yield $Y(h\nu)$. As expressed in Eq. (3-7), $Y(h\nu)$ is decided by H^+ coincidence counts (N_{CH}) and Auger electron counts (N_{CA}). I start from the discussion of N_{CA}. In this case, I also used Eq. (4-3) for N_{CA}. In the AEPICO measurement, I fixed the kinetic energy E_A for an AEPICO spectrum. Thus it is not necessary to integrate E_A in Eq. (4-3). Therefore, N_{CA} is expressed as follows;

$$N_{CA}(h\nu, E_A)$$
$$= \int_x I_0 \mu(h\nu) \exp\{-\mu(h\nu)x\} P(E_A) B(E_A) \exp\left(-\frac{x}{L(E_A)}\right) T(E_A) D(E_A) dx dE_A . \cdots\cdots (4-9)$$

Next, I discuss the N_{CH}. Generally, the counts rate of coincidence signal is given as a product of two single rates. In my experiment, there are two single rates: One is electron count rate and the other is H^+ count rate. The electron count rate reflects the Auger decay probability $P(E_A)$. It should be noted that $P(E_A)$ hardly depends on $h\nu$ above the C K-edge. Therefore, N_{CH} is expressed as follows;

$$N_{CH}(h\nu, E_H)$$
$$= P(E_A) N_{H^+}(h\nu, E_A)$$
$$= P(E_A) \iint_{E_H, x} I_0 \mu(h\nu) \exp\{-\mu(h\nu)x\} \eta_d(h\nu, E_A') B^{H^+}(E_H) \exp\left(-\frac{x}{L^{H^+}(E_H)}\right) T^{H^+}(E_H) D^{H^+} dx dE_H .$$
$$\cdots\cdots (4-10)$$

It should be noted that C-H dissociation yield $\eta_d(h\nu, E_A)$ includes only the contribution of fundamental effect and depends on the Auger decay processes. Using Eq. (4-9) and (4-10), $Y(h\nu, E_A)$ is expressed as follows;

$$Y(h\nu, E_A)$$

$$= \frac{P(E_A)\iint_{E_H,x} \mu(h\nu)\exp\{-\mu(h\nu)x\}\eta_d(h\nu, E_A)B^{H^+}(E_H)T^{H^+}(E_H)D^{H^+}dxdE_H}{\int_x \mu(h\nu)\exp\{-\mu(h\nu)x\}P(E_A)B(E_A)\exp\left(-\frac{x}{L(E_A)}\right)T'(E_A)D(E_A)dxdE_A} \quad \cdots\cdots(4-11)$$

In Eq. (4-11), $P(E_A)$ and $\mu(h\nu)$ are cancelled out. In the same manner as Eq. (4-7), I assumed that $B(E_A)$, $L(E_A)$, $T(E_A)$, $D(E_A)$, $B(E_H)^{H+}$, $T(E_H)^{H+}$ and D^{H+} are independent from $h\nu$. Consequently, Eq. (4-11) can be simplified to be

$$Y(h\nu, E_A) \approx C' \cdot \eta_d(h\nu, E_A), \quad \cdots\cdots(4-13)$$

where C′ is a constant. Hence, it is derived that $Y(h\nu, E_A)$ also reflects the C-H dissociation yield. In this case, however, the C-H dissociation yield reflects only the contribution from fundamental effect.

Ⅳ-2. **Fundamental and total C-H dissociation yield**

In this section, I discuss about C-H dissociation yield of benzene. First, I consider how $\eta_d(h\nu, E_A)$ depends on E_A. I show the $Y(h\nu, E_A)$ spectrum at excitation energy $h\nu$ = 430 eV in figure 4-3. In the figure, $Y(h\nu, E_A)$ is almost constant and hardly depends on E_A except a data at E_A = 275 eV. This result indicates that the C-H dissociation induced by inner shell excitation hardly depends on Auger decay processes. This can be explained by assuming ASD model as follows;;. Since benzene has π conjugated system, two holes formed in valence band *via* normal Auger decay are immediately delocalized in π conjugated system. Accordingly, C-H dissociation that follows this delocalization should be independent from Auger decay. The delocalization may make the coulomb repulsion energy decrease. This result seems to be one of fact which explain the reason why aromatic compounds are of anti-radiation nature.

Next, I discuss about the relationship between $\eta_d(h\nu)$ and $\eta^t_d(h\nu)$. On the basis of Eq. (3-8), the ratios of total C-H dissociation yield η^t_d(285eV)/η^t_d(430eV) and η^t_d(287eV)/η^t_d(430eV) were about 1/4 and 1/1, respectively. While, on the basis of Eq. (2-13), the ratios of fundamental C-H dissociation yield η_d(285eV)/η_d(430eV) and η_d(287eV)/η_d(430eV) were about 1/10 and 1/1, respectively. I summarize the results in table 4-1.

As shown in Table 4-1, the ratio η^t_d(287eV)/η^t_d(285eV) (≈ 4) is smaller than the ratio η_d(287eV)/η_d(285eV) (≈ 10). Both the intensity rates $\eta^t_d(h\nu)$ and $\eta_d(h\nu)$ at the excitations $\pi^*(e_{2u}) \leftarrow 1s$ and $X_D \leftarrow 1s$ originate from the inner shell resonant excitation effect. However, for $\eta^t_d(h\nu)$, the inner shell resonant excitation effect for $\eta_d(h\nu)$ were smeared out. To consider this problem, let us examine contributions of secondary effects shown in Fig.3-15 again. For the excitations $\pi^*(e_{2u}) \leftarrow 1s$ and $X_D \leftarrow 1s$, both the excitation energies are below I_P. Thus the dominant contribution of secondary effect is only due to Auger electron. By the comparison between the AES for $\pi^*(e_{2u}) \leftarrow 1s$ and the AES for $X_D \leftarrow 1s$, I regarded the contribution of Auger electron is constant for excitation energy. Accordingly, the contribution of the secondary effect for η^t_d(285 eV) is the same

with that for η^t_d(287 eV). The same amount of "Auger" secondary effect make the fundamental effect smear out. To consider the contribution rates of fundamental and secondary effect, I schematically separated the $\eta^t_d(h\nu)$ spectrum into three parts as shown figure 4-4. In the figure, there are three kinds of contributions, *i.e.*, the contributions of Auger electron effect, fundamental effect, and *K*-photoelectron effect. I assumed that the *V*-photoelectron part can be ignored. At first, let us discuss about *K*-photoelectron part. I could not observe the increasing tendency in TIY/AEY spectrum below 310 eV. As mentioned above, the contribution of *K*-photoelectron is proportional to $h\nu - E_K$. If there is the contribution of *K*-photoelectron effect, one must observe that TIY/AEY increase in proportion to $h\nu - E_K$. Actually, TIY/AEY is almost constant in the energy region $295 < h\nu < 310$ eV. And *K*-photoelectron is not emitted below I_P ($\approx$ 290 eV). From these reasons, it is assumed that the contribution of *K*-photoelectron is ignored in the energy region below 310 eV. Secondly, I regard the Auger contribution as almost constant. Thirdly, the remained part is attributed to the contribution of fundamental effect. I show the schematic diagram of the contributions of the three parts at the excitation energy $h\nu$ = 285 eV and 287 eV in figure 4-5. For η^t_d(285 eV) and η^t_d(287 eV), I estimated the magnitude x_A of Auger contribution from the results summarized in table 4-1 as follows;

$$\frac{\eta^t_d(285\text{eV})}{\eta^t_d(287\text{eV})} = \frac{\eta_d(285\text{eV}) - x_A}{\eta_d(287\text{eV}) - x_A}$$

$$\frac{1}{10} = \frac{\left(1/4 - x_A\right)}{(1 - x_A)}$$

$$x_A = 1/6 .$$

Consequently, I obtained the contribution rate at each excitation energy as summarized in the table 4-2.

Here we must note that there is a contrary result for fundamental effect. From this estimation, I obtained η_d(287 eV) / η_d(430 eV) = 5/2. In the estimation from coincidence yield $Y(h\nu)$, however, I obtained η_d(287 eV) / η_d(430 eV) $\approx$ 1. One possible explanation for this contradiction is due to *K*-photoelectron as

shown in Fig.1-1. If a *K*-photoelectron emitted from a molecule excites or ionizes a neighbor molecule, secondary H^+ ion can be desorbed. Let us assume a case in which a molecule that emits *K*-photoelectron also emits fundamental H^+. The kinetic energy E^K_{PE} of *K*-photoelectron is about 140 eV at $h\nu = 430$ eV. Assuming the distance *R* between benzene molecules a few tens Å, the time that *K*-photoelectron with $E^K_{PE} = 140$ eV reaches the neighbor molecule is estimated to be less than 10^{-15} s. When secondary H^+ is desorbed by an attack of the *K*-photoelectron emitted from the same molecule, both the fundamental and secondary H^+ have to be desorbed within fairly short times. Consequently, it may be probable that counts of secondary H^+ induced by *K*-photoelectron are included in the coincidence counts. It should be noted that this effect is not necessary to be considered for the coincidence counts of $h\nu = 285$ and 287 eV because there is no contribution from *K*-photoelectron.

IV-3. **Inner shell excitation effect on C-H dissociation in bulk**

As discussed above, inner shell resonant excitation effect on C-H dissociation of benzene showed quite different C-H dissociation yield depending on the character of excited state. And such effect were smeared out by secondary effect. Here, I will change the view from surface to bulk. I think that the bond breaking emerges as desorption from surface, while it emerges as damage in bulk. Studying the C-H dissociation in bulk, what kind of damage can be observed due to inner shell excitation effect? A possible approach for the question is to study the radiation damage of anthracene single crystals. Anthracene is a typical aromatic hydrocarbon compound as the same as benzene, and well known to be used as a standard material for scintillator [66]. The fluorescence efficiency of anthracene is degraded by irradiation gradually [32]. This phenomenon is due to that radiation-induced products quench the fluorescence of lowest singlet exciton (S_1 fluorescence). It is established that there are two kind of radicals produced by radiation at liquid nitrogen temperature; one is hydrogen detached radical (9-anthracyl radical, 9-AR) and the others is hydrogen attached radical (9-dibenzo-cyclohexadienyl radical, 9-DCR) [83]. These radicals are also called as color center because the nature of these radicals is similar to the nature of color centers in alkali halides. Among the two color centers, the dominantly produced color center is 9-DCR at room temperature [84, 85]. The hydrogen attached radical is also known to be dominant product in benzene solid [86]. Hence, one can regards that radiation damage in anthracene solids is similar with that in benzene solids.

Recently, it is reported that color center formation is caused not by charge transfer triggered process but MO changing triggered process [87]. It should be noted that dissociated hydrogen (or hydrogen ion) *via* this process makes a hydrogen attached color center in bulk. This means that color center formation quantum yield $\eta_c(h\nu)$ must reflect the C-H dissociation yield in bulk. Shimoyama *et al.* [88] reported $\eta_c(h\nu)$ in the carbon *K*-edge energy region. I show the results in figure 4-6. White circles and dotted lines show the $\eta_c(h\nu)$ and NEXAFS of anthracene solid, respectively. As shown in Fig.4-6, the data of $\eta_c(h\nu)$ are almost

constant across the *K*-edge except η_c(500 eV). The fact that $\eta_c(h\nu)$ did not decrease at the excitation of $\pi^* \leftarrow 1s$ ($h\nu$ = 286.8 eV) seems to mean that the secondary effect is dominant for C-H dissociation in bulk. In bulk, a molecule is surrounded by another molecules into all direction. This may give the larger contribution of secondary effect than surface. And the especially large value of η_c(500 eV) may be caused by the contribution of *K*-photoelectron. For the DIET of benzene, the contribution of *K*-photoelectron emerged from around $h\nu$ = 310 eV. To investigate the relationship between the DIET and color center formation in aromatic hydrocarbon compounds, it is interest to clear the threshold energy at which the contribution of *K*-photoelectron emerges for future work.

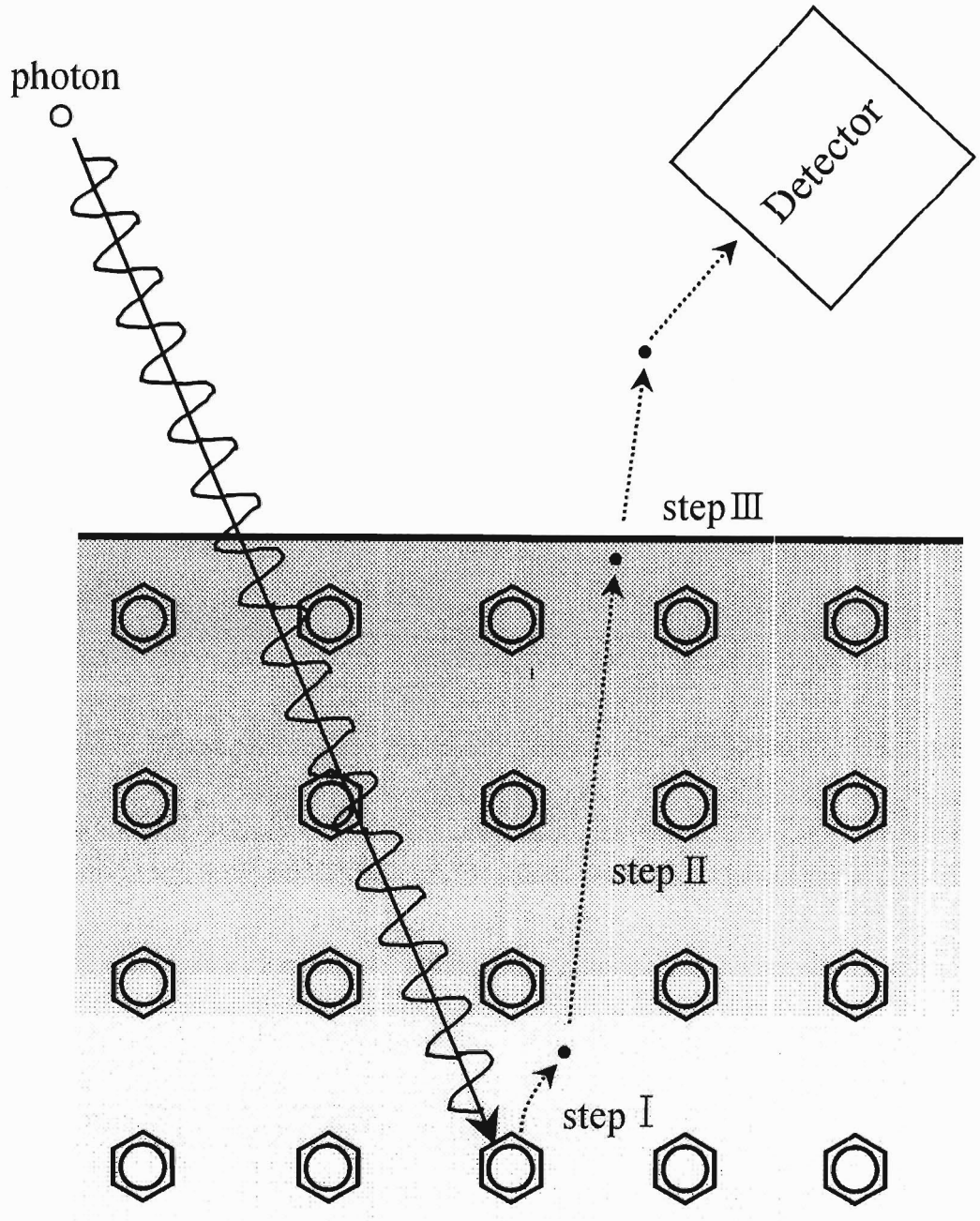

Figure 4-1. Schematic diagram of 3 step model.
Step (Ⅰ): Photoabsorption and following Auger decay and C-H dissociation, Step (Ⅱ): Arrival of Auger electron or H^+ to the surface, Step(Ⅲ): escape from the benzene surface. Finally, Detection of Auger electron or H^-.

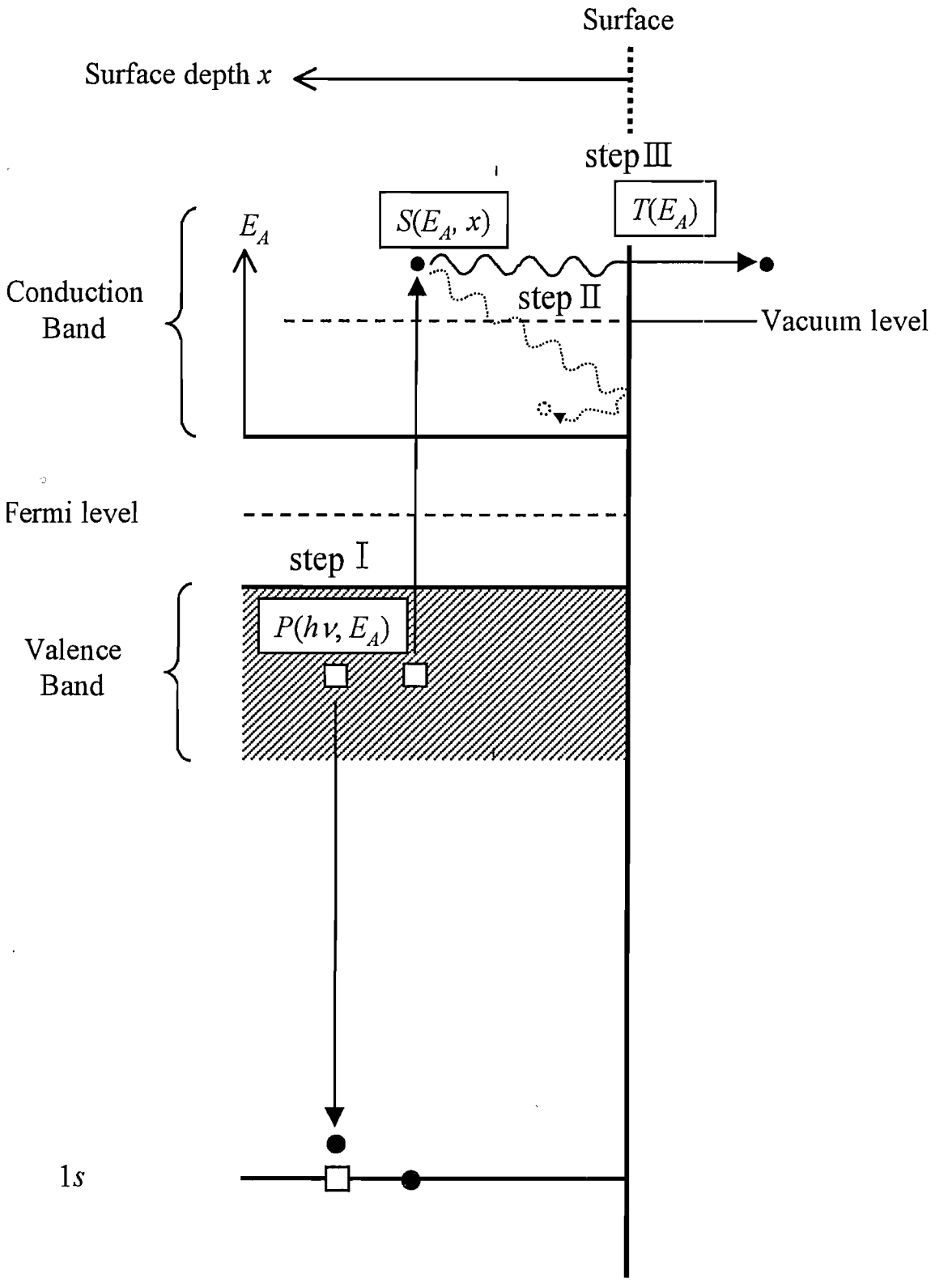

Figure 4-2. Schematic energy diagram of 3 step model for Auger electron.
$P(h\nu, E_A)$:Auger decay probability, $S(E_A, x)$: surface arriving probability
$T(E_A)$: penetration probability. See the detail in text.

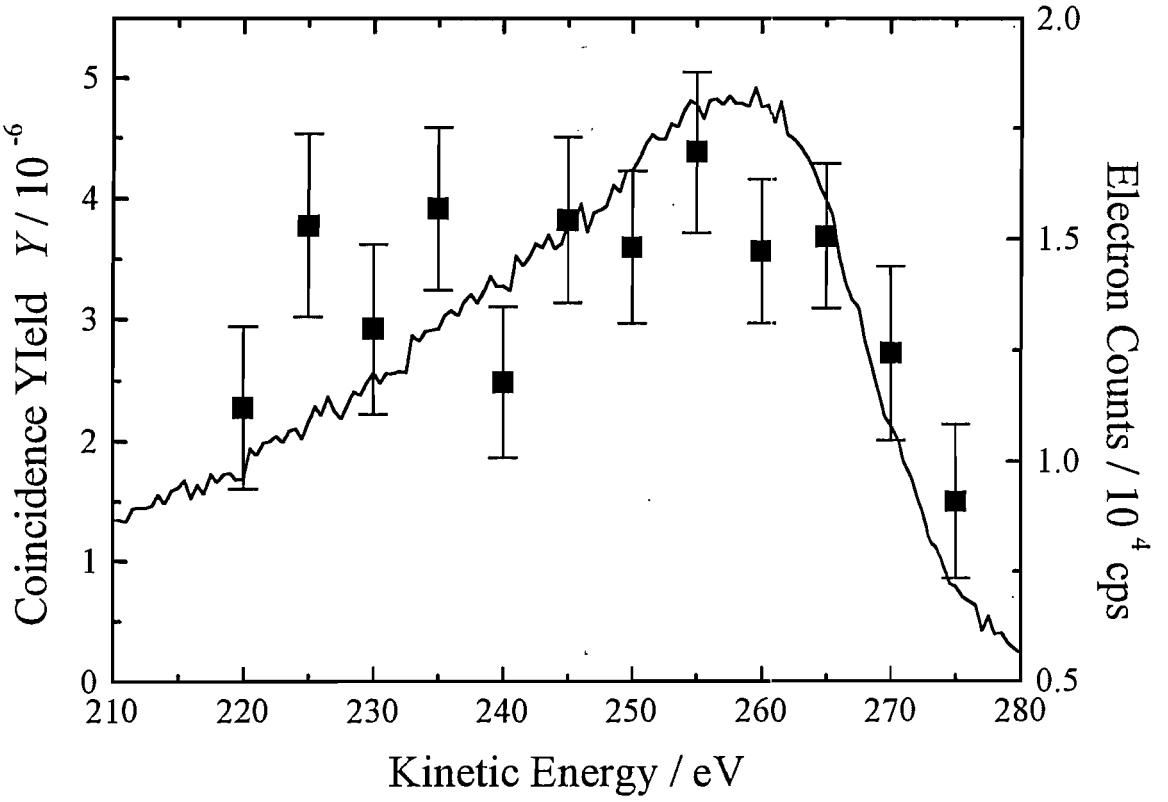

Figure 4-3. AES (solid line) and coincidence yield $Y(h\nu)$(■) for the excitation $h\nu = 430$ eV (ionization ← 1*s*).

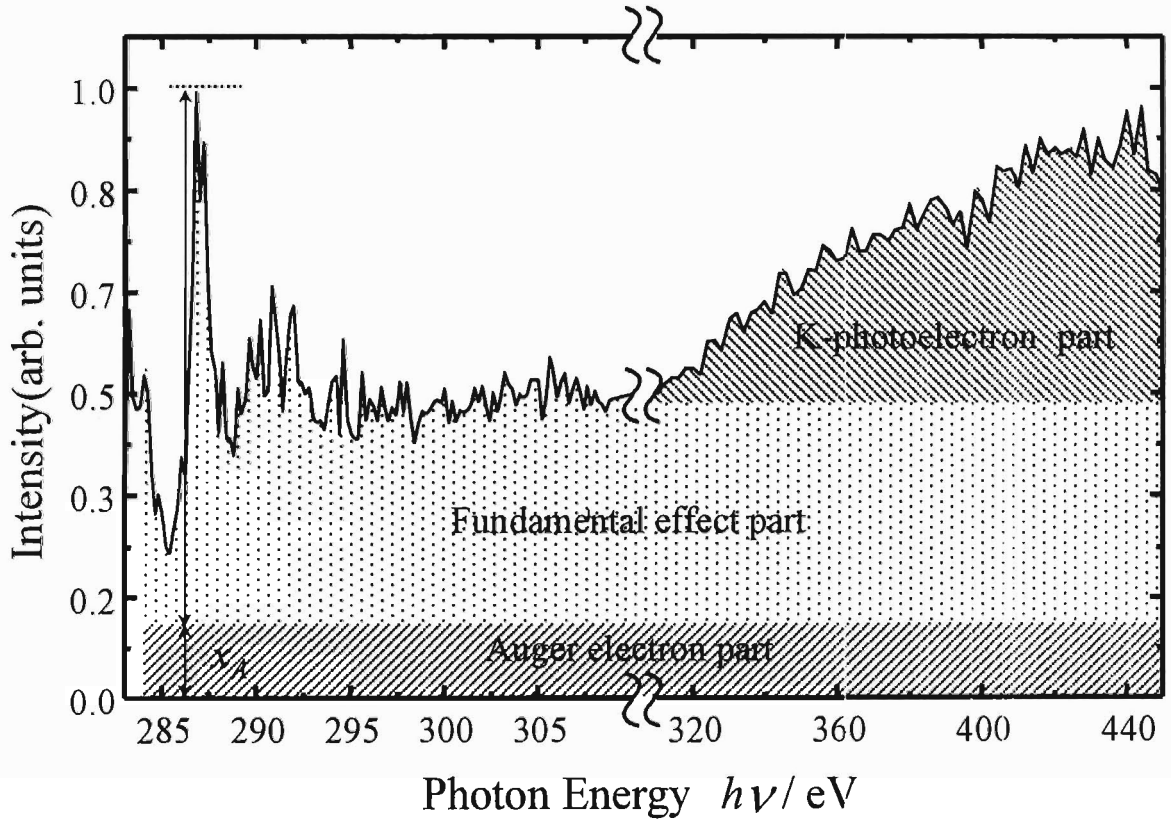

Figure 4-4. TIY/AEY spectrum and contribution separation of secondary and fundamental effects. x_A: magnitude of Auger electron contribution.

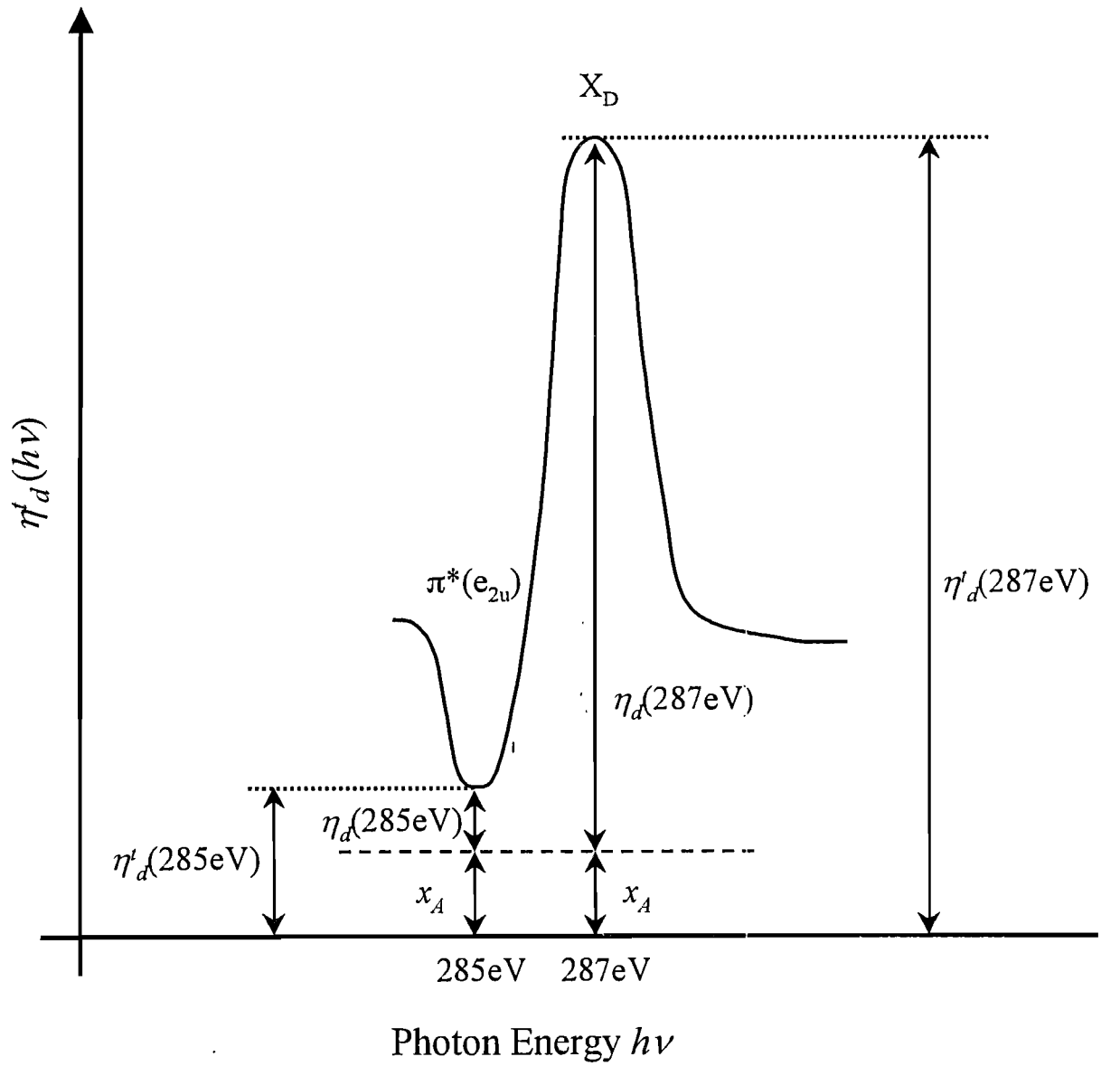

Figure 4-5. Schematic diagram of contributions of $\eta^t_d(h\nu)$ and $\eta_d(h\nu)$ at the inner shell resonant excitations $\pi^*(e_{2u}) \leftarrow 1s$ and $X_D \leftarrow 1s$.
x_A: magnitude of Auger electron contribution

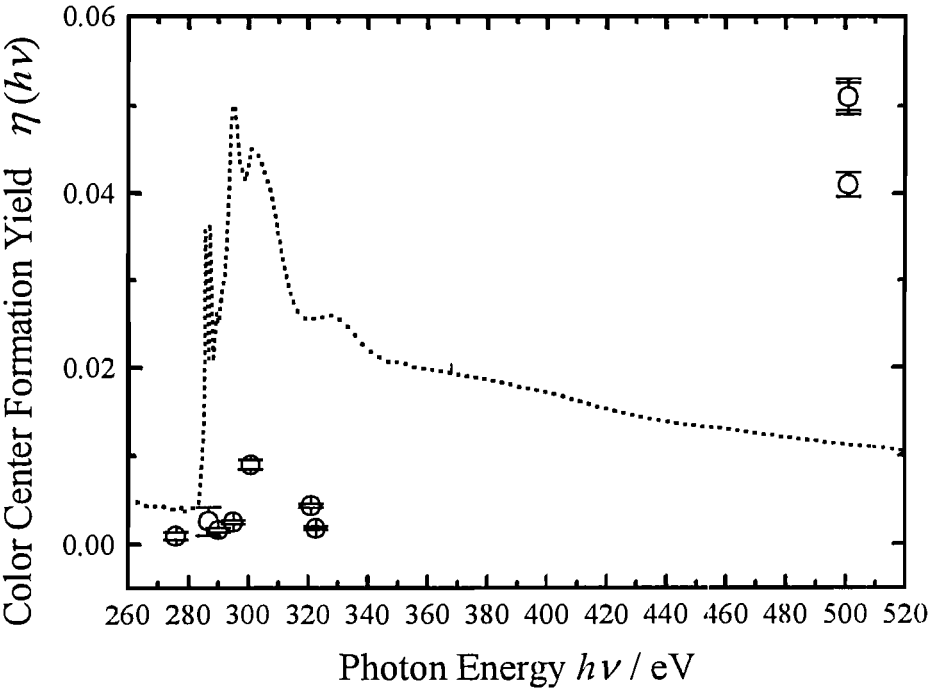

Figure 4-6-(a)

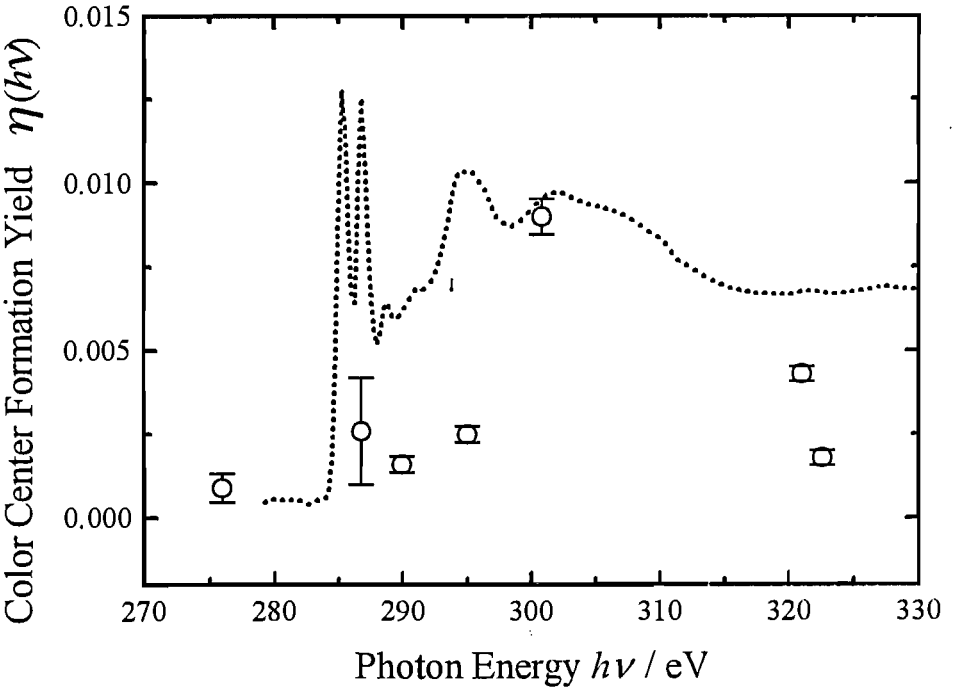

Figure 4-6-(b)

Figure 4-5. Color center formation quantum yield $\eta_c(h\nu)$ (○) of anthracene single crystals and NEXAFS (dotted line) of condensed anthracene. (a) wide energy region (b) narrow energy region

Table 4-1: C-H dissociation yield

	$\pi^*(e_{2u})$ $h\nu$=285eV	X_D $h\nu$=287eV	ionization $h\nu$=300eV	ionization $h\nu$=430eV
intensity ratio of $\eta^f_d(h\nu)$	1/4	1	1/2	1
intensity ratio of $\eta_d(h\nu)$	1/10	1	—	1

Table 4-2: Contribution ratios of fundamental and secondary effect

	$\pi^*(e_{2u})$ $h\nu$=285eV	X_D $h\nu$=287eV	ionization $h\nu$=300eV	ionization $h\nu$=430eV
Auger electron contribution ratio	1/6	1/6	1/6	1/6
K-photoelectron contribution ratio	—	—	—	1/2
Fundamental effect contribution ratio	1/12	5/6	1/3	1/3

V. Summary

1. We measured Auger electron yield (AEY), total ion yield (TIY) spectra of condensed benzene (C_6H_6) in carbon *K*-edge energy region. AEY spectra and TIY spectra correspond to absorption spectra and H^+ yield spectra, respectively.
2. In TIY/AEY spectrum, which reflects H^+ desorption yield that includes fundamental and secondary effects, we observed clear peak at the inner shell resonant excitation $X_D \leftarrow C(1s)$ ($h\nu$ = 287eV) and dip at the inner shell resonant excitation $\pi^*(e_{2u}) \leftarrow C(1s)$ ($h\nu$ = 285eV). The ratios of TIY/AEY($h\nu$) were obtained as follows;

   $\{TIY/AEY(285eV)\}/\{TIY/AEY(430eV)\} \approx 1/4$,
   $\{TIY/AEY(287eV)\}/\{TIY/AEY(430eV)\} \approx 1$,
   and $\{TIY/AEY(300eV)\}/\{TIY/AEY(430eV)\} \approx 1/2$.
3. The ratio of $\{TIY/AEY(285eV)\}/\{TIY/AEY(287eV)\}$ ($\approx$ 1/4) can be explained on the basis of Auger stimulated desorption model as follows. When core electron is excited into anti-bonding unoccupied orbital (in this case, X_D orbital), desorption yield is enhanced, while, when core electron is excited into non-bonding unoccupied orbital (in this case, $\pi^*(e_{2u})$ orbital), desorption yield is suppressed. And I concluded that the ratio of $\{TIY/AEY(300eV)\}/\{TIY/AEY(430eV)\}$ ($\approx$ 1/2) is attributed to secondary effect of *K*-photoelectron.
4. To extract fundamental effect on H^+ desorption yield, we measured Auger electron photoion coincidence (AEPICO) spectra for three kinds of specific excitations; $\pi^*(e_{2u}) \leftarrow C(1s)$ ($h\nu$ = 285eV), $X_D \leftarrow C(1s)$ ($h\nu$ = 287eV), and ionization $\leftarrow C(1s)$ ($h\nu$ = 430eV). From the AEPICO spectra, I obtained coincidence yield $Y(h\nu)$ ($\equiv$ coincidence H^+ counts / Auger electron counts) as follows; $Y(285eV) = 5.7\times10^{-7} \pm 3.1\times10^{-7}$, $Y(287eV) = 4.5\times10^{-6} \pm 1.7\times10^{-6}$, $Y(430eV) = 4.4\times10^{-6} \pm 6.6\times10^{-7}$. Thus the ratio of $Y(285eV)/Y(287eV)$ was about 1/10. I concluded that the inner shell resonant excitation effect on H^+ desorption yield from condensed benzene is suppressed from 1:10 to 1:4 by secondary effect.
5. I derived a relationship between total C-H dissociation yield $\eta'_d(h\nu)$ and TIY/AEY, and a relationship between fundamental C-H dissociation yield $\eta_d(h\nu)$ and $Y(h\nu)$ assuming 3 step model. From the relationships, I derived

simple formulae with some assumptions: TIY/AEY $\approx$ C $\cdot$ $\eta^t_d(h\nu)$ and $Y(h\nu) \approx$ C' $\cdot$ $\eta_d(h\nu)$, where C and C' are constant. Thus I concluded that TIY/AEY is regarded as C-H dissociation yield which include fundamental and secondary effects, and $Y(h\nu)$ is regarded as C-H dissociation yield which results from only fundamental effect.

6. Comparing $\eta^t_d(h\nu)$ and $\eta_d(h\nu)$, I succeeded to separate TIY/AEY into three parts of contributions; fundamental effect, Auger electron, and K-photoelectron. For the surface reaction on C-H dissociation, I concluded that the magnitude of fundamental effect is comparable to that of secondary effect. And I indicated that it may be probable that counts of secondary H^+ induced by *K*-photoelectron are included in the coincidence counts at the excitation energy $h\nu = 430$eV.
7. To study the difference between surface reaction and bulk reaction on C-H dissociation, I compared the C-H dissociation yield of condensed benzene with the color center formation quantum yield $\eta_c(h\nu)$ of anthracene single crystals. For $\eta_c(h\nu)$, a suppression at the excitation $\pi^* \leftarrow$ C(1*s*) could not observed. Thus I concluded that secondary effect is dominant in bulk for C-H dissociation yield of aromatic hydrocarbon compounds.

VI. References

[1] V. Rehn and R. A. Rosenberg, in *Advances in Surface and Interface Science*, vol. 1: Techniques, Eds. R. Z. Bacharach, Plenum Press, New York (1992)

[2] M. L. Knotek, *Rep. Prog. Phys.*, **47**, 1499 (1984)

[3] D. E. Ramaker, in *Desorption Induced by Electronic Transitions, DIET- II*, Vol. 4 of Springer Series in Surface Sciences, Eds. W. Brenig and D. Menzel, Springer-Verlag, Berlin (1985) p. 10

[4] N. Ueno and K. Tanaka, *Jpn. J. Appl. Phys.*; **36**, 12B(1997)

[5] D. Coulman, A. Puschmann, U. Höffer, H.-P. Steinrück, W. Wurth, P. Feulner, and D. Menzel, *J. Chem. Phys.*, **93**, 1(1990)

[6] K. Fujii, T. Sekitani, K. Tanaka, S. Yamamoto, K. K. Okudaira, Y. Harada, N. Ueno, *J. Electron Spectrosc. Relat. Phenom.*, **88-91**, 837(1998)

[7] D. Menzel, G. Rocker, D. Coulman, P. Feulner, and W. Wurth, *Phys. Scr.*, **41**, 58 (1990)

[8] H. Yamaoka, *Irradiation Effect of Polymer*, in *Irradiation Effect in Material*, Shokabo, Tokyo (1994) p. 168, in Japanese

[9] T. Seguchi, *Polymer*, **44**, 144 (1995), in Japanese

[10] T. J. Hardwick, *J. Phys. Chem.*, **64**, 1623 (1969)

[11] G. R. Freeman, *J. Chem. Phys.*, **33**, 71 (1969)

[12] W. G. Burns, *Trans. Faraday. Soc.*, **58**, 961 (1962)

[13] G. R. Freeman, *Can. J. Chem.*, **38**, 1043 (1960)

[14] T. Sasuga, in *High Performance Aromatic Polymer Materials, Advanced Polymer Materials*, Vol. 2, Eds. Y. Iwakura, T. Imai, and K. Iwata, Maruzene (1990) p. 92, in Japanese

[15] M. Y. Amusia, *Atomic Photoeffect*, Plenum Press, New York (1990)

[16] T. A. Carlson, *Photoelectron and Auger spectroscopy*, Plenum Press, New York (1975)

[17] *X-Ray Science and Technology*, Eds. A. G. Michette and C. J. Buckley, Institute of Physics Publishing, Bristol and Philadelphia (1993) p. 61

[18] T. Koopmans, *Physica*, **1**, 104(1934)

[19] F. P. Larkins, *Chem. Phys. Lett.*, **455**, 335 (1978)

[20] M. Thompson, M. D. Baker, A. Christie, and J. F. Tyson, in Auger Electron Spectroscopy, Eds. P. J. Elving and J. D. Winefordner, Willey, New York (1985) p. 99

[21] H. Hanashiro, Y. Suzuki, T. Sasaki, A. Mikuni, T. Takayanagi, K. Wakiya, H. Suzuki, A. Danjo, T. Hino, and S! Ohtani, *J. Phys. B: Atom Mol. Phys.*, **12**, L775 (1979)

[22] V. Schmidt, S. Krummacher, F. Wuilleumier, and P. Dhez, *Phys. Rev. A*, **24**, 1803 (1981)

[23] T. A. Carlson and R. M. White, *J. Chem. Phys.*, **44**, 12(1966)

[24] T. A. Carlson and M. O. Krause, *J. Chem. Phys.*, **56**, 3206 (1972)

[25] W. Eberhardt, T. K. Sham, R. Carr, S. Krummacher, M. Strongin, S. L. Weng, and D. Wesner, *Phys. Rev. Lett.*, **50**, 14(1983)

[26] K. Müller-Dethlefs, M. Sander, L. A. Chewter, and E. W. Schlag, *J. Phys. Chem.*, **88**, 6098 (1984)

[27] J. Murakami, M. C. Nelson, S. L. Anderson, and D. M. Hanson, *J. Chem. Phys.*, **85**, 5755 (1986)

[28] M. C. Nelson, J. Murakami, S. L. Anderson, and D. M. Hanson, *J. Chem. Phys.*, **86**, 8 (1987)

[29] A. Halpern and G. Stöcklin, *Rad. Res.*, **58**, 329-337(1974)

[30] F. Sato, N. Saito, J. Kusano, K. Takizawa, S. Kawado, T. Kato, H. Sugiyama, Y. Kagoshima and M. Ando, *J. Electrochem. Soc.*, **145**, 9(1998)

[31] Y. Kondo, S. Hoshina, S. Hirota, I. Goto, Y. Kon'no, M. Yanagihara, H. Kimura and T. Hnyuu, *Phys. Rev. Lett.*, **70**, 6(1993)

[32] A. Kimura, K. Nakagawa, K. Tanaka, M. Kotani and R. Katoh, *Nucl. Instr. and Meth. in Phys. Res. B*, **91**, 67 (1994)

[33] A. A. Sokolov and I. M. Ternov, *Sov. Phys.-JETP*, **4**, 396 (1957)

[34] K. Kimura, in *UVSOR Activity Report 1997*, Eds. M. Watanabe and K. Fukui

[35] F. Uesugi and I. Nishiyama, *Appl. Surf. Sci.*, **54**, 284 (1992); *Appl. Surf. Sci.*, **60/61**, 587 (1992); *Appl. Surf. Sci.*, **62**, 151 (1992); *Appl. Surf. Sci.*, **79/80**, 203 (1994); *IEICE Trans. Electron.*, **E76-C**, 47 (1993)

[36] M. C. K. Tinone, K. Tanaka, J. Maruyama, N. Ueno, M. Imamura, and N. Matsubayashi, *J. Chem. Phys.*, **100**, 8 (1994)

[37] M. C. K. Tinone, N. Ueno, J. Maruyama, K. Kamiya, Y. Harada, T. Sekitani, and K. Tanaka, *J. Electron Spectrosc. Rel. Phenom.*, **80**, 117 (1996)

[38] H. Akazawa and Y. Utsumi, *Synchrotron Radiation*, **8**, 1 (1995), in Japanese

[39] D. Menzel and R. Gomer, *J. Chem. Phys.*, **42**, 3311 (1964)

[40] P. A. Redhead, *Can. J. Phys.*, **42**, 886 (1964)

[41] M. L. Knotek and P. J. Feibelman, *Phys. Rev. Lett.*, **40**, 964(1978)

[42] D. E. Ramaker, C. T. White, and J. S. Murday, *J. Vac. Sci. Technol.*, **18**, 748 (1981)

[43] D. E. Ramaker, C. T. White, and J. S. Murday, *Phys. Lett.*, A **84**, 211 (1982)

[44] K. Mase, M. Nagasono, S. Tanaka, T. Urisu and Y. Murata, *Rev. Sci. Inst.*, **68**, 1703 (1997)

[45] F. C. Brown, R. Z. Bachrach, and N. Lien, *Nucl. Instrum. Methods*, **152**, 73 (1978)

[46] D. Briggs and M. P. Seah, *Practical Surface Analysis by Auger and X-ray Photoelectron Spectroscopy*, John Wiley & Sons (1983)

[47] D. E. Eastman, *Phys. Rev. Sect. B*, **2**, 1 (1970)

[48] K. Tanaka, *Synchrotron Radiation*, **4**, 1 (1991), in Japanese

[49] D. C. Koningsberger and R. Prins, *X-Ray Absorption in Chemical Analysis*, A Willey-Interscience Publication, **92** (1988)

[50] D. Menzel, G. Rocker, H.-P. Steinrück, D. Coulman, P. A. Heinmann, W. Huber, P. Zebisch and D. R. Lloyd, *J. Chem. Phys.*, **96**, 1724 (1992)

[51] J. A. Horsley, J. Stöhr, A. P. Hitchcock, D. C. Newbury, A. L. Johnson, and F. Sette, *J. Chem. Phys.*, **83**, 6099(1985)

[52] G. Rocker, P. Feulner, R. Scheuerer, L. Zhu, and D. Menzel, *Phys. Scr.*, **41**, 1014(1990); D. Menzel, *Appl. Phys.*, **A 51**, 163(1990)

[53] A. P. Hitchcock and C. E. Brion, *J. Electron Spectrosc. Relat. Phenom.*, **10**, 317(1977)

[54] J. Stöhr and D. A. Outka, *Phys. Rev.*, B **36**, 7891 (1987)

[55] J. L. Solomon, R. J. Madix, and J. Stöhr, Surf. Sci., 255, 12 (1991)

[56] W. H. E. Schwarz, T. C. Chang, U. Seeger and K. H. Hwang, *Chem. Phys.*, **117**, 73 (1987)

[57] E. Lindholm, L. Åsbrink, *Lecture notes in chemistry*, Springer, Berlin, **38**(1985) secs. I.5, K.4.

[58] W. Butscher, W. H. E. Schwarz, and K. H. Thunemann, in *Inner-shell and X-ray physics of atom and solids*, edited by D. J. Fabian, H. Kleinpoppen, and L. Watson, Plenum Press, New York (1981) p. 841

[59] A. Dennis, J. Langlet, ad J. P. Malrieu, *Theoret. Chim. Acta.*, **38**, 49 (1975)

[60] W. H. E. Schwarz, T. C. Chang, *Intern. J. Quantum. Chem. Symp.*, **10**, 91

(1976)
[61] M. Benard, *Theoret. Chim. Acta.*, 61, 379 (1982); *Chem. Phys. Lett.*, **91**, 363 (1983)
[62] V. N. Akimov, A. S. Vinogradov, A. A. Pavlychev, and V. N. Sivkov, *Optica I Spektroskya*, **59**, 342 (1985)
[63] S. Aminpirooz, L. Becker, B. Hillert, and J. Haase, *Surf. Sci. Lett.*, **244**, L152 (1991)
[64] I. Shimoyama, T. Mochida, K. Nakagawa, H. Takeshita, E. Ikenaga, T. Sekitani, K. Tanaka, *Meeting Abstracts of the Physical Society of Japan, Sectional Meeting '95 of Phys. Soc. Japan*, 28a W16 (1996), September 27-30, 1995, the University of Osaka Prefecture, Sakai, Japan (in Japanese)
[65] W. K. Siegbahn, C. Nording, G. Johansson, J. Hedman, P. F. Heden, K. Hamrin, U. Gelius, T. Bergmark, L. O. Werme, R. Manne, and Y. Baer, *ESCA Applied to Free Molecules*, North-Holland, Amsterdam (1969)
[66] C. J. Taylor, W. K. Jentschke, M. E. Remley, F. S. Eby, and P. G. Kruger, *Phys. Rev.*, **84**, 1034 (1951)
[67] K. Mase, M. Nagasono, S. Tanaka, T. Urisu, T. Sekitani, E. Ikenaga, and K. Tanaka, in preparation
[68] K. Mase, M. Nagasono, S. Tanaka, T. Urisu, T. Sekitani, E. Ikenaga, and K. Tanaka, *Surf. Sci.*, **390**, 97 (1997)
[69] M. Nagasono, K. Mase, S. Tanaka, T. Urisu, *Surf. Sci.*, **390**, 102 (1997)
[70] T. Sekitani, E. Ikenaga, H. Matsuo, S. Tanaka, K. Mase, K. Tanaka, J. Electron Spectrosc. Relat. Phenom., **88-91**, 831 (1998)
[71] W. Eberhardt, E. W. Plummer, C. T. Chen, R. Carr, and W. K. Ford, *Nucl. Instrum. Methods Phys. Res. Sect.*, A **246**, 825(1986)
[72] W. Eberhardt, E. W. Plummer, I.-W. Lyo, R. Carr, and W. K. Ford, *Rev. Lett.*, **58**, 207 (1987)
[73] W. Eberhardt, R. Murphy, in *Desorption Induced by Electronic Transitions, DIET-III*, Vol. 13 of Springer Series in Surface Sciences, Eds. R. H. Stulen and M. L. Knotek, Springer, Berlin (1988) p. 32
[74] W. Eberhardt, *Phys. Scr.*, **T17**, 28(1987)
[75] R. Murphy and W. Eberhardt, *J. Chem. Phys.*, **89**, 4054 (1988)
[76] D. M. Hanson, C. I. Ma, K. Lee, D. Lapiano-Smith, and D. Y. Kim, *J. Chem. Phys.*, **93**, 9200 (1990)
[77] D. M. Hanson, in *Desorption Induced by Electronic Transitions, DIET-V*," Vol. 31 of Springer Series in Surface Sciences, Eds. A. R. Burns, E. B.

Stechel, and D. R. Jennison, Springer, Berlin (1993) p. 110

[78] Y. Sato, K. Ueda, H. Chiba, E. Shigemasa, and A. Yagishita, *Chem. Phys. Lett.*, **196**, 475 (1991)

[79] K. Ueda, H. Chiba, Y. Sato, T. Hayaishi, E. Shigemasa, and A. Yagishita, *Phys. Rev.*, A **46**, R5 (1992); K. Ueda, K. Ohmori, M. Okunishi, H. Chiba, Y. Shimizu, Y. Sato, T. Hayaishi, E. Shigemasa, and A. Yagishita, *J. Electron Spectrosc. Relat. Phenom.*, **79**, 411 (1996)

[80] E. Shigemasa, T. Koizumi, Y. Ito, T. Hayaishi, K. Okuno, A. Danjo, Y. Sato, and A. Yagishita, *Rev. Sci. Instrum.*, **63**, 1505 (1992); E. Shigemasa, T. Hayaishi, K. Okuno, A. Danjo, K. Ueda, Y. Sato, and A. Yagishita, *J. Electron Spectrosc. Relat. Phenom.*, **79**, 495 (1996)

[81] M. L. Knotek and J. W. Rabalais, in *Desorption Induced by Electronic Transitions, DIET- II*, Vol. 4 of Springer Series in Surface Sciences, Eds. W. Brenig and D. Menzel, Springer-Verlag, Berlin (1985) p. 77

[82] W. E. Spicer, *Optical Properties of Solids*, F. Abelès(ed.), North-Holland, Amsterdam (1972) p.758

[83] Y. Akasaka, K. Masuda and S. Namba, *J. Phys. Soc. Japan*, **30**, 1686 (1971)

[84] L. A. Harsh and R. C. Hughes, *Mol. Crys.*, **5**, 141 (1968)

[85] T. Inoue, *J. Phys. Soc. Japan*, **25**, 914 (1968)

[86] S. Ohnishi, T. Tanei, and I. Nitta, J. Chem. Phys., 37, 2402 (1962)

[87] I. Shimoyama, K. Nakagawa, *UVSOR activity report 1997*, p. 94; to be published

[88] I. Shimoyama, Y. Kishigami, M. Tanaka, K. Nakagawa, F. Matsui, H. W. Yoem, and T. Ohta, *Meeting Abstracts of the Physical Society of Japan*, 53, 2, 26pYP7, *Sectional Meeting '98 of Phys. Soc. Japan*, September 25-28, 1998, the University of Ryukyus and Okinawa International University, Okinawa, Japan (in Japanese); to be published